

Studies on Novel Inhibitor of Mitotic Kinesin Eg5:

A validated Chemotherapeutic Target

By

Ogunwa Tomisin Happy



長崎大学
NAGASAKI UNIVERSITY

A Thesis submitted to Nagasaki University for the degree of
Doctor of Philosophy

Graduate School of Fisheries and Environmental Sciences
Nagasaki University, Japan

August, 2019

Acknowledgements

First and foremost, special gratitude to God whose help was nearest when the need was greatest. It was by his grace I am alive to achieve the results presented in this report. I will like to express my deep appreciation to my supervisors, Prof. Miyanishi Takayuki, Prof Oda Tatsuya, and Prof. Yamashita Kimihiro for their guidance and support during the research work reported in this thesis. I am grateful to Dr. Omotuyi Idowu Olaposi for training and supports in my computational analyses. I want to thank Dr. Elekofehinti Olusola for his advice. Dr. Juliann Nzembi Makau, Dr. Oloniniyi Olamide, and Dr. Chantal Agbemabiese provided wonderful career encouragements and guidance. My gratitude to all the students at Prof. Miyanishi and Prof. Okada's laboratory who always helped with translations of Japanese documents. Prof. Shinsaku Maruta and his research team at Soka University, Hachioji, Tokyo, and Prof. Roberta Galeazzi and Dr. Emiliano Laudadio of Università Politecnica delle Marche, Ancona, Italy were tremendously helpful in providing relevant collaboration for the biochemical analyses and molecular dynamics simulation, respectively.

I am highly indebted to my mother, Mrs. Lucy Tenelape Ogunwa for standing by all her children to achieve great feat in our family. My entire academic career would never have been possible without the care, love and supports received from my mentors; Associate Professor Omonkhua A.A., Pastor and Deaconess G.I. Jayeola, Pastor and Mrs. Oyetunji R., Mrs. Ojo Abike Lizzy (Nee Adeyogbe), Mrs. Adewola O.E., Mr. Olofin, Mr. Fakinlede F, Pastor Akinnusi I.J., and Aridunnu family as well as my siblings, and financial support from Mr. Seinde Fadeni. The continual encouragement, love, understanding, support and prayers received from my wife, Mrs. Ogunwa Titilayo Abigeal and my son Tomisin Semilore Kiseki, are highly appreciated. Finally, I acknowledge the sponsorship enjoyed from Japanese MEXT scholarship and the financial support from Nagasaki University during the course of my st

Abstract

Chemical compounds, from natural and synthetic sources, with potential to inhibit kinesin Eg5 ATPase and other functions are continually sought over the years as they are very suitable and effective chemotherapeutic agents. Eg5 is a mitotic kinesin with crucial role in the formation and maintenance of mitotic spindle bipolarity, an essential apparatus during proper cell division. Inhibition of Eg5 during mitosis may result in mitotic arrest and apoptosis because functional spindle does not assemble. Hence, inhibitors of Eg5 have been investigated in studies aimed at controlling proliferation of cancer cells, validating the protein as a target for chemotherapeutic candidates. Inhibitors that bind the allosteric Eg5 pocket are preferable to the ATP-competitive inhibitor to avoid potential interaction with other ATP-dependent proteins. Also, inhibitors such as ispinesib, monastrol, *S*-trityl-L-cysteine (STLC), etc. that bind the allosteric pocket formed by $\alpha 2/\alpha 3$ /Loop5 regions display specificity to Eg5 among other kinesins. Although several synthetic inhibitors of Eg5 are known, only few inhibitors from natural products have been investigated till date—despite that natural products are readily available source of bioactive compounds with pharmacological potency and reduced side effects.

In the experiments reported in this thesis, morelloflavone from *Garcinia dulcis* leaves was discovered as novel inhibitor of the mitotic kinesin Eg5. The compound was selected among forty plant-derived biflavonoids and tested for its inhibitory potential against Eg5 based on *in silico* analysis of binding modes, molecular interactions, binding energies, and functional groups that interact with Eg5. Computational models predicted that morelloflavone binds the putative allosteric pocket of Eg5, within the cavity surrounded by amino acid residues of Ile-136, Glu-116, Glu-118, Trp-127, Gly-117, Ala-133, Glu-215, Leu-214, and Tyr-211. Binding energy was -8.4 kcal/mol, with a single hydrogen bond formed between morelloflavone and Tyr-211. The binding configuration was comparable to that of a reference inhibitor, *S*-trityl-L-

cysteine. *In vitro* analysis confirmed that morelloflavone inhibited both the basal and microtubule-activated ATPase activity of Eg5 in a manner that does not compete with ATP binding. Morelloflavone also suppressed Eg5 gliding along microtubules. These results suggest that morelloflavone binds the allosteric binding site in Eg5 and thereby inhibits ATPase activity and motor function of Eg5.

To provide dynamical insights on the interaction and inhibitory mechanisms, molecular dynamics simulation was undertaken on Eg5-morelloflavone complexes in the presence of nucleoside-phosphates (ADP and ATP). Results were compared with those of known Eg5 inhibitors; ispinesib and *S*-trityl-L-cysteine (STLC). Data obtained strongly support a stable Eg5-morelloflavone complex, with significantly low binding energy and reduced flexibility of Eg5 at some regions including loop5 and switch I. Furthermore, the loop5 Trp127 was trapped in a downward position to keep the allosteric pocket of Eg5 in the so-called “closed conformation” comparable to STLC. Altered structural conformations were also visible within various regions of Eg5 including switch I, switch II, $\alpha 2/\alpha 3$ helices and tubulin-binding region, indicating that morelloflavone might induce modifications in Eg5 structure to compromise its ATP/ADP binding and conversion process as well as its interaction with microtubules.

Taken together, morelloflavone is a novel inhibitor of mitotic kinesin Eg5. Since morelloflavone is a naturally-occurring biflavonoid obtained from *Garcinia* spp, and is associated with suppression of ATP hydrolysis and microtubule gliding of Eg5, the compound may be useful in the control of proliferating cancer cells. Its chemical scaffold may be relevant in the design and development of new antimetabolic candidates. The reports provided herein also contribute to validation of the folkloric use of *Garcinia dulcis* (a medicinal plant) in the treatment of cancer. Finally, the efficient screening protocol developed and utilized in this research will be handy in further discovery of many more novel Eg5 allosteric inhibitors.

List of Abbreviations

Å	Ångström
ADME	Absorption, distribution, metabolism and excretion
ADP	Adenosine Diphosphate
ATP	Adenosine triphosphate
DMSO	Dimethyl sulfoxide
EDTA	Ethylenediaminetetraacetic acid
Eg5	Mitotic kinesin Eg5
EGTA	Ethylene glycol tetraacetic acid
g	Gram
HEPES	4-(2-hydroxyethyl)-1-piperazineethanesulfonic acid
hr	Hour
IC ₅₀	Half maxima inhibitory concentration
K-acetate	Potassium acetate
Kcal/mol	Kilocalorie per mole
KCl	Potassium chloride
kDa	Kilodalton
KIF11	Kinesin-like protein Factor 11
KOH	Potassium hydroxide
MF	Morelloflavone
MFa	Enantiomer “A” of morelloflavone
MFb	Enantiomer “B” of morelloflavone
MgCl ₂	Magnesium Chloride
MgSO ₄	Magnesium sulphate
min	Minute

mL	Milliliter
mm	Millimeter
mM	Millimolar
MS	Microsoft
MTS	Microtubules
NCBI	National Center for Biotechnology Information
Pi	Inorganic phosphate
r.m.s.d	Root-mean-square deviation
r.m.s.f	Root-mean-square fluctuation
Rg	Radius of gyration
SD	Standard deviation
sdf	Structure data file
STLC	S-trityl-L-cysteine
μg	Microgram
μL	Microliters

Table of contents

Abstract	i
List of abbreviations	iii
Table of contents	v
List of figures	viii
List of tables	x
CHAPTER 1	1
General introduction	2
1.1 Overview of kinesins	2
1.2 The mitotic kinesin Eg5	7
1.3 Objectives of research	12
1.4 Research approach and methodology	14
CHAPTER 2	
Morelloflavone as a novel inhibitor of mitotic kinesin Eg5	15
2.1 Introduction	16
2.2 Materials and methods	17
2.2.1 <i>In silico</i> screening	17
2.2.2 <i>In vitro</i> experimental validation	19
2.3 Results and discussion	21
2.3.1 <i>In silico</i> screening reveals morelloflavone as a potential Eg5 inhibitor	21

2.3.2	Morelloflavone inhibits both basal and microtubule-activated ATPase activities of Eg5	26
2.3.3	Mechanism of interaction between morelloflavone and Eg5	39
2.3.4	Morelloflavone suppresses Eg5 motor gliding along microtubules	32
2.4	Conclusion	33
2.5	Supplementary materials	34

CHAPTER 3

	Insights into the molecular mechanisms of Eg5 inhibition by (+)-morelloflavone	39
3.1	Introduction	40
3.2	Materials and Methods	43
3.2.1	Starting structures	43
3.2.2	Biosystems setup	44
3.2.3	Molecular dynamics (MD) simulation	44
3.3	Results and discussion	46
3.3.1	MF exhibits stability in complex with Eg5 at the allosteric pocket	47
3.3.2	MF induces Eg5-loop5/ α 2/ α 3 pocket closure comparable to STLC	49
3.3.3	MF induces compactness and stabilizes Eg5 allosteric pocket	53
3.3.4	MF binding on allosteric site alters Eg5 structural conformation	54
3.3.5	Binding free energy estimation for Eg5-inhibitor complexes: MM/PBSA	59
3.3.6	MF alters affinity of nucleotides to the active site of Eg5	62
3.4	Conclusion	64
3.5	Supplementary materials	65

CHAPTER 4

General discussion and conclusion	68
4.0 General discussion	69
4.1 Conclusion	73
Literature cited	74

List of Figures

Fig. 1-1 A simplified model of the function of kinesins Eg5 during mitosis	7
Fig. 1-2 Motor domain of mitotic kinesin Eg5 and interaction with microtubule	10
Fig. 1-3 Selected known inhibitors of kinesin Eg5	12
Fig. 1-4 The general <i>modus operandi</i> adopted for the research work reported in this thesis	14
Fig. 2-1 2D structure of Eg5 inhibitors (morelloflavone and STLIC)	17
Fig. 2-2 Structure and function of kinesin Eg5	22
Fig. 2-3 Binding of morelloflavone to Eg5	25
Fig. 2-4 <i>In vitro</i> ATPase activity of Eg5 in presence of inhibitor (morelloflavone)	27
Fig. 2-5 Effect of morelloflavone on microtubule-activated Eg5 ATPase activity	30
Fig. 2-6 Motility of Eg5	32
Fig. SM2-1 Predicted binding poses of selected biflavonoids on Eg5	34
Fig. SM2-2 Morelloflavone binding sites predicted by PSB-SLIM	35
Fig. 3-1 Chemical structure of (+)-morelloflavone	42
Fig. 3-2 Flow-chart for the computational strategy used in this study	42
Fig. 3-3 Stability and compactness parameters of Eg5 complexes	49
Fig. 3-4 Distances (in nm) between Eg5 Trp127 and Glu215 residues, and Trp127 and Tyr211	51
Fig. 3-5 RMSD of allosteric pocket around 8 Å of complexes in presence of ADP and ATP	54
Fig. 3-6 Structural behavior of Eg5 in the presence and absence of inhibitors	56
Fig. 3-7 Potential of mean force along the reaction coordinate for the dissociation of inhibitors in Eg5 protein	61
Fig. 3-8 Binding affinity of ADP with Eg5 during MD trajectories calculated using MM/PBSA on the 100 ns trajectories	63

Fig. SM3-1 Cartoon representation of Eg5 crystal (motor domain) showing amino acid residues Trp127 and Glu215 (yellow stick), and Trp127 and Tyr211 (orange stick)	65
Fig. SM3-2 Estimated b-factors for the apo protein on ResQ server	65
Fig. SM3-3 Comparison between RMSF and experimental b-factors	66
Fig. 4-1. Preliminary results to compare Eg5 inhibitory effects of morelloflavone and its constituent flavonoids (apigenin and luteolin)	70
Fig. 4-2. <i>In silico</i> binding and interaction model of apigenin and luteolin, components of morelloflavone, on Eg5 allosteric pocket	71

List of Tables

Table 1-1 Human kinesin nomenclature and function	3
Table 1-2 Name and amino acid residues of various domains of Eg5	10
Table 2-1 Estimated binding energy, molecular interaction, and IC ₅₀ values for morelloflavone and a few known Eg5 inhibitors	13
Table SM2-1 Biflavonoids screened <i>in silico</i>	36
Table 3-1 Energy estimation (MM/PBSA)	62

CHAPTER ONE

General Introduction

1.1 Overview of kinesins

Kinesins are a large superfamily of motor proteins that play key roles in eukaryotic cell division and intracellular trafficking (Wittmann, 2001; Rath and Kozielski, 2012). Higher vertebrate genomes have been reported to contain at least forty-five genes which codes for diverse kinesins (Table 1-1), majority of which are implicated in variety of human diseases. These proteins are termed “molecular motor machines” due to their involvement in cellular processes such as intracellular transport, cytokinesis, neurogenesis, and mitosis (Figure 1-1). They travel unidirectionally along the microtubule in a processively manner to fulfil their biological roles. Till date, more than 650 members of the kinesin superfamily have been identified (Miki *et al.*, 2005; Rath and Kozielski, 2012) and, are found in all eukaryotes. However, they are reportedly absent in archaea and bacteria. It is claimed that about a third of the kinesin superfamily members participate in different stages of cell division while a few among them can play dual roles in both cell division and transport. Interference with the biological functions of some crucial proteins during mitosis has been proposed as an alternative to cancer cell elimination via mitotic progression in humans (Debonis *et al.*, 2004; El-Nissan, 2013). The members of the kinesin superfamily that play important roles in intracellular cell division are shown in Figure 1-1.

On the basis of structure and phylogenetic analyses of the motor domain of the kinesins, they are classified into fourteen (14) subfamilies (Lawrence *et al.*, 2004; Wordeman, 2010) which are detailed in Table 1-1. However, all these proteins have been classified into just two groups based on their functions which are non-mutually exclusive. The kinesins are essential during different stages of cell division (Figure 1-1). They also play crucial roles in intracellular organelle and vesicle transport (Hirokawa *et al.*, 2009). Kinesins are composed of limited set of modular domains and hence, can be classified as N-, C- or M-type kinesins depending on the location of the motor domain. Most kinesins are known to move toward the microtubule

plus-end and the motor domain is found at the N-terminus of the protein. These are simply referred to as N-type kinesins. Other kinesins having their motor domain specifically located at the C-terminus are labelled as C-type kinesins and move toward the minus end of microtubules (minus-end directed motors). A few kinesins have their motor domain in the middle of the polypeptide chain and are termed M-type kinesins. They do not move along the microtubules; however, they can depolymerize them. The motor domain of kinesins is the most conserved region across the proteins and contains both the microtubule binding domain as well as the catalytic site responsible for ATP binding/hydrolysis.

Table 1-1. Human kinesin nomenclature and function (Rath and Kozielski, 2012)

Acronym	Full Name	Alternative Nomenclature	Kinesin Family	Function
KIF1A	kinesin family member 1A	ATSV (axonal transport of synaptic vesicles), C2orf20 (chromosome 2 open reading frame 20), FLJ30229	Kinesin-3	Neuron-specific axonal transporter of synaptic vesicle precursors
KIF1B	kinesin family member 1B	CMT2, CMT2A, HMSNII, KIAA0591, KLP, NBLST1	Kinesin-3	Microtubule plus end-directed monomeric motor protein for transport of mitochondria, involved in axonal transport
KIF1C	kinesin family member 1C	KIAA0706, LTXS1	Kinesin-3	Regulates podosome dynamics in macrophages
KIF2A	kinesin family member 2A	KIF2 (kinesin heavy chain member 2), KNS2, HK2, HsKin2	Kinesin-13	Microtubule minus end-depolymerising motor crucial for bipolar spindle formation
KIF2B	kinesin family member 2B	FLJ53902	Kinesin-13	Involved in kinetochore-microtubule dynamics to promote mitotic progression
MCAK (KIF2C)	kinesin family member 2C	KNSL6 (kinesin-like 6), MCAK (mitotic centromere-associated kinesin)	Kinesin-13	Microtubule plus end-depolymerising motor required for chromosome congression and alignment
KIF3A	kinesin family		Kinesin-2	Microtubule plus end-directed motor for

	member 3A	-		membrane organelle transport, required for assembly of the primary cilium
KIF3B	kinesin family member 3B	KIAA0359	Kinesin-2	Microtubule plus end-directed motor for membrane organelle transport
KIF3C	kinesin family member 3C	-	Kinesin-2	Maybe involved in maturation of neuronal cells
KIF4A	kinesin family member 4A	chromokinesin-A, FLJ12530, FLJ12655, FLJ14204, FLJ20631, HSA271784, KIF4, KIF4-G1	Kinesin-4	Chromosome condensation, anaphase spindle midzone formation and cytokinesis
KIF4B	kinesin family member 4B	chromokinesin-B	Kinesin-4	Chromosome condensation, anaphase spindle midzone formation and cytokinesis
KIF5A	kinesin family member 5A	SPG10 (spastic paraplegia 10), D12S1889, MY050, NKHC,	Kinesin-1	Involved in spastic paraplegia type 10 and Charcot-Marie-Tooth type 2
KIF5B	kinesin family member 5B	KNS1, KNS, UKHC	Kinesin-1	Involved in vesicle transport; interacts with a variety of viruses to allow for their replication within the cell
KIF5C	kinesin family member 5C	NKHC2, KINN, KIAA0531, FLJ44735	Kinesin-1	Binding partner of casein kinase 2 involved in apical trafficking
KIF6	kinesin family member 6	C6orf102 (chromosome 6 open reading frame 102), dJ137F1.4, dJ188D3.1, dJ1043E3.1, DKFZp451I2418, MGC33317	Kinesin-9	Unknown
KIF7	kinesin family member 7	JBTS12	Kinesin-4	Hedgehog signalling
KIF9	kinesin family member 9	MGC104186	Kinesin-9	Regulation of matrix degradation by macrophage podosomes
CENPE (KIF10)	Centromere-associated	KIF10, PPP1R61 (protein	Kinesin-7	Microtubule-kinetochore capture and mitotic

	protein E	phosphatase 1, regulatory subunit 61)		checkpoint signalling
EG5 (KIF11)	kinesin family member 11	KNSL1 (kinesin-like 1), KIF11, HKSP (Kinesin Spindle Protein), TRIP5, Thyroid receptor-interacting protein 5	Kinesin-5	Separation of the duplicated centrosome during spindle formation
KIF12	kinesin family member 12	RP11-56P10.3	Kinesin-12	Unknown
KIF13A	kinesin family member 13A	RBKIN, bA500C11.2, FLJ27232	Kinesin-3	Transports mannose-6-phosphate receptor to the plasma membrane
KIF13B	kinesin family member 13B	GAKIN, KIAA0639	Kinesin-3	Involved in regulation of neuronal cell polarity
KIF14	kinesin family member 14	CMKRP, KIAA0042, MGC142302	Kinesin-3	Involved in cytokinesis, chromosome congression and alignment
KIF15	kinesin family member 15	KNSL7 (kinesin-like 7), HKLP2, KLP2, NY-BR-62, FLJ25667	Kinesin-12	Involved in bipolar spindle formation in absence of Eg5
KIF16B	kinesin family member 16B	C20orf23 (chromosome 20 open reading frame 23), FLJ20135, dJ971B4.1, SNX23	Kinesin-3	Critical for early embryonic development by transporting the FGF receptor
KIF17	kinesin family member 17	KIAA1405, KIF3X, KIF17B	Kinesin-2	Neuron-specific molecular motor in neuronal dendrites
KIF18A	kinesin family member 18A	DKFZP434G2226, Kip3p, Klp67A, KipB, klp5/6+	Kinesin-8	Chromosome congression
KIF18B	kinesin family member 18B	-	Kinesin-8	Chromosome congression and alignment and microtubule depolymerisation
KIF19	kinesin family member 19	FLJ37300, KIF19A	Kinesin-8	Unknown
MKLP-2 (KIF20A)	kinesin family member	RAB6KIFL (RAB6-interacting, kinesin-like 6),	Kinesin-6	Cytokinesis

	20A	MKLP-2, RabK6, rabkinesin-6, rabkinesin6, FLJ21151		
MPP1 (KIF20B)	kinesin family member 20B	MPHOSPH1 (M-phase phosphoprotein 1), MPP1, CT90, KRMP1	Kinesin-6	Likely required for completion of cytokinesis
KIF21A	kinesin family member 21A	FEOM1 (fibrosis of the extraocular muscles 1), FLJ20052, KIAA1708, FEOM3A, NY-REN-62	Kinesin-4	Unknown
KIF21B	kinesin family member 21B	DKFZP434J212, KIAA0449, FLJ16314	Kinesin-4	Unknown
Kid (KIF22)	kinesin family member 22	KNSL4 (kinesin-like 4), Kid (kinesin-like DNA-binding protein), OBP-1, OBP-2	Kinesin-10	Generates polar injection forces essential for chromosome congression and alignment
MKLP-1 (KIF23)	kinesin family member 23	KNSL5 (kinesin-like 5), MKLP-1 (mitotic kinesin-Like Protein 1), MKLP1, CHO1	Kinesin-6	Cytokinesis
KIF24	kinesin family member 24	C9orf48 (chromosome 9 open reading frame 48), bA571F15.4, FLJ10933, FLJ43884	Kinesin-13	Regulates centriolar length and ciliogenesis
KIF25	kinesin family member 25	KNSL3 (kinesin-like 3)	Kinesin-14	Unknown
KIF26A	kinesin family member 26A	DKFZP434N178, KIAA1236, FLJ22753	Kinesin-11	Regulates GDNF-Ret signaling in enteric neuronal development
KIF26B	kinesin family member 26B	FLJ10157	Kinesin-11	Regulates adhesion of the embryonic kidney mesenchyme
KIF27	kinesin family	DKFZp434D0917, RP11-575L7.3	Kinesin-4	Hedgehog signaling

	member 27			
HSET (KIFC1)	kinesin family member C1	KNSL2 (kinesin-like 2), HSET, Human Spleen Embryo Testes, XCTK2, Kar3, Ncd	Kinesin-14	Essential for bipolar spindle assembly and proper cytokinesis
KIFC2	kinesin family member C2	-	Kinesin-14	Transports vesicles in a microtubule-dependent manner in a retrograde direction ^{62,63} KIFC3kinesin
KIFC3	kinesin family member C3	FLJ34694, DKFZp686D23201	Kinesin-14	Cooperates with cytoplasmic dynein in Golgi positioning and integration

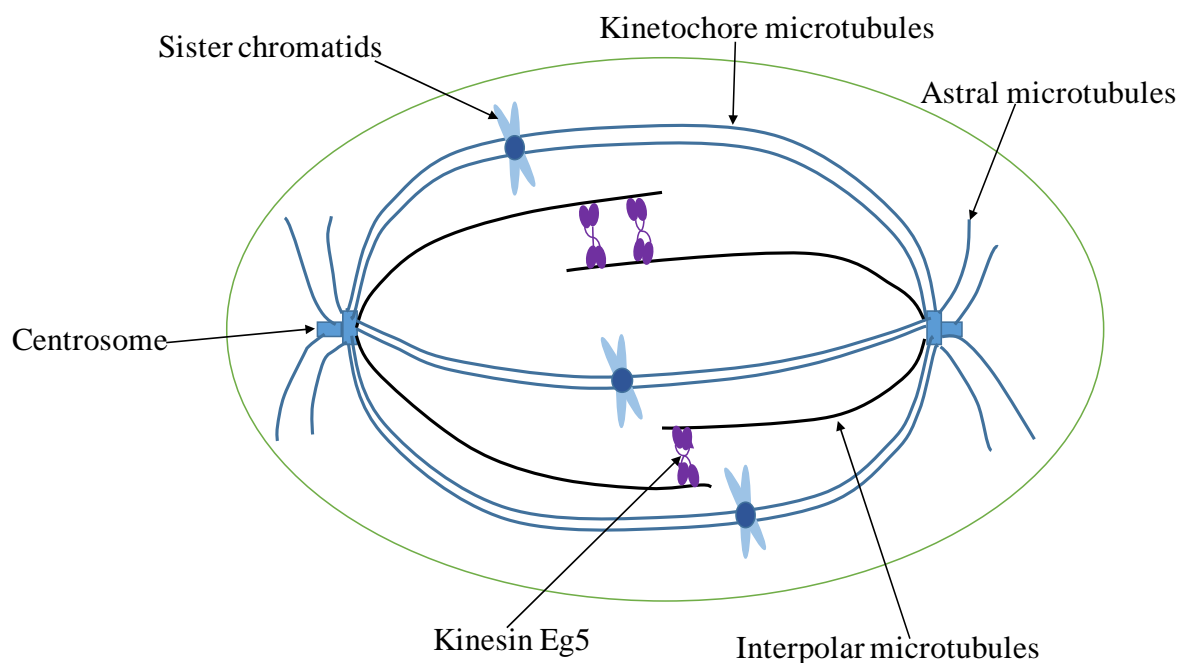


Figure 1-1. A simplified model of the function of kinesin Eg5 during mitosis. Eg5 is highlighted in purple.

1.2 The mitotic kinesin Eg5

Kinesin Eg5 is a plus-end-directed NH₂-terminal motor protein which controls mitosis via bipolar spindle formation and centrosome separation. The protein comprises a conserved homotetrameric structure composing of two identical heavy chains and two identical light chains. The heavy chain contains a N-terminal motor domain (Figure 1-2A) that binds and

hydrolyzes ATP, a C-terminal tail domain, and an α -helical coiled coil stalk domain. The head domain also has binding pockets for inhibitors (Figure 1-2B). Kinesin Eg5 has a unique structure appropriate for bringing about relative motions of the microtubules themselves. The protein functions via a 'sliding filament' mechanism, crosslinking adjacent microtubules into bundles throughout the spindle (Kashina *et al.*, 1996; Sharp *et al.*, 1999; Kapitein *et al.*, 2005), and exerting outward or braking forces on antiparallel microtubules to coordinate bipolar spindle assembly and to drive or constrain poleward flux and anaphase B spindle elongation (Valentine *et al.*, 2006; Kaseda *et al.*, 2009; Scholey, 2009; Subramanian and Kapoor, 2012). Its bipolar homotetrameric structure which places two pairs of motor domains at each end of an extended stalk enabled kinesin Eg5 to crosslink microtubules and induce MT-MT sliding during centrosome separation in the formation of the bipolar spindle (Figure 1-2C).

Kinesin Eg5 has been described as an important member of the "blocked in mitosis" (BimC) subfamily of the kinesins (Blangy *et al.*, 1995; Debonis *et al.*, 2004). The motor domain of Eg5 consists of numerous α helices, β sheets and loops (Table 1-2), and contains binding pockets for nucleotides (ATP and ADP) and inhibitors (Figure 1-2B). ATP-competitive inhibitors, such as the thiazoles (Figure 1-3A), directly bind the ATP binding site (also called the active site). Approximately 12 Å away from the nucleotide-binding site is an allosteric pocket established by the $\alpha 2$ helix, $\alpha 3$ helix and loop5 regions of Eg5 (Figure 1-3B). Several small-molecule inhibitors, from synthetic and natural origin, targeting the protein $\alpha 2/\alpha 3/L5$ pocket have been reported. They block both ATPase and microtubule-gliding activities of Eg5 (Figure 1-2C). However, chemical structures of the inhibitors are not highly conserved but varied widely despite that they identify and bind same pocket. Among the synthetic compounds, monastrol was the first Eg5-specific inhibitor that was discovered (Mayer *et al.*, 1999; Maliga *et al.*, 2002). S-trityl-L-cysteine (STLC) is another potent inhibitor that binds Eg5 more tightly than monastrol (Debonis *et al.*, 2004; Skoufias *et al.*, 2006). Other potent inhibitors, including

ispinesib (Lad *et al.*, 2008; Talapatra *et al.*, 2012), K885 (Nakai *et al.*, 2009) and ARRY-520 (Woessner *et al.*, 2009), have also been reported (Figure 1-3B). The few known Eg5 inhibitors isolated from natural products (medicinal plants, seaweeds, or microorganisms) are shown in Figure 1-3C (Nakazawa *et al.*, 2003; Debonis *et al.*, 2004; Reddie *et al.*, 2006; Oishi *et al.*, 2010). The molecular mechanism of the Eg5 inhibition via allosterism has been well-studied, and involves alterations in the ability of the protein to bind and move on microtubules through prevention of ADP release without affecting the release of the KSP-ADP complex from the microtubule (Lad *et al.*, 2008; Chen *et al.*, 2017).

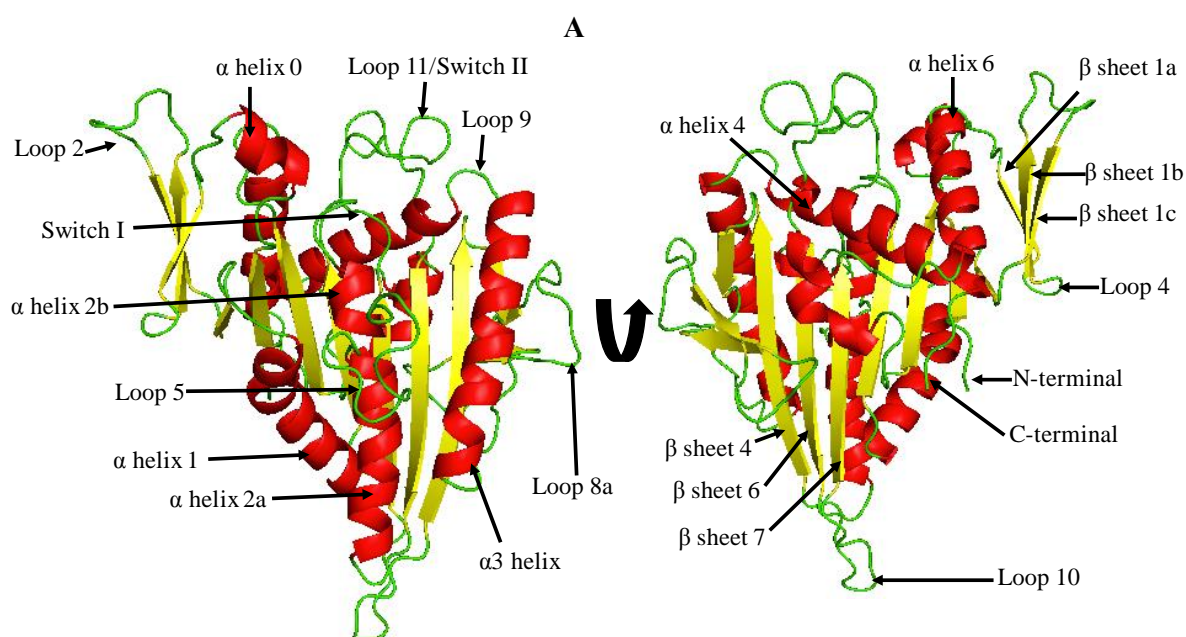
Since kinesin Eg5 is required to build the mitotic spindle, inhibiting its activity would interfere with cell division. Targeting molecules into the binding pockets on Eg5 could therefore potentially form part of anti-cancer therapy, preventing the rapid proliferation of cancer cell divisions. Cancer still remains as one of the most serious human diseases with large number of death till date. Available reports have confirmed that when Eg5 is inhibited in replicating cells, centrosomal separation and mitotic spindle assembly are prevented, resulting in phenotypic monopolar spindles (“monoasters”) formation. Such abnormal phenotypic occurrence resulting from Eg5 inhibition are essential in the eventual activation of mitotic spindle assembly checkpoint which promotes either mitotic arrest during metaphase/anaphase junction or apoptosis (Stem and Murray, 2001; Weil *et al.*, 2002; Marcus *et al.*, 2005). The monoastral spindles are formed because normal centrosome migration to the polar region/opposite sides of the cell are blocked (Mayer and Kapoor, 1999; Kapoor *et al.*, 2000; Stem *et al.*, 2001). Therefore, kinesin Eg5 has become a target for cancer treatment (Guido *et al.*, 2015).

An advantage in targeting kinesin Eg5 in cancer treatment is its almost absence in non-proliferating tissues in contrast to many proliferating tissues. Hence, the effects of Eg5 inhibitors through cell cycle arrest during mitosis are expected to be profound on tumor cells than in non-proliferating cells. Eg5 is also not found in central nervous system of adult because

they do not participate in post-mitotic processes. This indicate that compounds which inhibit Eg5 may not have grave adverse effects associated with taxanes and vinca alkaloids which target microtubules with nonspecific effects on both normal and proliferating cells.

Table 1-2. Name and amino acid residues of various segments of Eg5 motor domains

Alpha helices	Beta sheets	Loops
$\alpha 0$ (Asn29 – Ala35)	$\beta 0$	L1 (Ser36 – Ile40)
$\alpha 1$ (Lys77 – Met95)	$\beta 1$ (Gln20 – Cys25)	L2 (Thr54 – Ser62)
$\alpha 2a$ (Asp134 – Gly149)	$\beta 1a$ (Val41 – Asp44)	L3 (Gly73 – Lys76)
$\alpha 2b$ (Glu110 – Gly116)	$\beta 1b$ (Glu49 – Arg53)	L4 (Pro45 – Arg47)
$\alpha 3$ (Asn206 – Thr226)	$\beta 1c$ (Arg63 – Thr67)	L5 (Gly117 – Gly133)
$\alpha 3a$ /Switch I (Ala230 – Ser235)	$\beta 2$ (Met70 – Phe72)	L6 (Asn150 – Glu153)
$\alpha 4$ (Asn289 – Glu304)	$\beta 3$ (Asn98 – Gly105)	L7 (Asn165 – Glu166)
$\alpha 5$ (Pro310 – Lys324)	$\beta 4$ (Phe154 – Tyr164)	L8a (Leu171 – Glu182)
$\alpha 6$ (Ala339 – Lys357)	$\beta 5$ (Glu167 – Asp170)	L8b (Asp187 – Gly193)
	$\beta 5a$ (Arg183 – Asp186)	L9 (Leu227 – Asn229)
	$\beta 5b$ (Val194 – Lys197)	L10 (Thr249 – Glu253)
	βs (Ile202 – Val204)	L11/Switch II (Leu265 – Asn288)
	$\beta 6$ (His236 – Thr248)	L12/ “K-loop” (Arg305 – Val309)
	$\beta 7$ (Glu254 – Asp265)	L13 (Gly325 – Thr328)
	$\beta 8$ (Arg329 – Ile336)	L14 (Ser337 – Pro338)
		P-loop (Gln106 – Gly109)



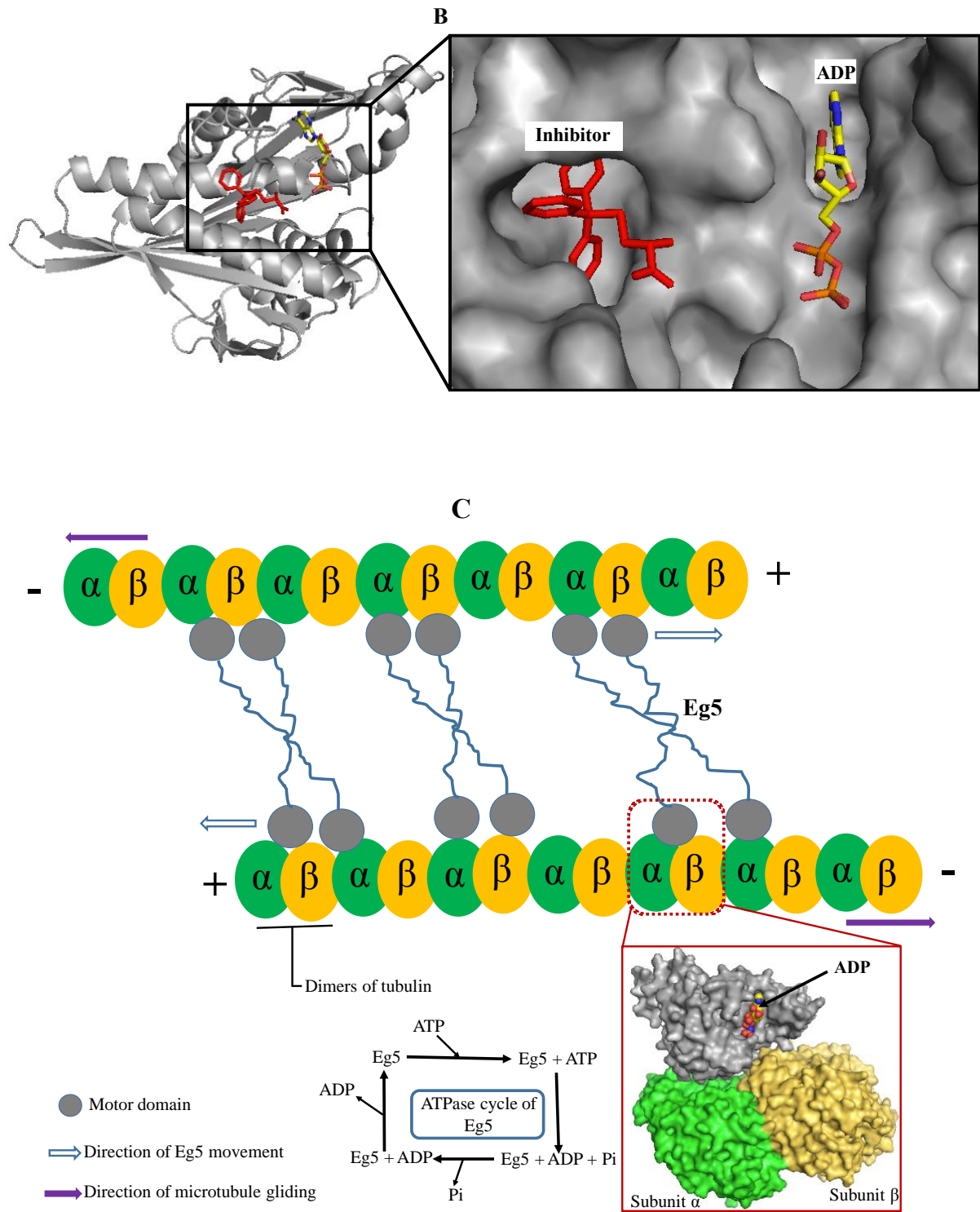
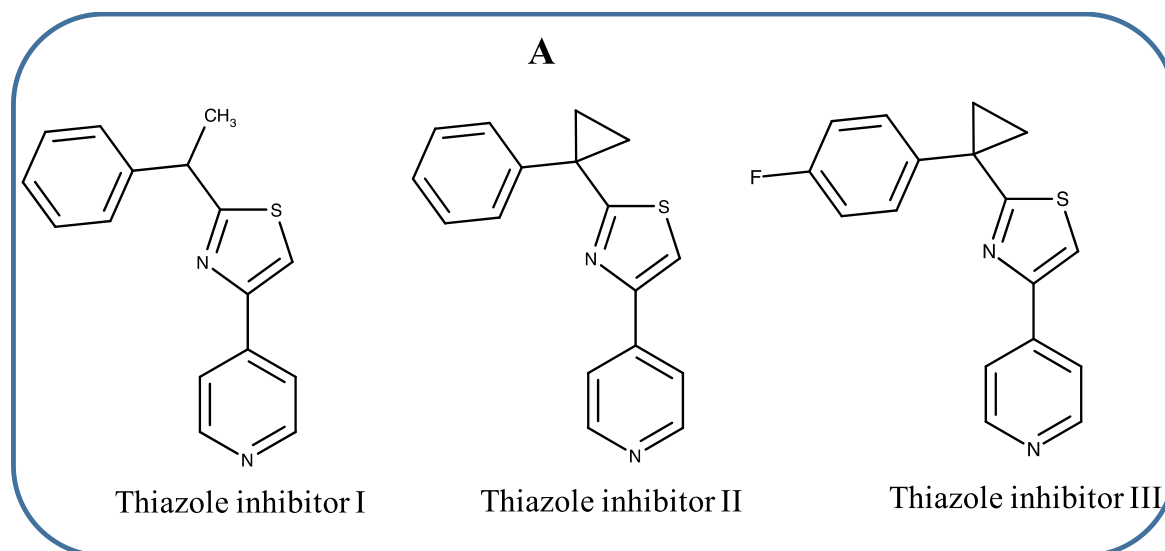


Figure 1-2. Structure of motor domain of mitotic kinesin Eg5. (A) Eg5 segments comprising the alpha helices (red), beta sheets (yellow) and loops (green). (B) Binding pockets on Eg5. (C) Depiction of Eg5 gliding on microtubules; inset: Eg5 in complex with microtubules (PDB ID: 2WBE).

1.3. Research objectives

The specific objectives of this research include:

- To thoroughly study available crystal structures of kinesin Eg5 and gain insights into the structural and conformational modifications associated with inhibitors interactions with Eg5.
- To search for novel scaffolds with capacity to interact with Eg5 and interfere with its biological function, particularly at the allosteric binding site.
- To identify new kinesin Eg5 inhibitors from natural products and determining their potency.
- To investigate the effects of the novel inhibitors on the ATPase activity of Eg5.
- To ascertain the effects of the novel inhibitors on the motility function of Eg5.
- To unravel the mechanism of interaction between the novel inhibitors and Eg5 at the atomistic level.



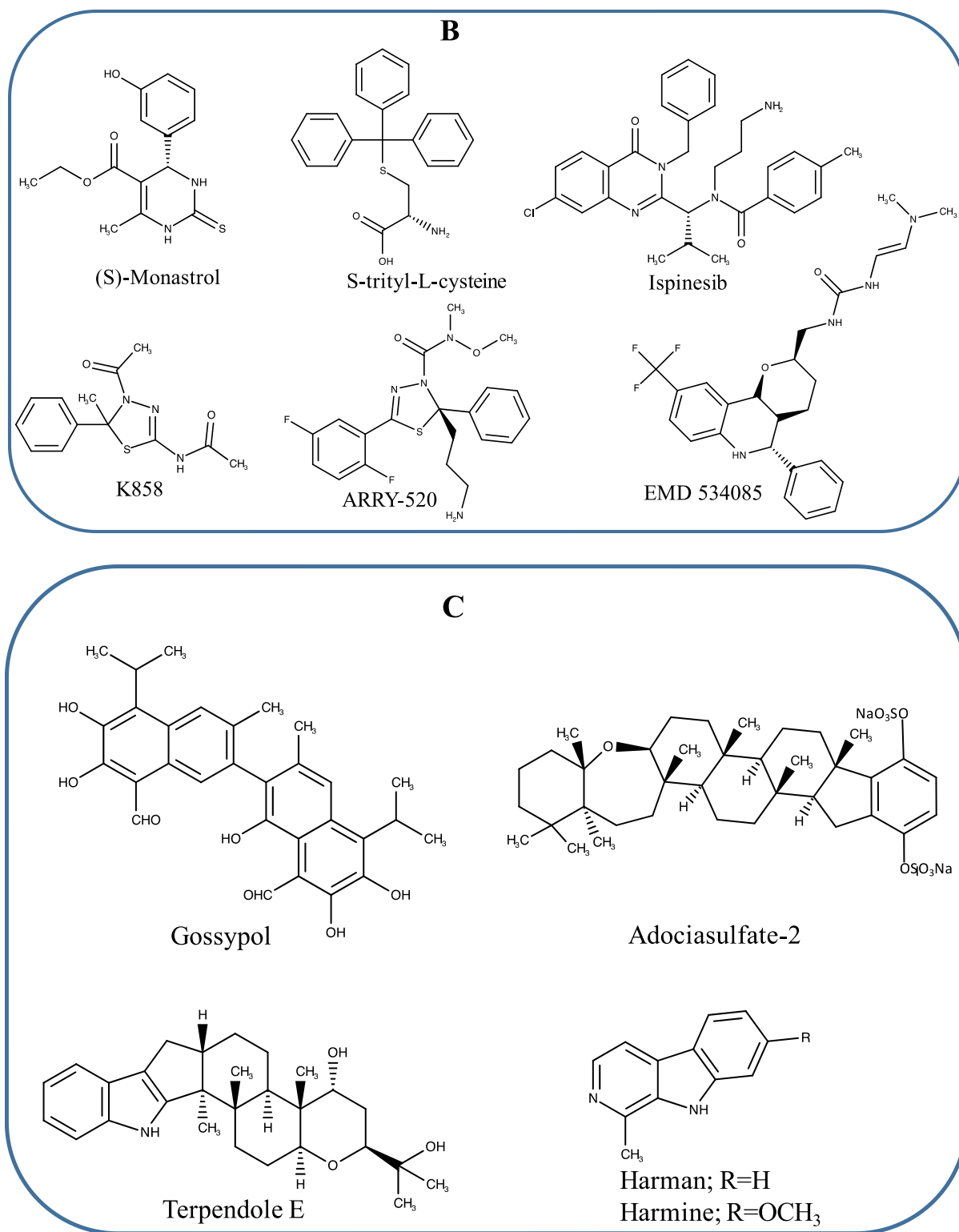


Figure 1-3. Selected known inhibitors of kinesin Eg5. (A) ATP-competitive inhibitors (B) synthetic allosteric inhibitors and (C) inhibitors from natural products.

1.4 Research approach and methodology

The general protocol employed in the current studies includes the computational and *in vitro* (protein kinetics/biochemical) analyses. The *modus operandi* is highlighted in the chart (Figure 1-5) below:

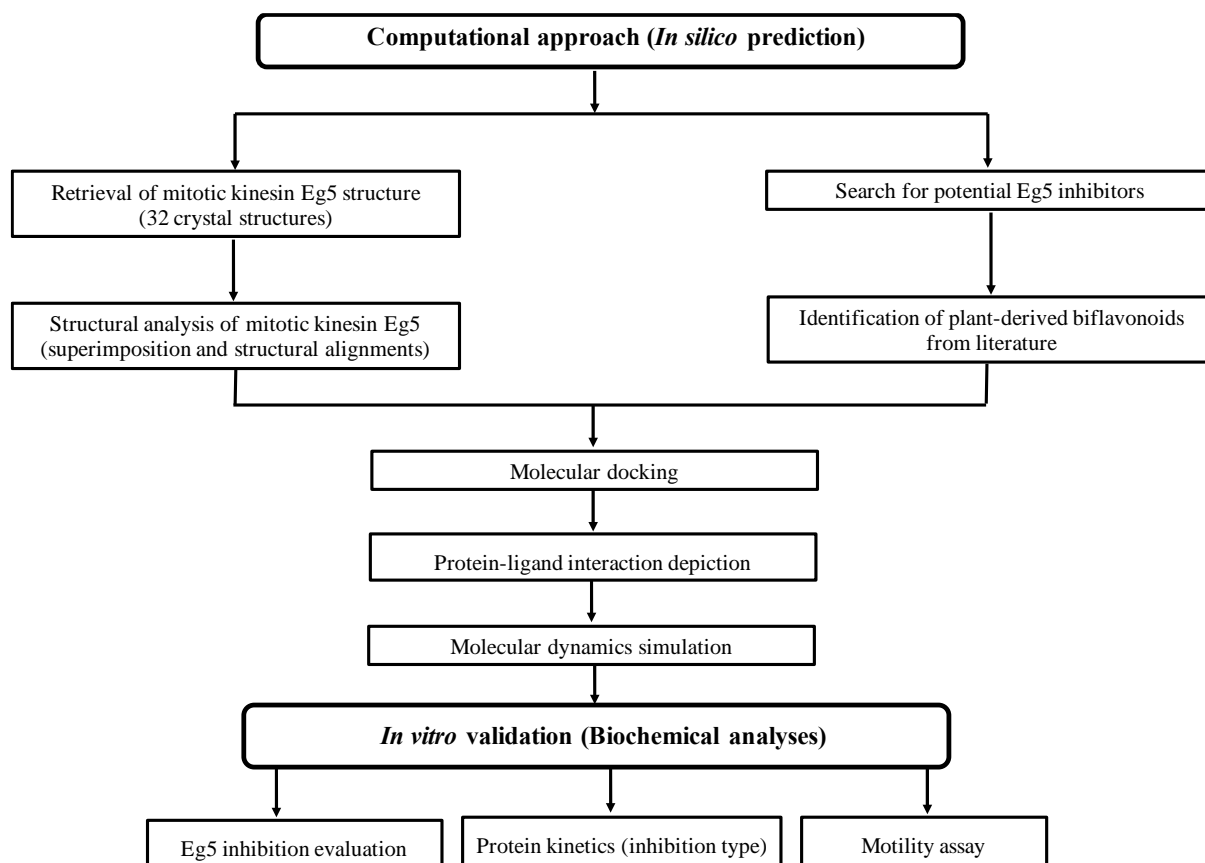


Figure 1-4. The general *modus operandi* adopted for the research work reported in this thesis.

CHAPTER TWO

Morelloflavone as a novel inhibitor of mitotic kinesin Eg5

2.1 Introduction

The mitotic kinesin Eg5 is critical to the formation and maintenance of bipolar mitotic spindle, an essential structure during cell division. Accordingly, inhibition of Eg5 may result in mitotic arrest and apoptosis (Compton, 2000; Skoufias *et al.*, 2006; El-Nassan, 2013). Hence, Eg5 inhibitors have been investigated as potential drugs against cancer cells (Rath and Kozielski, 2012; Myers and Collins, 2016). Nevertheless, only a few Eg5 inhibitors from natural resources have been investigated, even though potent anticancer effects have been detected in numerous medicinal plants (Solowey *et al.*, 2014; Greenwell and Rahmna, 2015; Choudhury *et al.*, 2016). Of note, natural products are attractive as therapeutics because of reduced side effects, potency, and patient preference over synthetic counterpart (Katiyar *et al.*, 2012; Veeresham, 2012; Cragg and Newman, 2013). Compounds that inhibit Eg5 have been isolated from marine algae and microorganisms, including terpendole E (Nakazawa *et al.*, 2003), adociasulfate-2 (Reddie *et al.*, 2006), gossypol (Debonis *et al.*, 2004), harmine and Harman (Oishi *et al.*, 2010). On the other hand, biflavonoids composed of two covalently linked flavones are a major class of compounds from medicinal plants with known anti-cancer properties but minimal adverse effects (Kang *et al.*, 2009; Jeon *et al.*, 2015; Xiong *et al.*, 2016; Yao *et al.*, 2017). Morelloflavone is one such biflavonoid, and consists of luteolin and apigenin (Pinkaw *et al.*, 2009). The compound was first isolated from *Garcinia morella* by Karanjaokar *et al.* in 1967 (Karanjaokar *et al.*, 1967). Morelloflavone is unique to *Garcinia* species such as *G. dulcis*, *G. subelliptica*, *G. brasiliensis*, *G. livingstonei*, *G. multiflora*, and *G. Morella*, and is accumulated in leaves, nuts, and heartwood (Lin *et al.*, 1997; Pinkaw *et al.*, 2009; Yang *et al.*, 2010; Ito *et al.*, 2013). Morelloflavone is the most well-known flavonoid in *G. dulcis* leaves (Pinkaw *et al.*, 2009). *In vitro*, morelloflavone inhibits enzymes like 3-hydroxy-3-methylglutaryl-coenzyme A (HMG-CoA) reductase (Tuansulong *et al.*, 2011), secretory phospholipase A₂, specifically groups II and III forms (Gil *et al.*, 1997), snake venom phospholipase A₂ (Pereñez

et al., 2014), tyrosinase (Masuda *et al.*, 2005), fatty acid synthase (Li *et al.*, 2002), papain, cruzain, and trypsin (Gontijo *et al.*, 2015). Morelloflavone also exhibits anti-oxidant (Hutadilok-Towatana *et al.*, 2007), anti-atherogenic (Decha-Dier *et al.*, 2008), anti-microbial (Verdi *et al.*, 2004), anti-angiogenic (Pang *et al.*, 2009), anti-inflammatory, and anti-hypercholesterolemic activities (Gil *et al.*, 1997; Tuansulong *et al.*, 2011; Pereañez *et al.*, 2014).

In this study, morelloflavone was identified *in silico* as a potential Eg5 inhibitor among a library of forty natural biflavonoids. Inhibitory activity was confirmed *in vitro*, and possible mechanisms of its interaction with the Eg5 were investigated.

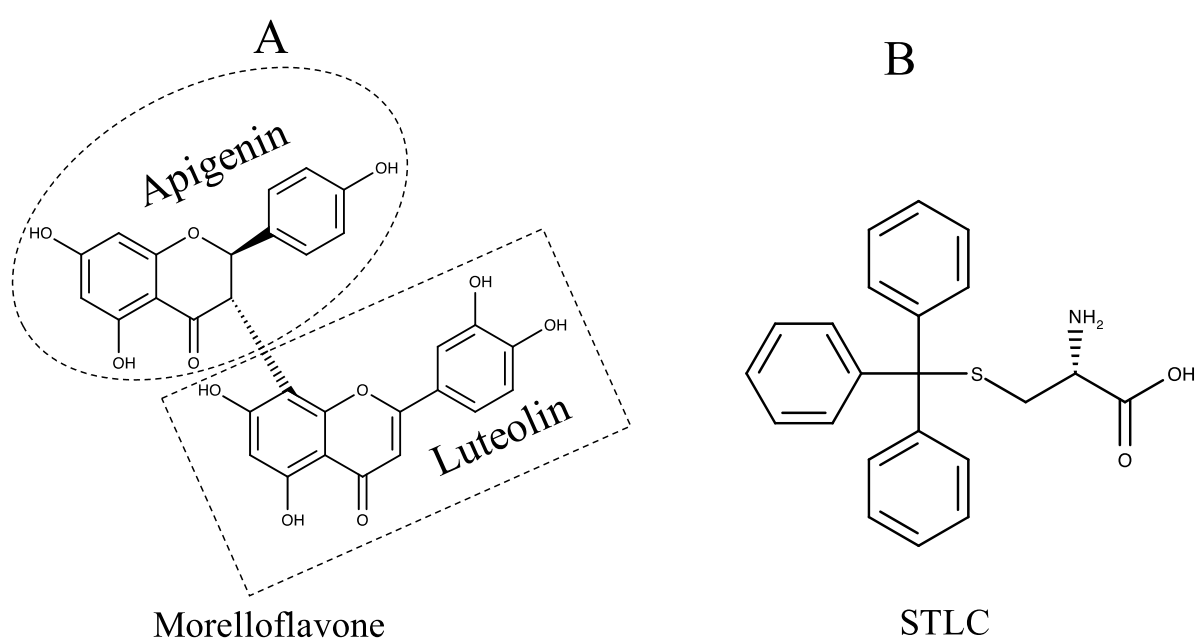


Figure 2-1. 2D structure of Eg5 inhibitors. (A) (+)-Morelloflavone, a flavonoid dimer comprising of apigenin (in dotted circle) and luteolin (in dotted rectangle) (Li *et al.*, 2002; Tuansulong *et al.*, 2011). (B) STLC (Skoufias *et al.*, 2006).

2.2 Materials and methods

2.2.1 *In silico* screening

2.2.1.1 Ligand selection, preparation and optimization.

Forty biflavonoids from various medicinal plants were selected for *in silico* analysis. The chemical structure of morelloflavone used was obtained from the report of Li *et al.*, (2001).

The chemical structures of all other biflavonoids were also retrieved from the literature (Iwu *et al.*, 1990; Lin *et al.*, 1997; Zembower *et al.*, 1998; Romani *et al.*, 2002; Kin *et al.*, 2008; Yang *et al.*, 2010; Tuansulong *et al.*, 2011; Ito *et al.*, 2013; Gontijo *et al.*, 2017; Yu *et al.*, 2017). S-trityl-L-cysteine (STLC), a known Eg5 inhibitor for which a co-crystal structure is available (PDB ID: 3KEN), was used as a reference. 2D structures of the biflavonoids were drawn in ChemAxon (<https://www.chemaxon.com>), and converted to 3D based on the Merck molecular force field (MMFF94) in the conformers suite of Marvin-Sketch. The 3D structure of STLC was retrieved from the NCBI PubChem compound database (<http://www.ncbi.nlm.nih.gov/pccompound>).

2.2.1.2 Protein selection and preparation.

The starting coordinates for Eg5 were retrieved from RSCB Protein Data Bank (<http://www.rcsb.org/pdb>) as 3KEN, which corresponds to Eg5 with ADP and STLC bound to the nucleotide-binding and allosteric sites, respectively. Ligands and crystallographic water molecules were removed prior to molecular docking studies.

2.2.1.3 Molecular docking and scoring.

Ligand docking and binding site analysis were performed in the Autodock Vina suite in PyMol (Seeliger and de Groot, 2010; Trott and Olson, 2010). In brief, blind docking was first performed with grid parameters $x = 200$, $y = 200$ and $z = 200$ to filter out ligands that are not recognized by the allosteric site in Eg5. These parameters also ensure that all available binding pockets in Eg5 are accessible, with sufficient room for full ligand rotation and translation. Next, the allosteric binding site, as delineated in PDB data, was specifically targeted with default grid parameters ($x = 60$, $y = 60$ and $z = 60$), but with coordinates of origin $x = 18.31 \text{ \AA}$, $y = 8.38 \text{ \AA}$, and $z = 15.17 \text{ \AA}$ to include all the amino acids in the active site. Spacing between grid points was maintained at 0.375 \AA . All ligands were docked to the loop5/ α 2/ α 3 allosteric binding pocket (L5: Gly117 - Gly134, α 2: Lys111-Glu116 and Ile135-Asp149, α 3: Asn206-Thr226)

(Jiang *et al.*, 2007; Moores, 2010). While the rotatable bonds in the ligands were not restrained, the protein molecule was treated as a rigid structure. Multiple docking runs were performed for each ligand with the number of modes set to 10 to achieve more accurate and reliable results. Estimated binding energies were estimated for the best fits.

2.2.2 *In vitro* experimental validation

2.2.2.1 Chemicals.

Morelloflavone was purchased from Ambinter (France). All other chemicals were analytical grade.

2.2.2.2 Eg5.

Recombinant Eg5 was prepared as described previously (Ishikawa *et al.*, 2014).

2.2.2.2.1 Expression and purification of the mitotic kinesin Eg5 monomer

Briefly, cDNA of the motor domain of mouse wild-type Eg5 (WT, residues 1-367) was amplified by polymerase chain reaction and ligated into the pET21a vector. The Eg5 WT expression plasmids were used to transform *Escherichia coli* BL21 (DE3). Eg5 WT was purified by using a Co-NTA column which was washed with lysis buffer containing 30mM imidazole, and bound Eg5 was eluted with lysis buffer containing 150mM imidazole. The obtained fractions were analysed by sodium dodecyl sulphate-polyacrylamide gel electrophoresis (SDS-PAGE). Dialysis of purified Eg5 was done using a buffer containing 30mM Tris-HCl [pH 7.5], 120mM NaCl, 2mM MgCl₂, 0.1mM ATP and 0.5mM DTT, and stored at -80°C till needed for experiments.

2.2.2.2.2 Purification and polymerization of tubulin

Tubulin was purified from porcine brain using the method described by Hackey (1988). Polymerization of the tubulin was carried out for 30 min at 37°C in a buffer containing 100mM

Piperazine-1,4-bis(2-ethanesulfonic acid) [PIPES] (pH 6.8), 1mM *O,O'*-Bis(2-aminoethyl)ethyleneglycol- *N,N,N',N'*-tetraacetic acid [EGTA], 1mM MgCl₂ and 1mM GTP. Taxol was later added to a final concentration of 10 mM. The polymerized microtubules were collected by centrifugation at 280 000xg for 15 minutes at 37°C. The supernatant was discarded whereas the microtubule pellet was collected in a buffer containing 100mM PIPES [pH 6.8], 1mM EGTA, 1mM MgCl₂, 1mM GTP and 10mM taxol. For the microtubule gliding assay, microtubules were labelled with rhodamine. Rhodamine-labelled tubulin was mixed with unlabeled tubulin at a ratio of 1:5 and polymerized for 40 minutes at 37°C in buffer (100mM PIPES, 2mM EGTA, 1mM MgSO₄). Taxol was then added to a final concentration of 20 mM.

2.2.2.3 ATPase assay.

ATPase activity was measured at 25°C in ATPase assay solution (20 mM HEPES-KOH, [pH7.2] containing 50 mM KCl, 2 mM MgCl₂, 0.1 mM EGTA, 0.1 mM EDTA and 1.0 mM β-mercaptoethanol). Using 0.5 μM Eg5 (for basal ATPase activity) or 0.1 μM Eg5 (for microtubule-activated ATPase activity). To measure inhibitory activity, Eg5 was pre-incubated for 5 minutes in the presence of absence of 3.0 μM microtubule, and supplemented with 0-150 μM morelloflavone dissolved in DMSO. ATPase activity was initiated by adding 2.0 mM ATP, terminated after 5 minutes by adding 10% trichloroacetic acid, and estimated based on inorganic phosphate (Pi) released into the supernatant, as quantified by the Youngburg method (Youngburg and Youngburg, 1930) and described by Ishikawa *et al.* (2014). To assess the effects of morelloflavone on microtubule-dependent activity, ATPase turnover was also measured in the presence of 80 μM morelloflavone and 0-15 μM microtubule. To assess competitive inhibition, ATPase activity was evaluated in the presence of 0-400 μM ATP, 0, 50, and 100 μM morelloflavone, 0.5 μM microtubule, and 0.1 μM Eg5.

2.2.2.4 *In vitro* microtubule gliding assay.

Eg5 motor activity was evaluated by microtubule gliding assay (Ishikawa *et al.*, 2014; Sadakane *et al.*, 2018). Briefly, coverslips were coated with anti-6x histidine monoclonal antibody (Wako) in assay solution (10 mM Tris-acetate [pH 7.5], 2.5 mM EGTA, 50 mM K-acetate, 4mM MgSO₄). Subsequently, 0.1 μ M Eg5 in assay solution A (10 mM Tris-acetate [pH 7.5], 4mM MgSO₄, 50 mM potassium acetate, 2.5 mM EGTA, 0.5 mg/mL casein, and 0.2% β -mercaptoethanol) was flushed through the flow chambers, and left there for 5 minutes. The chamber was then washed with rhodamine-labeled microtubule in assay solution B (20 mM taxol added to assay solution A), followed by 2 minutes incubation. Subsequently, assay solution B was flushed through the chambers, followed by 100-250 μ M morelloflavone and 1.0 mM ATP in assay solution C (assay solution B, 0.01mg/mL catalase, 1.5 mg/mL glucose, and 0.05 mg/mL glucose oxidase) (Youngburg and Youngburg, 1930; Sadakane *et al.*, 2018). Finally, rhodamine-labeled microtubules were visualized using an Olympus BX50 microscope equipped with a 3CCD camera (JK-TU53H, Toshiba, Japan).

2.2.3 Data analysis.

Protein-ligand complexes and molecular interactions were visualized in PyMol. ATPase activity was plotted against morelloflavone concentration to obtain the IC₅₀ values. Biochemical experiment data are reported as mean \pm standard deviation (SD). Significant differences between groups were tested by Welch's t-test or Student's t-test.

2.3 Results and discussion

2.3.1 *In silico* screening reveals morelloflavone as a potential Eg5 inhibitor

To identify compounds from natural products that may interact with Eg5, forty biflavonoids (Table IS) were compiled and screened by using molecular docking. First, blind docking was performed to allow each biflavonoid to seek out its most preferred binding site on Eg5. Of all

compounds, morelloflavone (Figure 1A), which is comprised of apigenin and luteolin conjugated via 3',8" linkage (Konoshima *et al.*, 1969; Li *et al.*, 2002; Tuansulong *et al.*, 2011), bound the L5/ α 2/ α 3 allosteric pocket with appreciable affinity, with binding modes comparable to those of the reference ligand STLC (Figure 1B) (Moores, 2010). The binding energy was -8.4 kcal/mol. Particularly, an enantiomer (+)-morelloflavone, with known absolute configuration, conformation, and chiral properties was used as its structure in this study (Li *et al.*, 2002). Other biflavonoids with different linkage patterns did not bind or fit well into the Eg5 allosteric pocket, possibly because of steric hindrance (Figure 1S). This supports an earlier claim that the type of linkage in biflavonoids is a significant determinant of bioactivities (Lee *et al.*, 2008).

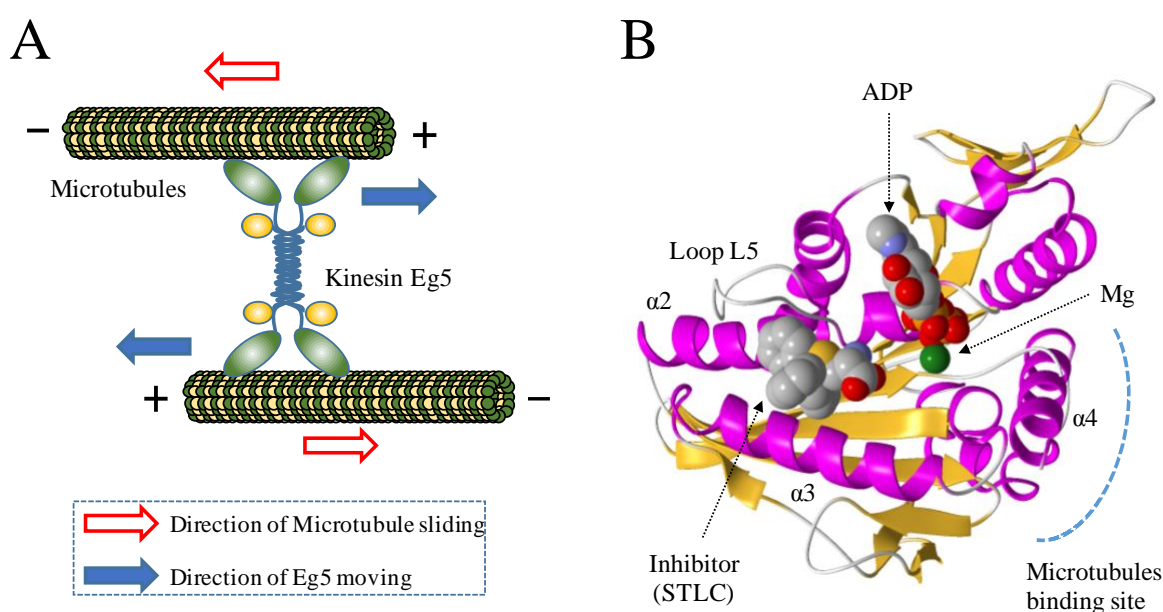


Figure 2-2. Structure and function of kinesin Eg5. (A) The protein moves towards the plus end of microtubules, pushing the anti-parallel microtubules apart and separating the duplicated centrosomes while establishing a bipolar spindle (Skoufias *et al.*, 2006; El-Nissan, 2013). (B) Crystal structure of the ATP-binding domain of Eg5 (PBD ID: 3KEN) with ATP bound. An extended loop (L5) is unique to Eg5 and contributes to the specificity and selectivity for inhibitors that bind to the allosteric binding pocket.

On site-specific molecular docking, morelloflavone was again found to potentially interact with Eg5 at the L5/ α 2/ α 3 allosteric pocket and might inhibit ATPase and microtubule gliding activities (Figure 2), as assessed by binding modes, binding energies, molecular interactions, and important functional groups that interact with Eg5. Figure 3A shows morelloflavone (yellow stick) in complex with Eg5 at the same pocket as STLC (cyan stick) with comparable binding pose. STLC contains three phenyl rings that fit well into the allosteric binding pocket, and induces conformational change in Eg5 structure to impede ADP release from the nucleotide binding pocket as well as Eg5-driven gliding of antiparallel spindle microtubules (Skoufias *et al.*, 2006).

Table 2-1. Estimated binding energy, molecular interaction, and IC₅₀ values for morelloflavone and a few known Eg5 inhibitors.

Ligand	<i>In silico</i> binding energy (kcal/mol)	Hydrogen bonds	Residues involved in hydrogen bonding	Bond length (Å)	Residues involved in hydrophobic interactions	IC ₅₀ for basal ATPase activity (μM)	IC ₅₀ for microtubule-activated ATPase activity (μM)
Morelloflavone	-8.4	1	Tyr211	1.8	Arg119, Ala218, Leu214	100	96
Monastrol	-8.7	2	Glu116, Glu118	2.8, 2.7	Arg119, Pro137	6.1 *	34*
S-Trytil-L-cysteine	-10.0	3	Glu116, Gly117, Arg221	3.2, 2.7, 3.6	Glu116, Arg119, Tyr214, Pro137	1 **	0.14 **
Ispinesib	-11.1	1	Glu116	2.9	Trp127, Tyr211, Pro137, Leu214, Ala218	0.032 ***	0.003 ***

In silico estimations were obtained by Autodock Vina in PyMol. IC₅₀ values for basal ATPase and microtubule-activated ATPase activity for morelloflavone were determined *in vitro* in this study (Figure 4), and those for reference ligands (STLC, ispinesib, and monastrol) were obtained from the literatures (* Maliga *et al.*, 2002; ** Debonis *et al.*, 2004; ***Talapatra *et al.*, 2012).

Visualization of Eg5-morelloflavone interaction in PyMol revealed similar binding conformational geometry as STLC at the putative Eg5 allosteric pocket, suggesting that both compounds may have similar inhibitory mechanism. In particular, the aromatic rings of the luteolin and one aromatic ring of apigenin group in morelloflavone fit into similar binding regions as the phenyl residues of STLC (Figure 3B). Indeed, morelloflavone is embedded in a cavity formed by Ile-136, Glu-116, Glu-118, Trp-127, Gly-117, Ala-133, Glu-215, Leu-214, and Tyr-211, and forms a hydrogen bond with Tyr-211 (Fig. 3c). Tyr-211 was previously confirmed to be in the allosteric pocket of Eg5 (Jiang *et al.*, 2007; Kaan *et al.*, 2009; Wang *et al.*, 2012). Moreover, the luteolin group in morelloflavone is observed deeply buried within the hydrophobic core while the apigenin subunit occupies the solvent-exposed patches in the allosteric site (Figure 3A). Some hydroxyl moieties and the two carbonyl groups in morelloflavone (Figure 1) may play key roles in affinity, binding pose, and interaction with Eg5, and thus its inhibitory potential (Lee *et al.*, 2008; Razzaghi-Asl *et al.*, 2015). Collectively, these observations suggest that the interaction of morelloflavone with Eg5 is similar to that of STLC, and that morelloflavone may induce a conformational change in Eg5 to inhibit its ATPase activity (Yan *et al.*, 2004; Skoufias *et al.*, 2006; Kaan *et al.*, 2009). However, the binding energy for morelloflavone is higher (-8.4 kcal/mol *in silico*) than that of reference ligands, suggesting lower affinity (Table I). Docking of monastrol and ispinesib, both known Eg5 inhibitors, also confirmed that morelloflavone may have lower affinity for Eg5 than

synthetic inhibitors. Notably, the binding energies for Eg5 inhibitors correlate well with IC₅₀ values (Table I). To validate these predictions, morelloflavone was evaluated *in vitro* against Eg5.

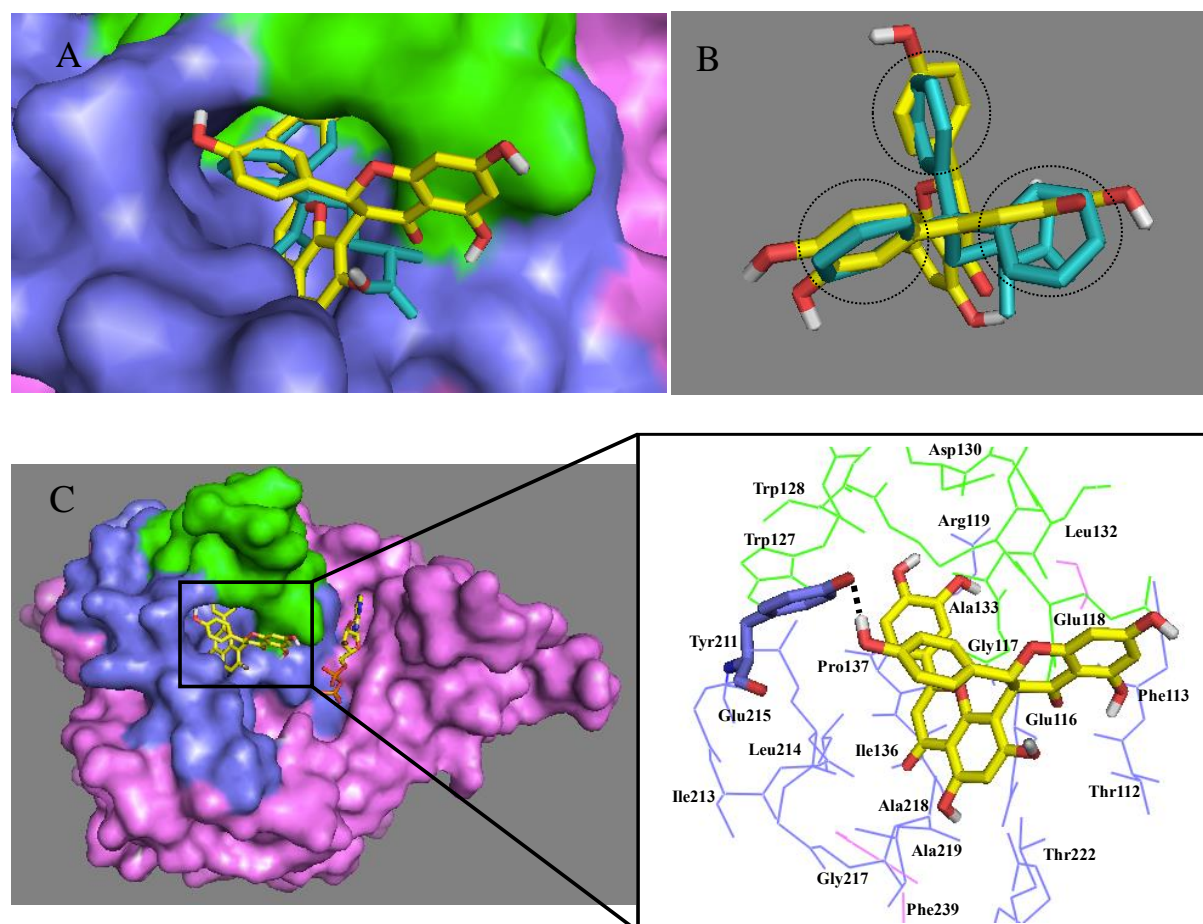


Figure 2-3. Binding of morelloflavone to Eg5. (A) Binding configuration of morelloflavone to the allosteric L5/ α 2/ α 3 binding site (L5: Gly117-Gly134, α 2: Lys111-Glu116 and Ile135-Asp149, α 3: Asn206-Thr226) in Eg5 (44). Loop 5 and α 2/ α 3 helices are highlighted in green and blue respectively. Other parts of the protein are uniformly illustrated in violet. The biflavonoid, (yellow stick) binds to same pocket as STLC (cyan), with the luteolin group buried in the allosteric pocket while the apigenin group lies in the solvent-exposed region. (B) Comparison of the binding poses of the aromatic rings in morelloflavone (yellow) and STLC (cyan), highlighted in dashed black circles. (C) Hydrogen bond (black dotted line) predicted

by PyMol between morelloflavone and the putative L5/ α 2/ α 3 allosteric pocket in Eg5, especially Tyr-211 (stick). ADP at the nucleotide-binding site is also shown. Morelloflavone and ADP are colored by atom type, with carbon in yellow, oxygen in red, hydrogen in white and nitrogen in blue. STLC is colored only in cyan to distinguish it from morelloflavone.

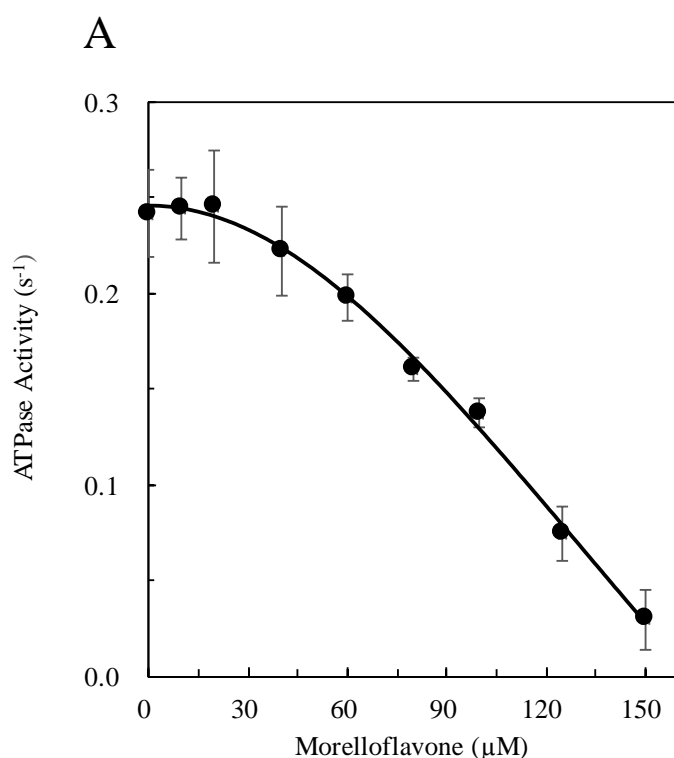
2.3.2 Morelloflavone inhibits both basal and microtubule-activated ATPase activities of Eg5

As common to all kinesins that move unidirectionally along microtubules, Eg5 utilizes ATP hydrolysis as energy source. Known allosteric Eg5 inhibitors were reported to trap the protein in the ADP-bound configuration, reducing its affinity to ATP and ultimately resulting in monoastral spindles in mitotic cells (Mayer *et al.*, 1999; Kapoor *et al.*, 2000; Maliga *et al.*, 2002; Lad *et al.*, 2008). To validate *in silico* predictions, ATPase activity of Eg5 was measured in the absence (basal ATPase) or presence of microtubules (microtubule-activated ATPase) at various concentrations of morelloflavone. The inhibitory effect of morelloflavone was dose-dependent, with IC₅₀ 100 μ M (Figure 4A) and 96 μ M (Figure 4B) against basal and microtubule-activated ATPase activity of Eg5, respectively. Although the turnover rate of the basal ATPase reaction was reported to be at least 12-fold slower than the microtubules-activated ATPase activity (Cochran *et al.*, 2005), evaluation of the Eg5 basal ATPase activity helps to understand properties of the inhibitor. The small difference in the IC₅₀ values for basal and microtubule-activated ATPase activities (Table I) suggests that the binding affinity of morelloflavone to Eg5 may not be significantly affected by the presence of microtubules. Binding energies estimated *in silico* were also positively correlated with experimentally-determined IC₅₀ values (Table I).

As shown in Figure 4C, the microtubule-activated ATPase was inhibited by 80 μ M morelloflavone in a manner dependent on microtubule concentration (0-15 μ M). This result

indicates that morelloflavone may modulate Eg5 affinity for microtubules. The K_{MT} value for microtubule association with Eg5 under the condition of the assay was $0.343 \pm 0.066 \mu\text{M}$ with V_{max} of $16.29 \pm 1.44 \text{ s}^{-1}$ in the absence of morelloflavone, but $3.803 \pm 0.585 \mu\text{M}$ with V_{max} , $13.27 \pm 0.83 \text{ s}^{-1}$ in the presence of $80 \mu\text{M}$ morelloflavone. Thus, morelloflavone significantly affects microtubule binding to Eg5.

The IC_{50} values obtained for morelloflavone in this work are higher than those of known natural Eg5 inhibitors such as adociasulfate-2, which blocks basal and microtubule-activated ATPase activity with IC_{50} $3.5 \mu\text{M}$ and $5.3 \mu\text{M}$ respectively (Brier *et al.*, 2006). Similarly, the microtubule-activated ATPase activity of Eg5 is inhibited by terpendole E with IC_{50} value of $23 \mu\text{M}$ (Nakazawa *et al.*, 2003), and by gossypol, harmine and harman with IC_{50} values of $10.8 \mu\text{M}$, $38 \mu\text{M}$ and $32 \mu\text{M}$, respectively (Debonis *et al.*, 2004; Oishi *et al.*, 2010). Hence, the inhibitory potential of morelloflavone against Eg5 appears to be relatively moderate.



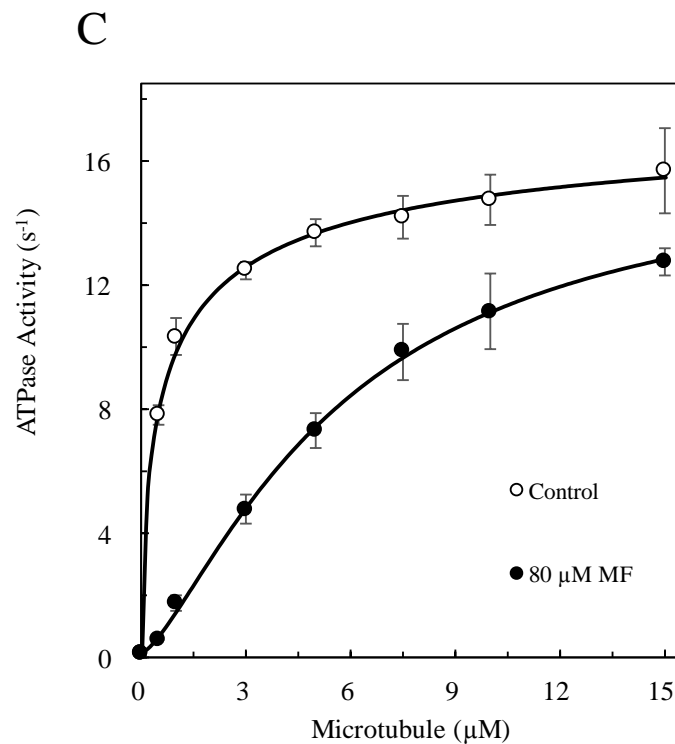
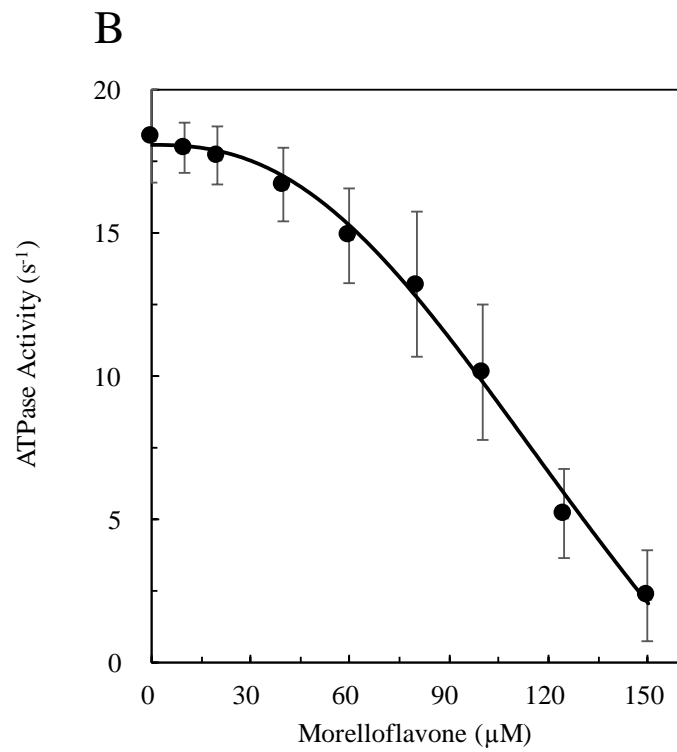


Figure 2-4. *In vitro* ATPase activity of Eg5 in presence of inhibitor. (A) Basal Eg5 ATPase activity measured in 20 mM HEPES-KOH [pH7.2], containing 50 mM KCl, 2 mM

MgCl₂, 0.1 mM EGTA, 0.1 mM EDTA, 1.0 mM β-mercaptoethanol and 0.5 μM Eg5. The reaction was initiated by adding 2.0 mM ATP, and ATPase activity was measured for 20 minutes at 25°C in the presence of 0-150 μM morelloflavone. Data were collected from three independent experiments. (B) Microtubule-activated Eg5 ATPase activity was measured for 5 minutes at 25°C in the presence of 3.0 μM microtubules, 0.1 μM Eg5 and 0-150 μM morelloflavone. (C) ATPase assay with 0-15 μM microtubule and 80 μM morelloflavone.

2.3.3 Mechanism of interaction between morelloflavone and Eg5

Blind docking experiments predicted that morelloflavone recognizes and binds to the L5/α2/α3 region near the nucleotide binding site (Figure 3). Further validation of this result was performed by the PSB-SLIM method (Lee and Zhang, 2012; Omotuyi and Ueda, 2015) against Eg5 free of all ligands and crystallographic waters. Based on the output structures, morelloflavone binds to the L5/α2/α3 allosteric site with a chance of 60% (3 in 5 outputs), and to the nucleotide-binding site with a probability of 40% (Figure 2S). Further, the binding site of morelloflavone on Eg5 was mapped *in vitro* using varying concentrations of ATP and morelloflavone. As shown in Figure 5A, morelloflavone did not compete with ATP. In particular, morelloflavone decreased the V_{\max} for ATP from 5.7 s⁻¹ to 4.9 s⁻¹ at 50 μM and 4.3 s⁻¹ at 100 μM. Similarly, the K_m for ATP increased from 24.9 μM in the absence of morelloflavone to 29.8 μM and 33.1 μM at 50 μM and 100 μM morelloflavone, respectively. Since a competitive inhibitor increases K_m without affecting the V_{\max} value (Maliga *et al.*, 2002), these results suggest that morelloflavone is not a competitive inhibitor, but rather binds to the allosteric site, thereby altering the structure of the ATP binding site (Figure 5B). The K_m for ATP in the absence of morelloflavone is comparable to the values reported by Cochran *et al.*, 2004; Cochran *et al.*, 2005 (20.7 μM and 25.1 μM), and by Lad *et al.*, 2008 (21 μM).

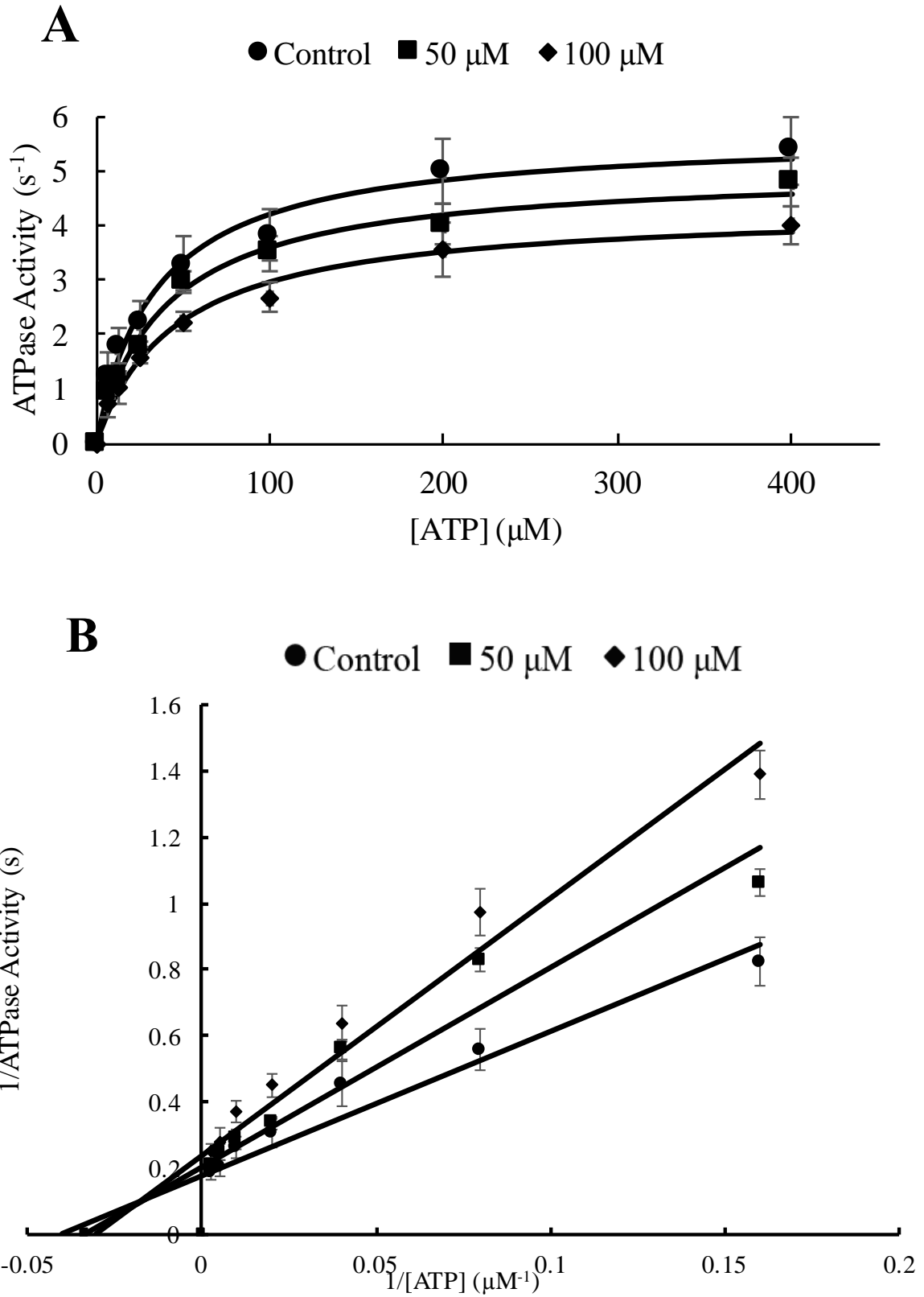
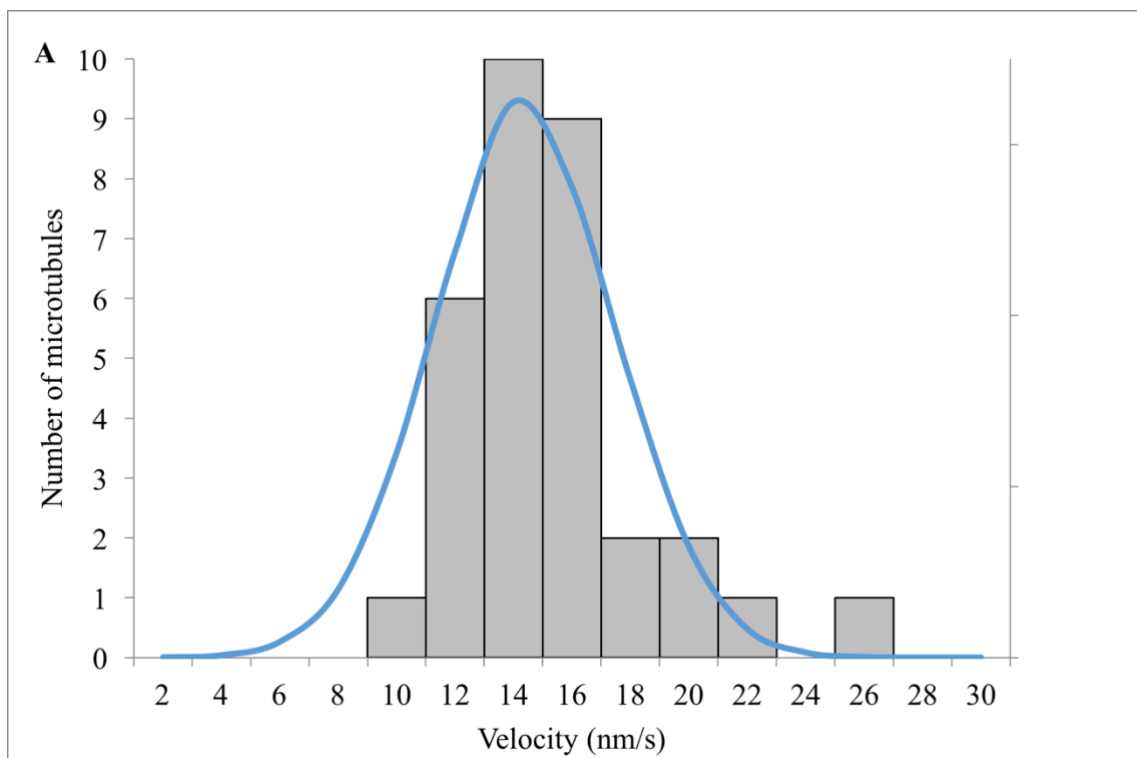


Figure 2-5. Effect of morelloflavone on microtubule-activated Eg5 ATPase activity. (A) ATPase activity of 0.1 μM Eg5 in the presence of 0.5 μM microtubule and 0 μM (circle), 50

μM (rectangle), and $100 \mu\text{M}$ (diamond) morelloflavone. Data were collected from three independent experiments. **(B)** Fitting to the Michaelis-Menten equation of enzyme velocity in the presence of morelloflavone against 0-400 μM ATP.

2.3.4 Morelloflavone suppresses Eg5 motor gliding along microtubules

To test whether the movement of Eg5 on fluorescently labeled microtubules is reduced in the presence of morelloflavone, motility assay was performed. It was found that motor gliding along microtubules was suppressed by morelloflavone in dose-dependent fashion, as seen in histograms of velocity (Figure 6). Gliding velocity was $14.4 \pm 3.2 \text{ nm/s}$ in the absence of morelloflavone (control), but $12.0 \pm 2.4 \text{ nm/s}$ (Figure 6B) and $6.8 \pm 2.4 \text{ nm/s}$ (Figure 6C) in the presence of $100 \mu\text{M}$ and $250 \mu\text{M}$ morelloflavone respectively. These results show that the biflavonoid significantly blocks microtubule gliding. It is important to emphasize that Eg5 mobility-dependent function has been robustly tested (Mandelkow and Mandelkow, 2002; Wang *et al.*, 2012; Sadakane *et al.*, 2018), and results herein are compatible with previous reports suggesting that Eg5 inhibitors induce slow release of ADP and weaken Eg5 affinity for microtubules (Moores, 2010).



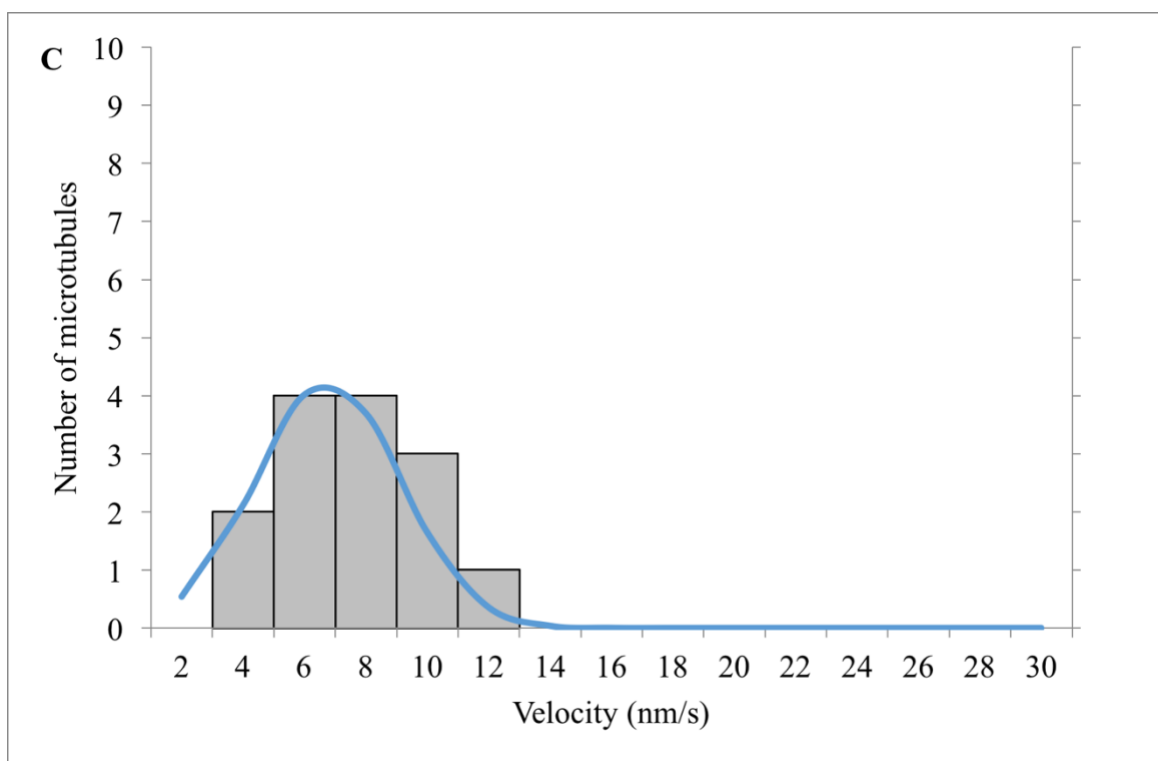
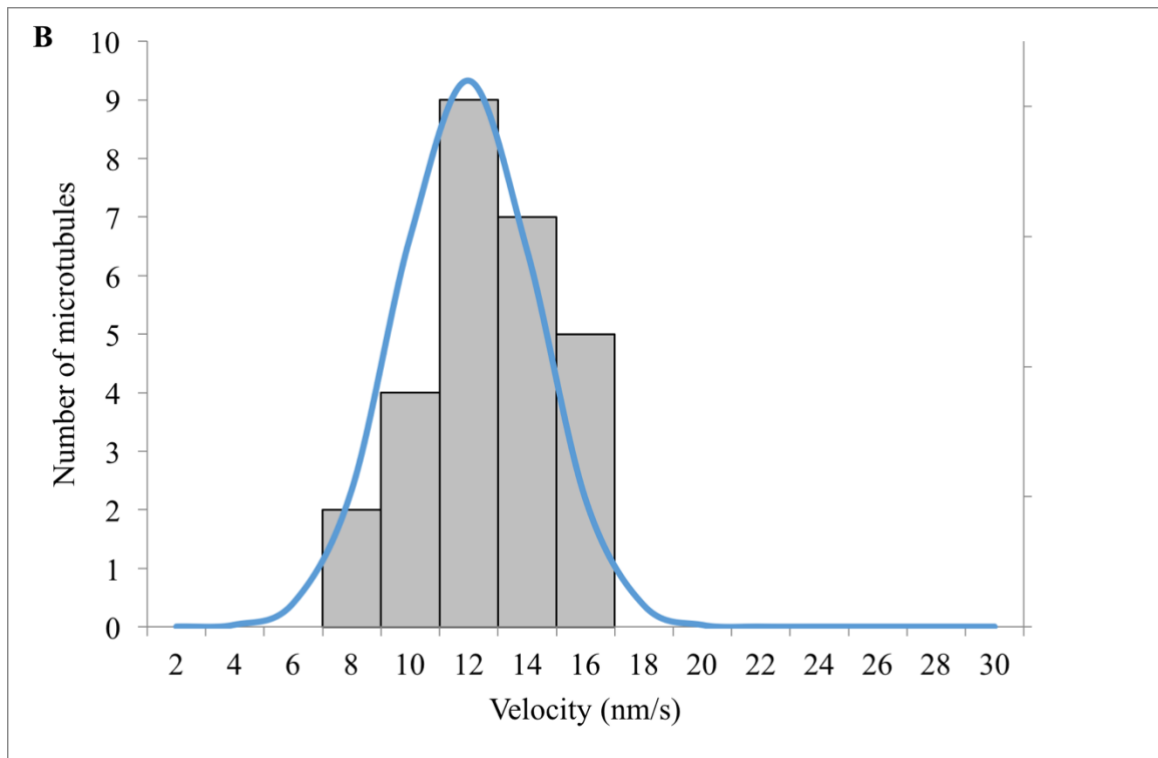


Figure 2-6. Motility of Eg5. (A) In the absence of morelloflavone. (B) In the presence of 100 μM morelloflavone. (C) In the presence of 250 μM morelloflavone. Data were collected in 10 mM Tris-HCl, pH 7.5, 50 mM potassium acetate, 4 mM MgCl_2 , 2.5 mM EGTA, 1.0 mM β -mercaptoethanol, and 20 μM taxol, 0.15 μM rhodamine-labeled microtubules, and 0.6 μM Eg5.

Movement of rhodamine-labeled microtubules was initiated by addition of 1.0 mM ATP, and observed for 30 min at 25 °C using fluorescence microscopy.

2.4 Conclusion

In silico screening of selected plant-derived biflavonoids indicated that morelloflavone may potentially interact with and inhibit mitotic kinesin Eg5 in a comparable manner as STLC, a known inhibitor of the enzyme. In agreement with the *in silico* data, morelloflavone inhibited both basal and microtubule-activated ATPase activity of Eg5 *in vitro*. Although the inhibitory activity is moderate, the result is consistent with the binding affinity estimated *in silico*. The mixed inhibition type observed also indicates that the biflavonoid binds at an allosteric site rather than directly competing with ATP at the nucleotide binding site. Finally, it was observed that morelloflavone suppresses Eg5 motor function on microtubules, implying that binding to the allosteric site may elicit conformational changes that inhibit enzyme activity. Hence, morelloflavone is a good candidate of Eg5 inhibitor. How morelloflavone interacts with Eg5 at atom level shall be investigated in the next phase of this project. Site-directed mutagenesis of amino acid residues at the predicted interface of Eg5 with morelloflavone may further confirm interactions, while crystallization of the ligand-protein complex may provide high-resolution information on such interactions.

2.5 Supplementary materials

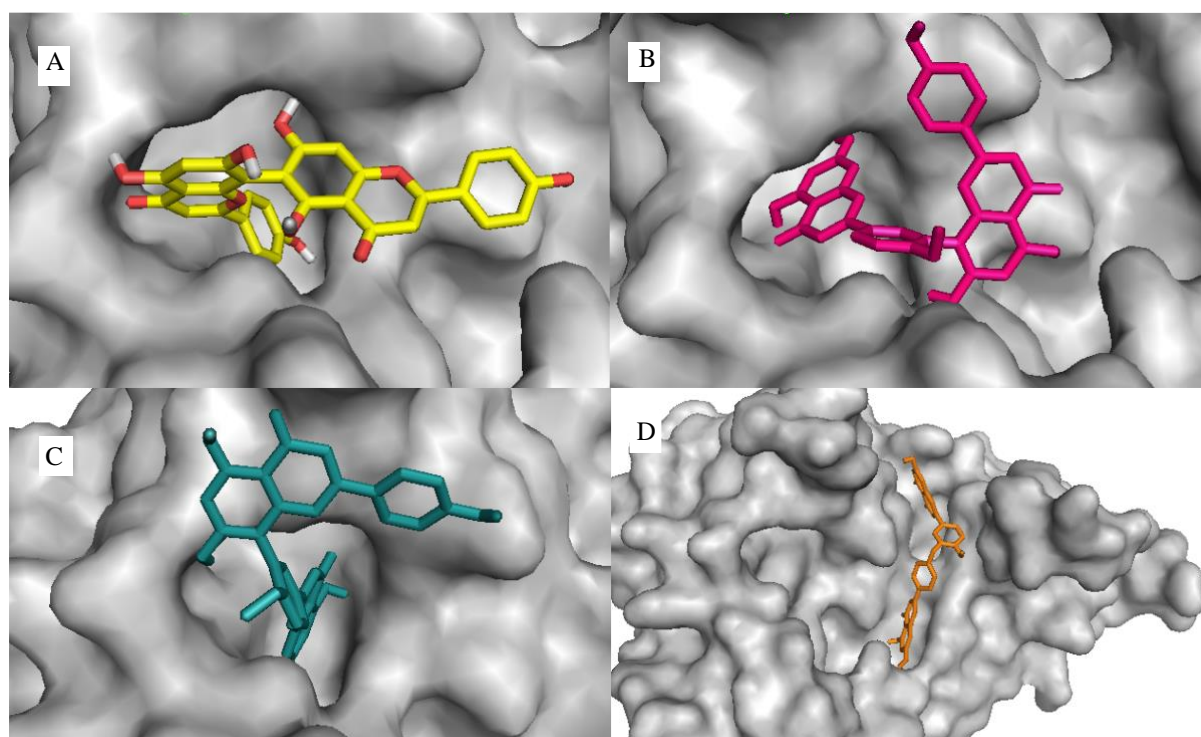


Figure SM2-1. Predicted binding poses of selected biflavonoids on Eg5. Biflavonoids are shown in sticks while kinesin Eg5 is shown as gray surface. (A) Agathisflavone. (B) Bilobetin. (C) Ginkgetin. (D) Ochnaflavone. Some biflavonoids recognize the L5/ α 2/ α 3 allosteric pocket but have “poor” binding configuration relative to the reference ligand STLC, while others bind only to the nucleotide-binding site. Binding to the allosteric site with comparable configuration to that of the reference ligand was an essential selection parameter in the screening.

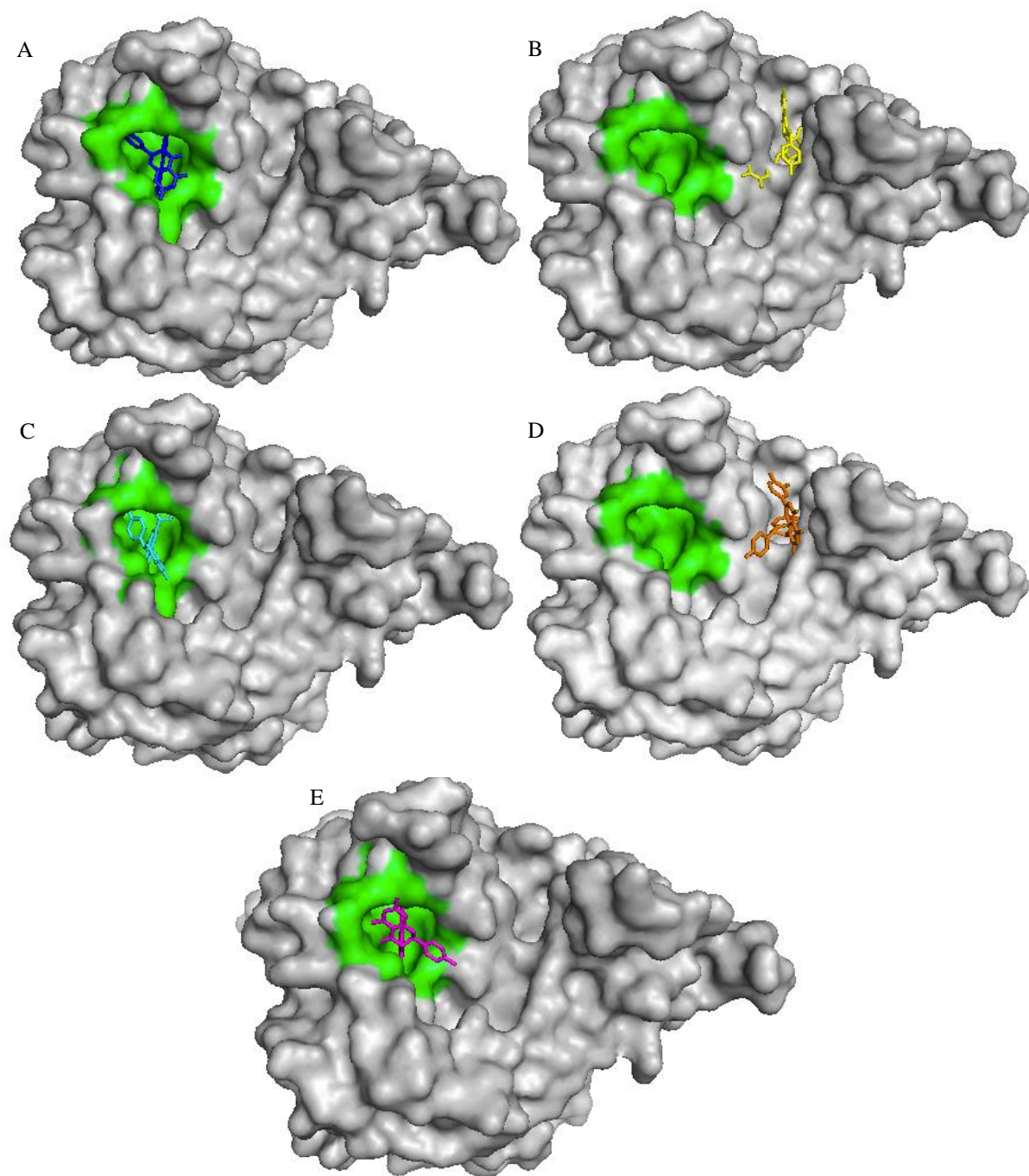


Figure SM2-2. Morelloflavone binding sites predicted by PSB-SLIM. Binding to the L5/ α 2/ α 3 allosteric pocket (green) and nucleotide-binding site was predicted in 3 (60%) and 2 (40%) outputs, respectively.

Table SM1. Biflavonoids screened *in silico*.

S/No	Biflavonoid	Binding energy (kcal/mol)	Predicted binding site
1.	Volkensiflavone	-8.4	Allosteric pocket
2	Succeedaneaflavone	-9.2	Allosteric pocket
3	Lanaroflavone	-9.7	Nucleotide-binding site
4	Prodelphinidine	-8.1	Allosteric pocket
5	Manniflavone	-10.1	Nucleotide-binding site
6	Kayaflavone	-8.5	Allosteric pocket
7	Hinokiflavone	-9.9	Allosteric pocket
8	GB1	-10.0	Allosteric pocket
9	Kolaflavanone	-9.9	Allosteric pocket
10	GB2	-10.0	Allosteric pocket
11	Ochnaflavone	-10.2	Nucleotide-binding site
12	Sumaflavone	-9.6	Nucleotide-binding site
13	Rhusflavone	-9.3	Nucleotide-binding site
14	Ginkgetin	-8.7	Allosteric pocket
15a	(+)-Morelloflavone	-8.4	Allosteric pocket
15b	(-)-Morelloflavone	-10.2	Allosteric pocket
16	Sequejasflavone	-9.5	Allosteric pocket

17	Procyanidin	-8.1	Allosteric pocket
18	Isoginkgetin	-8.8	Allosteric pocket
19	Cupressuflavone	-8.5	Nucleotide-binding site
20	Robustaflavone	-10.1	Nucleotide-binding site
21	Amentoflavone	-9.4	Allosteric pocket
22	Agathisflavone	-8.9	Allosteric pocket
23	Xanthorone	-8.5	Allosteric pocket
24	Podocarpusflavone A	-9.2	Allosteric pocket
25	Hydroxyxanthorone	-8.4	Allosteric pocket
26	Heveaflavone	-9.2	Allosteric pocket
27	Bilobetin	-8.8	Allosteric pocket
28	Taiwaniahomoflavone A	-9.4	Allosteric pocket
29	Taiwaniahomoflavone B	-9.7	Nucleotide-binding site
30	Spicataside	-9.2	Allosteric pocket
31	7-methyl-agathisflavone	-9.4	Nucleotide-binding site
32	7',7'' dimethylanaroflavone	-10.2	Nucleotide-binding site
33	Charmjasmin	-9.0	Nucleotide-binding site
34	Protoanthocyanidin	-9.2	Allosteric pocket

35	3',3" binaringenin	-10.1	Nucleotide-binding site
36	2',8" biapigenin	-8.1	Allosteric pocket
37	Sciadopitysin	-9.2	Allosteric pocket
38	Putraflavone	-9.4	Allosteric pocket
39	Podoverine B	-9.4	Allosteric pocket
40	Isocryptomerin	-9.8	Allosteric pocket

CHAPTER THREE

Insights into the molecular mechanisms of Eg5 inhibition by (+)-morelloflavone

3.1 Introduction

An *in vivo* study by Li *et al.* (2016) reported morelloflavone (MF), a biflavonoid isolated from *Garcinia* spp., as an antitumor compound in glioma. However, the molecular mechanisms and protein target involved in the antitumor activity were not investigated. In the first experiment reported in this thesis, mitotic kinesin Eg5 was identified as the possible target for this bioactivity (Ogunwa *et al.*, 2018). Kinesin Eg5 is an essential protein with key roles in cell division. Its inhibition can lead to a halt in mitosis or an eventual apoptosis. Both *in silico* and *in vitro* experiments were used to provide evidence of Eg5 inhibition by MF in the study where MF inhibited Eg5 basal and microtubule-activated ATPase activities. The biflavonoid also suppressed the microtubule gliding of Eg5 *in vitro* (Ogunwa *et al.*, 2018). The inhibitory mechanism appears to involve direct binding to an allosteric site on Eg5 to structurally alter the ATP-binding pocket, thus inhibiting its enzymatic functions.

In the current study, the underlying mechanisms of Eg5-MF interaction were thoroughly investigated using molecular dynamics simulation. Although X-ray crystallization and NMR analyses can be used to depict a protein-ligand complex, these methods only provide a snapshot of the complex without detailed information on the changes occurring in the protein and ligand structure per time during their interaction. Molecular dynamics simulation, on the other hand, has proved very useful in unraveling such changes at particular time intervals. Interestingly, computational approach has proved suitable in predicting possible mechanisms of inhibition of previous Eg5 inhibitors as well as depicting the binding mode and molecular interactions of such novel inhibitors (Nagarajan *et al.*, 2012; Ogo *et al.*, 2015; Wang *et al.*, 2017).

In the current study, morelloflavone was docked to Eg5 loop5/ α 2/ α 3 binding pocket and subjected to 100 ns molecular dynamics simulation. Results obtained unraveled the possible mechanisms underlying the modulation of Eg5 function by the biflavonoid (Figure 3-1).

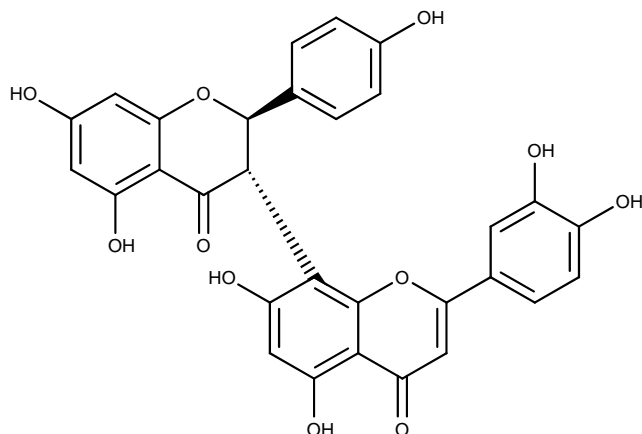


Figure 3-1. Chemical structure of (+)-morelloflavone (Li *et al.*, 2002).

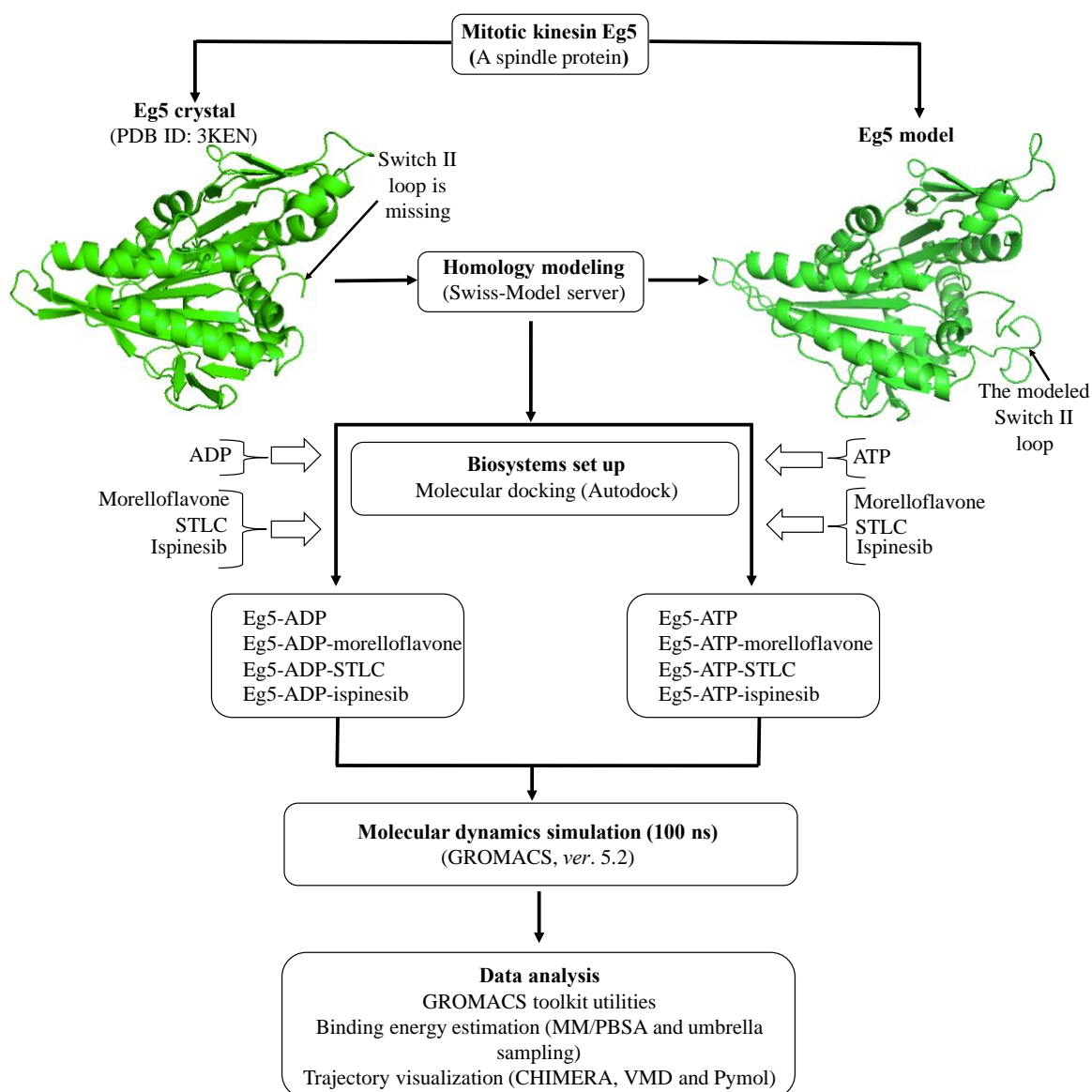


Figure 3-2. Flow-chart for the computational strategy used in this study.

3.2 Computational methods

3.2.1 Starting structures

The chemical structure of MF was built from data retrieved from the literature (Li *et al.*, 2002). ChemAxon software (MarvinSketch, 2015) was used to prepare cleaned-up 2D-coordinates of the MF, which was converted to 3D geometry using the Conformers suit of the software based on the Merck molecular force field (MMFF94). The FASTA format of Eg5 (PDB ID: 3KEN) was retrieved from PubMed to model the starting protein structure on Swiss-Model server [94]. The 3D structure of modeled Eg5 was visualized with PyMol (Delano, 2002) as a cartoon representation for observation of the co-crystallized ligands. All water molecules and ligands, except adenosine diphosphate (ADP), were deleted. Molecular docking was carried out using the modeled structure to obtain Eg5-ADP-MF complex as described previously (Ogunwa *et al.*, 2019). To generate Eg5-ATP-MF complex, the co-crystallized ADP was simply replaced with ATP having the adenine, ribose, and string of phosphate groups well aligned. Next, the bound MF molecule was deleted to obtain the control complexes (Eg5-ADP and Eg5-ATP). For comparison, crystal structures of Eg5 in complex with two potent inhibitors (STLC and ispinesib) were retrieved as Eg5-ADP-STLC (PDB ID: 3KEN) and Eg5-ADP-ispinesib (PDB ID: 4AP0), respectively, from the RCSB PDB Data Bank (www.rcsb.org). Missing segments of the protein structures were modeled. In addition, the cocrystallized ispinesib, which appeared to have lost the alkyl group, was substituted with a complete ispinesib structure obtained from the Macromodel MAESTRO suite. Finally, the cocrystallized ADP molecule in these structures was substituted with an ATP molecule to generate the Eg5-ATP-STLC and Eg5-ATP-ispinesib complexes. Autodock Vina on PYMOL was used for preparing these complexes (Seeliger and de Groot, 2010; Trott and Olson, 2010).

3.2.2 Biosystems setup

Energetic parameters for ADP and ATP were obtained from the AMBER parameter database (Meagher *et al.*, 2003). Inhibitors parametrization was carried out using the general AMBER force field (GAFF) (Wang *et al.*, 2004). For the protein structures, the H⁺⁺ server (Anandakrishnan *et al.*, 2012) was used to compute pK values of ionizable amino acids and the correct protonation state was assigned to the residues based on a pH value of 7. All the histidine residues were protonated at the epsilon position and all the aspartic and glutamic acids were retained in their anionic form. The protein and ligands were combined to obtain the biosystems for MD simulation starting from the docked cluster as previously reported (Ogunwa *et al.*, 2019). A cubic periodic boundary condition was then set up corresponding to a cubic box 10 nm long in all directions and with the complex at its center. Solvation of all the biosystems in a transferable intramolecular potential three-point (TIP3P) water model (Jorgensen and Madura, 1983) was carried out, followed by a neutralization using Na⁺/Cl⁻ ions (0.15 M). Prior to proceeding to minimization and dynamics, the geometry of the ligands was optimized at the B3LYP/6-31G* level using G09 (Frisch *et al.*, 2010), to obtain their charges and the missing AMBER parameters (Jakalian *et al.*, 2002; Duan *et al.*, 2003). The obtained system was then minimized with the steepest descent algorithm (10,000 steps) followed by 5,000 cycles using conjugate gradient algorithm until the threshold (Fmax<100 kJ/mol) was reached.

3.2.3 Molecular dynamics (MD) simulation

Groningen Machine for Chemical Simulations (GROMACS) version 5.0 (Van Der Spoel *et al.*, 2005; Aliev *et al.*, 2014) was used to run all atomistic simulation for trajectory analyses employing the AMBER-99SB-ILDN force field (Lindorff-Larsen *et al.*, 2010). Equilibration was carried out using an accurate leap-frog integrator for equations of atomic motion with a time-step of 0.002 fs at constant number of particles, volume and temperature (NVT) for 200 ps and constant number of particles, pressure and temperature (NPT) condition for 2 ns.

Temperature was kept at 310 K using V-rescale thermostat algorithm (Lee *et al.*, 2014) with a short preliminary 200 ps run in the NVT ensemble, applying the positional restraints to the protein with a force constant of 1000 kJ/mol, for the whole NVT run while Parrinello-Rahman barostat algorithm was used to maintain pressure at 1bar (Parrinello and Rahman, 1981). During these steps, protein and ligand as well as water and ions were coupled to their own temperature and pressure while a full positional constraint was imposed on the heavy atoms in all directions using the Linear Constraint Solver (LINCS) algorithm for bond constraint (Hess *et al.*, 1997). The particle mesh Ewald (PME) algorithm was used to estimate the electrostatic interactions (Darden *et al.*, 1993; Laudadio *et al.*, 2017; Mangiaterra *et al.*, 2017). The cut-off range for electrostatic and Van der Waals interactions was set to 1.2 Å for both. Using the more accurate Nosè-Hoover thermostat and setting the time constant for coupling to 0.5 ps, production phase simulation was performed for 100 ns in NPT ensemble on each of the biosystems with removal of all positional restraints (Nose, 1984; Galeazzi *et al.*, 2018).

3.2.4 Umbrella sampling and Data analysis

MD trajectories generated during 100 ns were analyzed using GROMACS toolkit utilities. RMSF, RMSD, Rg and hydrogen bond distribution for each system were determined (Hess *et al.*, 2008). *g_dist* tool was used to estimate the distance between residues (Nose, 1984). Umbrella sampling simulations are used to determine the ΔG of binding (Lemkul and Bevan, 2010) along the dissociation main axis that corresponds the reaction coordinate ξ (rc) chosen as the distance between the center of mass (COM) of Eg5 inhibitor molecules and the midpoint of the line connecting the backbone atoms of amino acids that compose the inhibitors binding site. The ξ chosen has been proved to be suitable to describe the transition between the inhibitors-bound and the inhibitors-unbound structures. Umbrella sampling simulations were run between $\xi = 16$ Å using a harmonic force constant, $k = 40$ kcal/mol. For each sampling window, the 100 ns equilibrated Eg5-ADP-inhibitor complexes obtained after 100 ns were used

for other 200 ps followed by another 1 ns MD for the umbrella sampling; the free energy profiles of the three studied systems were then compared and quantified. The changes in free energy along the reaction coordinate were calculated using WHAM (Grossfield, 2019). Free binding energy (G_{binding}) of Eg5-inhibitors complexes was determined by the MM/PBSA method using the *g_mmpbsa* tool (Kumari and Kumar, 2014). Snapshots were extracted at every 10 ps to calculate the free Gibbs energy values (Gabbianelli *et al.*, 2015; Tilio *et al.*, 2016; Fedeli *et al.*, 2017). PyMol was used for visualization and interaction analysis of the docked complexes. VMD and CHIMERA softwares were employed for trajectory visualization and analyses, while Xmgrace (Grace 5.1.21) was used for generating the plots (Humphrey *et al.*, 1996; Pettersen *et al.*, 2004; Turner, 2005; Galeazzi *et al.*, 2015).

3.3 Results and discussion

Figure 3-1 shows the chemical structure of MF, a *Garcinia* biflavonoid having a luteolin-apigenin structure (Li *et al.*, 2002). Eg5-MF complex stability, conformational and structural behaviors were investigated herein, and compared the results to those of known inhibitors of Eg5 (ispinesib and STLC) (Skoufias *et al.*, 2006; Lad *et al.*, 2008). In total, eight biosystems were prepared including (1) ADP-bound Eg5, (2) ATP-bound Eg5, (3) Eg5 in complex with ADP and STLC, (4) Eg5 in complex with ADP and ispinesib, (5) Eg5 in complex with ATP and STLC, (6) Eg5 in complex with ATP and ispinesib, (7) Eg5 in complex with ADP and MF and (8) Eg5 in complex with ATP and MF (Figure 3-2). Among these, the first two biosystems served as negative controls, the next four biosystems were used to sample known inhibitors of Eg5 for comparison to MF, and the last two biosystems were the test complexes to investigate the activity of MF towards Eg5. From 100 ns molecular dynamics (MD) runs carried out on each of the biosystems, data were critically analyzed to gain insights into the effect of MF on the Eg5 structure and catalytic function.

3.3.1 MF exhibits stability in complex with Eg5 at the allosteric pocket

First, the stability of all the complexes during the simulation timeframe was monitored, using the root means square deviation (RMSD) to observe when the trajectories plateaued and converged towards an equilibrium state. As shown in Figure 3-3, all the complexes stabilized around 50 ns and remained stable throughout the 100 ns simulation. Before reaching stability, the Eg5-ADP-MF complex showed fluctuation up to $1.03 \pm 0.12 \text{ \AA}$ (Figure 3-3A). The RMSD value of Eg5-ATP-MF was relatively low, as the system converged around $1.01 \pm 0.35 \text{ \AA}$ (Figure 3-3B). In the first 25 ns of the simulation trajectory, Eg5-ATP-MF had an RMSD comparable to that of Eg5-ATP. Thereafter, the RMSD increased to a level similar to that of Eg5-ATP-ispinesib and Eg5-ATP-STLC, and was maintained until the end of the simulation. It was apparent that the Eg5-ATP showed a very stable complex with the lowest RMSD ($0.75 \pm 0.05 \text{ \AA}$) and converged within the shortest time (20 ns) (Figure 3-3B). The ADP-bound Eg5 was less stable than ATP-bound Eg5 as the biosystem converged after 20 ns (Figure 3-3A). The difference in the nucleotides structure, i.e., the presence of a γ -phosphate in ATP which is missing in ADP, may contribute to the variation in the RMSD values. The relatively high RMSD values of Eg5-ATP-inhibitor complexes compared to the ATP-Eg5 complex suggest a structural deviation and conformational modifications in Eg5 occasioned by the presence of the inhibitors (MF, STLC, and ispinesib). Among the ADP-bound complexes, the highest RMSD value was observed with MF ($1.03 \pm 0.12 \text{ \AA}$). Early into the simulation, STLC- and ispinesib-bound Eg5 in the presence of ADP displayed comparable structural deviation, with a slight deviation at the end of the 100 ns timeframe (Figure 3-3A). Eventually, the RMSD of Eg5-ADP-ispinesib and Eg5-ADP complexes became converged at around $0.9 \pm 0.08 \text{ \AA}$ and $0.88 \pm 0.12 \text{ \AA}$, respectively, whereas that of Eg5-ADP-STLC was reduced to approximately $0.85 \pm 0.05 \text{ \AA}$. On the other hand, variation was observed in the ATP-bound counterpart of the complexes within the first 25 ns (Figure 3-3B). It is notable that the Eg5-ATP complex

exhibited a lower RMSD value than the Eg5-ADP complex. The difference in nucleotides structure may contribute to the variation in the RMSD values. Usually, Eg5 hydrolyses ATP to ADP and Pi at the nucleotide-binding site to facilitate the generation of a favourable configuration that can interact with microtubules (Farrell *et al.*, 2002; McGrath *et al.*, 2013). Convergence of Eg5 complexes at 50 ns in the current study suggests the stability of the biosystems during the simulation (Scarabelli *et al.*, 2014).

To verify the stability of the complexes, the biosystem structures were checked in the presence and absence of inhibitors using radius of gyration (Rg) analysis. As presented in Figure 3-3C, the Rg of the Eg5-ADP complex without inhibitor initially rose from 2.05 nm to nearly 2.4 nm early into the simulation (20 ns), but then continuously decreased to approximately 2.26 nm at the end of the simulation. However, this value was apparently higher than that obtained for the inhibitor-bound Eg5-ADP complexes (Figure 3-3C), suggesting an inhibitor-induced compactness in Eg5. For instance, the Rg value for Eg5-ADP-MF was reduced from 2.14 nm to less than 2.07 nm at 60 ns, and later slightly increased to 2.13 nm, which was the lowest among all complexes. In contrast, for the corresponding Eg5-ATP-MF complex, the Rg increased from 2.06 nm to 2.21 nm throughout the simulation (Figure 3-3D), which was lower than that of Eg5-ATP. The presence of γ -phosphate of ATP might play a role in the Rg increase. For STLC- and ispinesib-bound Eg5-ATP structures, Rg values were also lower compared to Eg5-ATP. These results suggest that the inhibitor-bound Eg5-nucleotide structures are very compact. Focusing on the inhibitors; they were stably resident within the loop5/ α 2/ α 3 allosteric pocket (Figure 3-3E), and the integrity of the Eg5 structure was maintained during the MD simulation, despite the observed fluctuations and displacements (Kumaresan *et al.*, 2011).

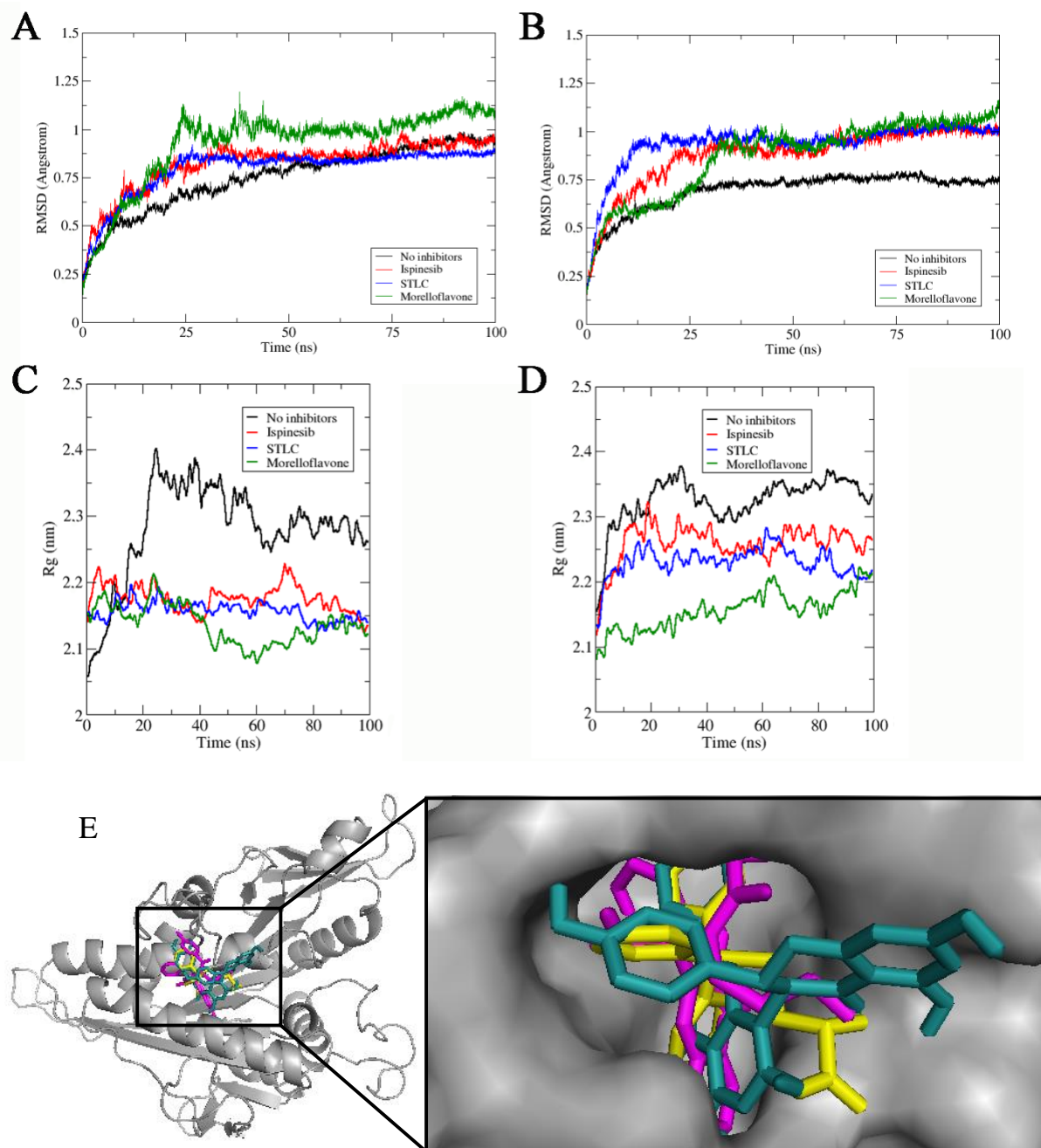


Figure 3-3. Stability and compactness of Eg5 complexes. (A) RMSD of complexes in the presence of (A) ADP, and (B) ATP. Rg values of complexes in the presence of (C) ADP and (D) ATP. (E) MF (green stick), STLC (yellow), and ispinesib (magenta) are stably resident within the loop5/ α 2/ α 3 binding pocket.

3.3.2 MF induces Eg5-loop5/ α 2/ α 3 pocket closure in a manner comparable to STLC

STLC and ispinesib reportedly both bind the allosteric pocket formed by the loop5/ α 2/ α 3,

despite having diverse chemical structures (Kim *et al.*, 2010; Talapatra *et al.*, 2012; Kaan 2013). Based on an Eg5-MF model generated by molecular docking, it was predicted that MF also binds at the allosteric loop5/ α 2/ α 3 pocket, ~ 12 Å from the nucleotide-binding site (Ogunwa *et al.*, 2019). To unveil the possible effect of MF binding on the loop5/ α 2/ α 3 pocket in comparison with the effects of STLC and ispinesib, the opening or closing of the allosteric binding pocket in Eg5 was studied by measuring the distance between selected residues located on α 3 and loop5, which formed the binding pocket. First, the distance between Trp127 and Glu215—two important residues—at the loop5/ α 2/ α 3 pocket was estimated. Trp127 is one of the functionally essential residues on loop5 that has been majorly implicated in the opening/closure of Eg5 allosteric pocket. Glu215, on the other hand, is located on α 3 of the protein (Supplementary Figure S3-1). As early as 20 ns into the simulation, the allosteric pocket of Eg5, in the absence of inhibitors (Eg5-ADP), began to open (as deduced from the eventual distance between residues Trp127 and Glu215) reaching 2.31 ± 0.2 Å, and failed to close till the end of the simulation (Figure 3-4A). Evidently, the presence of MF rapidly reversed opening of the pocket; the Trp127—Glu215 distance in the Eg5-ADP-MF complex decreased from 1.13 Å to as low as 0.45 Å (Figure 3-4A). Despite the apparent attempt by the binding pocket to return to its open conformation, the presence of the inhibitor successfully prevented the allosteric pocket from opening. Interestingly, the protein remained in this state until the end of the simulation. The STLC and ispinesib data revealed a relatively tight closure of the loop5/ α 2/ α 3 pocket, which may have implications for their potency. For Eg5-ATP complex, the loop5/ α 2/ α 3 pocket opened as early as 3.5 ns during the simulation, with an attempt to close at approximately 20 ns. However, this attempted closure was promptly reversed and the distance increased to 3.44 Å. All other attempts to return the binding pocket to its closed state, mainly at 18 ns, 22 ns, and 60 ns, resulted in large increase in the Trp127-Glu215 distance (Figure 3-4B), indicating that the Eg5 allosteric pocket was open in the absence of inhibitors.

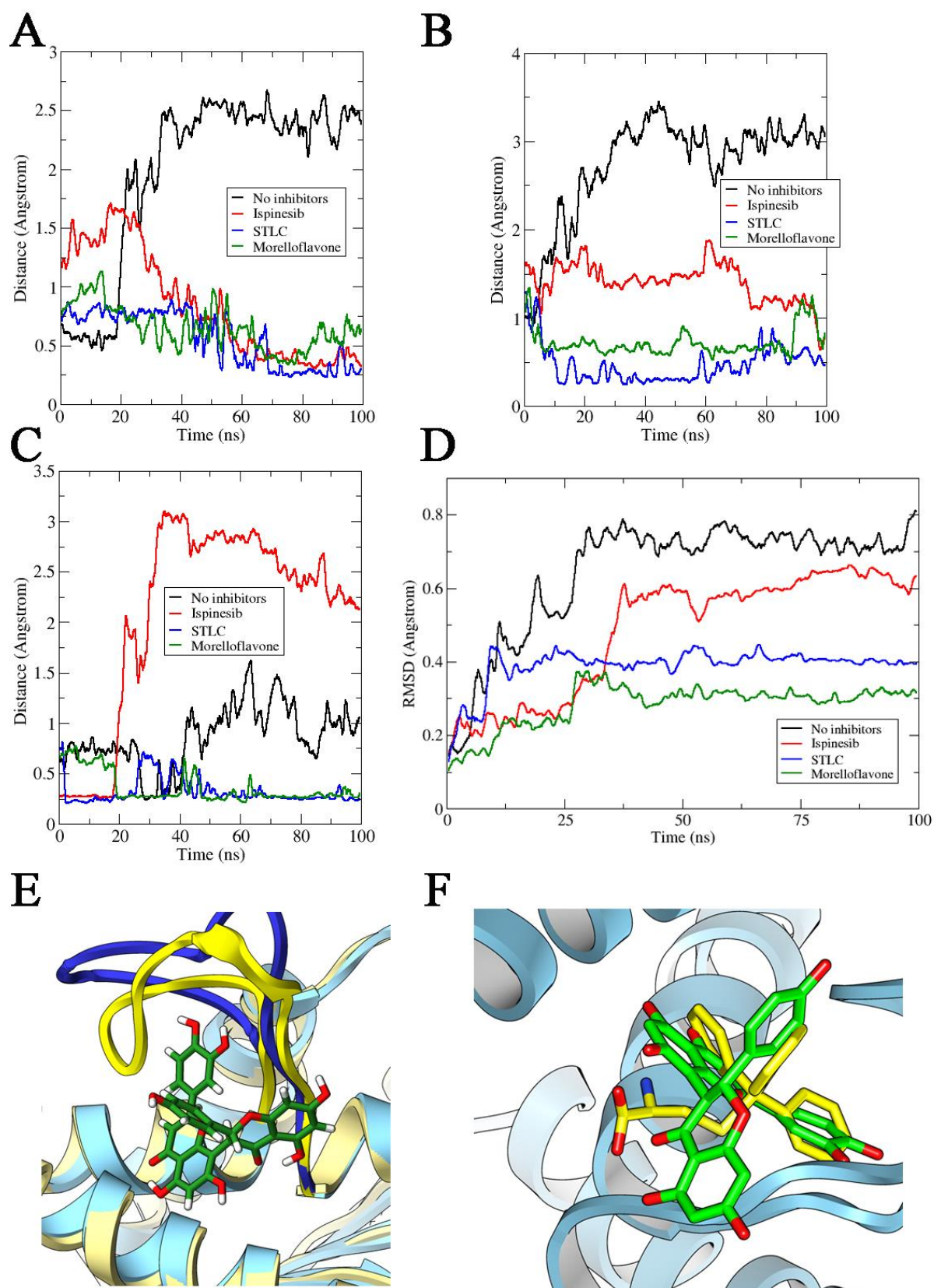


Figure 3-4. Distances (in Å) between Eg5 Trp127 and Glu215 residues in the presence of (A) ADP and (B) ATP. (C) Estimated distances (in Å) between Trp127 and Tyr211 on Eg5 in the

presence of ADP and inhibitors. (D) RMSD of loop5 in Eg5-ADP-inhibitor complexes. (E) Loop5 trapped in the close conformation by inhibitor (MF, reported in green). (F) Comparison between final conformations of STLC (in yellow sticks) and MF (in green sticks) in complex with Eg5 (in blue ribbons) and ADP. The movement of the two inhibitors toward loop5 is comparable.

However, binding of MF, STLC, or ispinesib induced the Eg5 allosteric pocket to switch from the open to the closed conformation. This observation on the loop5/ α 2/ α 3 pocket of Eg5 was further substantiated by evaluating the distance between Tyr211 and Trp127. Indeed, the distance between these residues decreased significantly in Eg5-ADP-MF and Eg5-ADP-STLC structures compared to Eg5 structures in the absence of inhibitors (Figure 3C), suggesting the trapping of loop5 in the downward position. Notably, these observations are compatible with various crystals of Eg5-inhibitor structures (Garcia-Saez *et al.*, 2007; Kaan *et al.*, 2009; Zhang *et al.*, 2011; Talapatra *et al.*, 2012).

Furthermore, the RMSD of loop5 during the MD simulations in the presence and absence of inhibitors was estimated. The results revealed lower values for inhibitor-bound Eg5 structures, suggesting a ligand-induced tightening of the allosteric pocket (Figure 3-4D). The values were 0.73 ± 0.06 Å for Eg5-ADP, 0.62 ± 0.05 Å for Eg5-ADP-ispinesib, 0.4 ± 0.03 Å for Eg5-ADP-STLC, and 0.31 ± 0.02 Å for Eg5-ADP-MF. Finally, the Eg5-MF complex was deeply inspected, and the loop5 could indeed be seen in the downward position when MF was bound (Figure 3-4E). Analyzing the poses at the end of the MD simulations, a very similar reorientation for MF and STLC within the loop5/ α 2/ α 3 pocket was observed. Both inhibitors moved closer to loop5 as confirmed from the interaction modes and the distance from loop5 (Figure 3-4F). This behavior remarks the likely similar mode of action of these molecules, which is compatible with their comparable binding configuration (Ogunwa *et al.*, 2019).

3.3.3 MF induces compactness and stabilizes the Eg5 allosteric pocket

To better understand the local effect of MF and other inhibitors on the Eg5 loop5/ α 2/ α 3 pocket, the degree of movements associated with the binding site throughout the simulation was investigated in more details, within a distance of 8 Å in all directions around the inhibitors. In this range, the residues Thr112, Phe113, Met115, Glu116, Gly117, Glu118, Arg119, Ser120, Trp127, Glu128, Leu132, Ala133, Gly134, Ile136, Pro137, Arg138, Leu171, Leu172, Tyr211, Ile213, Leu214, Glu215, Lys216, Ala218, Ala219, Lys220, Arg221, Thr222, and Phe239 were found and used to prepare an index file. The RMSD plots for the allosteric pocket in the Eg5-ADP and Eg5-ATP complexes were unsteady, with high fluctuations of up to 0.6 Å (Figure 3-5A and 3-5B). This may be due to the presence of loop5 within the region. The elongated and conserved loop5 (residues Gly117–Gly133) significantly contributes to the creation of the hydrophobic cleft in conjunction with α 2 and α 3 helices to accommodate interacting inhibitors. Some authors have suggested that loop5 can regulate the rate of conformational change occurring at the nucleotide-binding pocket (Zhang, 2011; McGrath *et al.*, 2013; Scarabelli *et al.*, 2014; Nagarajan *et al.*, 2018). Notably, the presence of MF in the allosteric site decreased such fluctuations. The Eg5-ADP-STLC complex showed the lowest RMSD values and stabilized around 0.42 Å at 100 ns. The RMSD patterns obtained for Eg5-ATP-inhibitor complexes were similar to those of ADP-bound Eg5-inhibitor complexes.

Next, the Rg of the allosteric binding site was investigated for all Eg5 complexes evaluated in this study (Figure 4C and 4D). It was found that ispinesib, which showed the lowest impact on the RMSD of the putative allosteric pocket of Eg5, actually induced the highest degree of compactness on the binding cleft. The compactness was stronger at the allosteric pocket compared to the global protein structure in both ADP- and ATP-bound complexes (Figure 3-5C and 3-5D). It was also observed that the compactness caused by MF binding to the loop5/ α 2/ α 3 binding pocket in the presence of nucleotides was stronger than that of STLC.

Although the known inhibitors of Eg5 displayed varied structural properties, most of them still identify and bind the allosteric site to exert their inhibitory effects. Together, these data indicated that, in addition to inducing closure of the loop5/ α 2/ α 3 allosteric pocket, MF stabilizes and compacts the allosteric pocket as part of its interaction mechanisms.

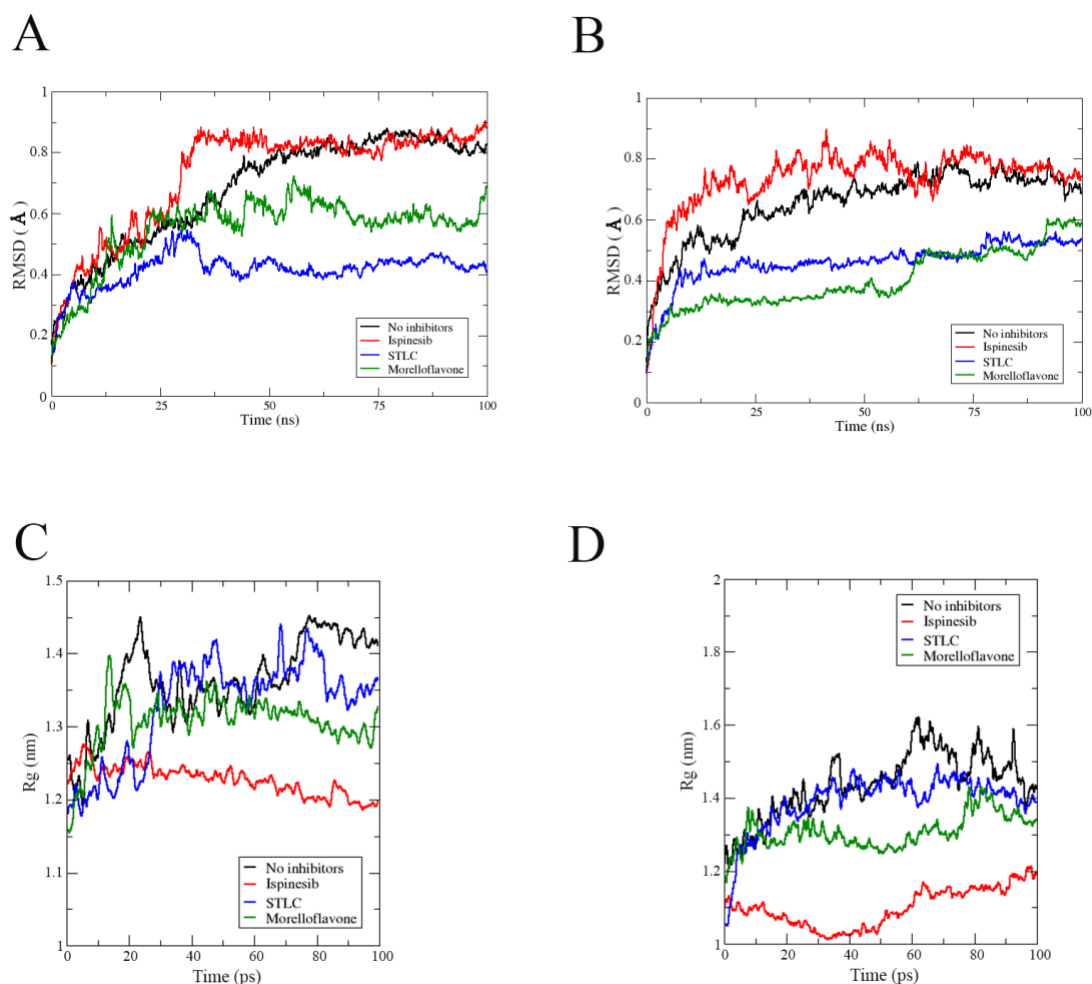


Figure 3-5. RMSD profiles of the allosteric pocket in Eg5 in the presence of (A) ADP and (B) ATP. Rg values of the Eg5 allosteric pocket in the presence of (C) ADP and (D) ATP.

3.3.4. Binding of MF on the allosteric site alters the Eg5 structural conformation

To explore the structural behavior of Eg5 in the presence or absence of MF, the distance between selected regions, such as switch I, switch II, α -helix 4 and the central β -sheet (β 6) of ADP-bound Eg5 was estimated, and compared the data with those obtained for STLC and ispinesib. Switch I region encompasses residues Met228–Ser235 (highlighted in yellow in

Figure 3-6A), whereas switch II comprises Leu266–Asn289 (red in Figure 3-6B). $\beta 6$ consists of His236–Met245 (orange in Figure 3-6B), and α -helix 4 encompasses Gln290–Val303 (light green in Figure 3-6A). For the analysis, an index file was created for each system, in which all the above residues were recorded and the distances between these regions were monitored throughout the MD simulation. As the switch I loop conformation is known to aid ATP binding through formation of a closed nucleotide-binding cleft (Parke *et al.*, 2010), it became important to evaluate the distance between switch 1 and α -helix 4 along the simulation trajectories. In biosystem without inhibitor, the initial distance between these two domains was 0.58 Å. Twenty nanoseconds into the simulation, an increase in this distance to 0.92 Å was observed, which was retained throughout the rest of simulation (Figure 3-6A). In the presence of inhibitors, switch I and α -helix 4 became very close to each other. In detail, the final distance was 0.54 Å, 0.22 Å and 0.26 Å for the Eg5-ADP-ispinesib, Eg5-ADP-STLC, and Eg5-ADP-MF complexes, respectively. These results indicate that the inhibitors influence the motions of Eg5 structure, and that STLC and MF may have a similar inhibitory mechanism. The space between switch 2 and $\beta 6$ was analyzed and a similar distance (size 0.25 Å) was observed for all Eg5 complexes at the beginning of simulations (Figure 3-6B). After 25 ns of simulations, this distance reached 0.66 Å in Eg5-ADP-ispinesib and was maintained around 0.65 Å until the end of the simulation. This is a peculiar behavior, which suggests the likely different mode of action of ispinesib with respect to the other inhibitors studied. In fact, for the other complexes, final distances ranged between 0.23 Å and 0.27 Å. Previous reports on wet experiments have suggested that inhibitors that bind to the Eg5 allosteric pocket can induce an Eg5 conformation with weak affinity to microtubules (Luo *et al.*, 2004; Lad *et al.*, 2008; Behnke-Parks *et al.*, 2011; Chen *et al.*, 2017).

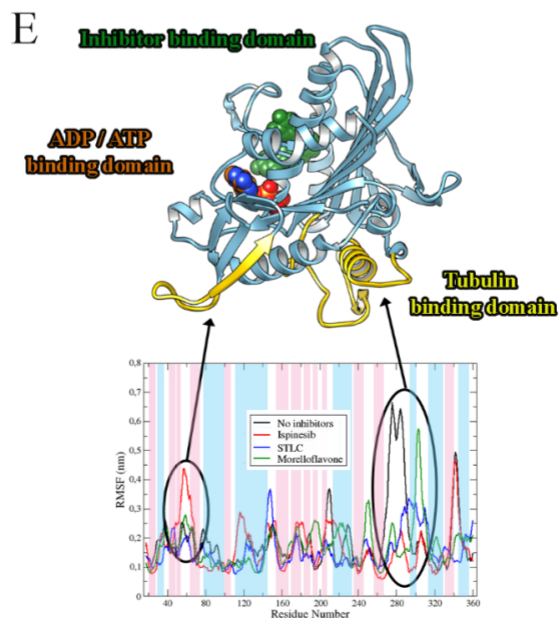
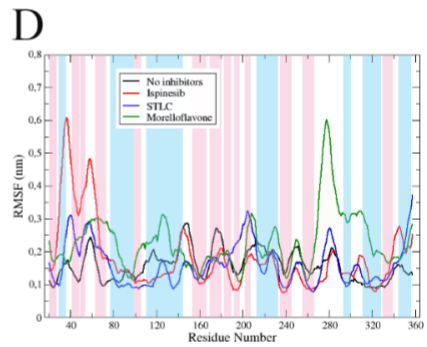
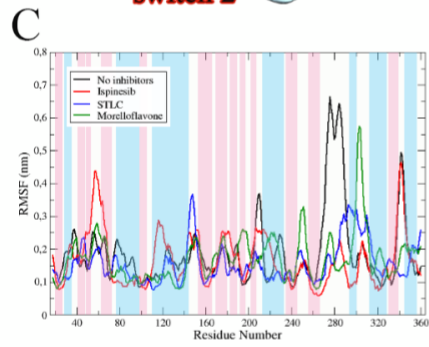
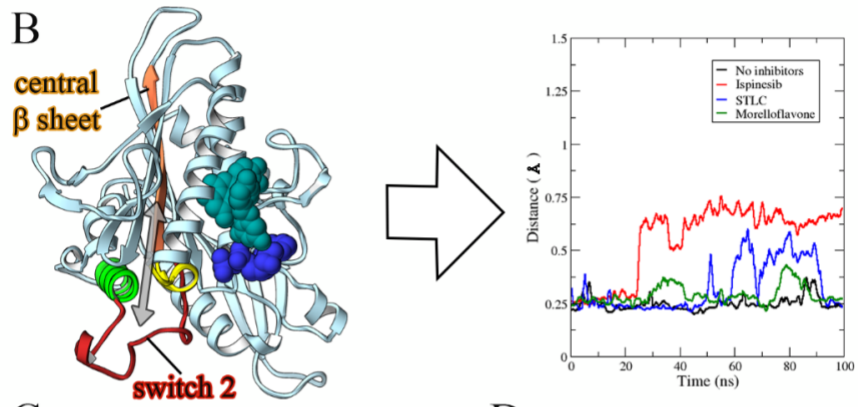
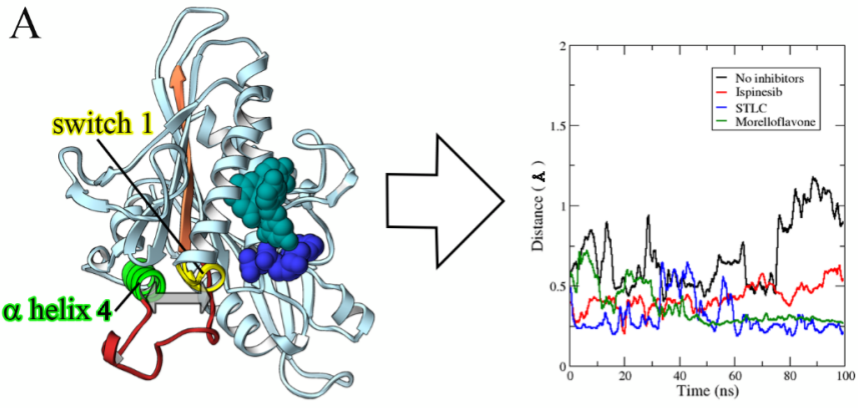


Figure 3-6. Structural behavior of Eg5 in the presence and absence of inhibitors. Distance of (A) switch I from α 2-helix and (B) switch II from the central β -sheet. Graphs are shown as Eg5 without inhibitors (black), with ispinesib (red), with STLC (blue), and with MF (green). Inhibitor (sphere, cyan) is bound to the allosteric pocket whereas the nucleoside-phosphate (sphere, blue) complexed with Eg5 at the ATP/ADP-binding site. The estimated distance between selected Eg5 segments plotted for STLC and MF are similar. RMSF profiles of (C) ADP-bound Eg5 complexes and (D) ATP-bound Eg5 complexes. (E) Fluctuations in Eg5 regions induced by MF. The β -sheets, α -helices, and loops secondary structure are highlighted in blue, pink, and white, respectively.

The binding of MF to the allosteric pocket of Eg5 prompts the evaluation of the flexibility of ATP- and ADP-bound Eg5 complexes in the absence and presence of the inhibitor so as to understand how the compound might alter the overall protein conformation. The root mean square fluctuation (RMSF) profiles shown in Figure 3-6C and 3-6D showed a similar trend of residual fluctuations at different regions of Eg5 for all the complexes. The unsteady profile in the RMSF plots reflects the structural alterations in the highly flexible regions of the protein which is consistent with its b-factor (Figure SM3-2). For instance, the β -sheet that is buried into the core of Eg5 has lower RMSF values than solvent-exposed regions, such as the neck linker and the loop regions. Eg5-ATP displayed reduced flexibility at the N-terminus of the neck linker region when compared to Eg5-ADP (Figure 3-6C and 3-6D). In the Eg5-ADP structure, the switch I region showed higher fluctuation than in Eg5-ATP. This may be due to the absence of γ -phosphate in ADP, which is consistent with a previous study that revealed that the lack of γ -phosphate in ADP-bound Eg5 allows the switch I portion of Eg5 to move frequently during simulation (Nagarajan *et al.*, 2018). Hence, the Eg5-ATP structure is more rigid than the Eg5-ADP complex. In this study, the fluctuations recorded for the switch II

region were lower in Eg5-ATP than in Eg5-ADP. These observations are often associated with the repeated contacts formed by switch I with γ -phosphate of ATP, and switch II which afforded a β -hairpin conformation (Scarabelli and Grant, 2014). Since these interactions are missing in ADP-bound Eg5, it permits the Eg5-ADP structure to adopt a range of diverse conformations resulting in enhanced flexibility. Another probable explanation for the relatively rigid state of switch II in the Eg5-ATP complex is a hydrophilic interaction between γ -phosphate oxygen of ATP and the nitrogen moiety of Gly268 (Nagarajan *et al.*, 2018), which can position the switch II loop in a manner that might cause steric hindrance against Eg5-microtubule binding. Furthermore, a hydrogen bond between the oxygen moiety of the ATP ribose ring and the amide nitrogen of Asn29 possibly afforded switch II less flexibility (Nagarajan *et al.*, 2018). It must be noted that this hydrogen bond is not formed in the presence of ADP since the missing γ -phosphate group in ADP allows the molecule to be placed slightly upward in the nucleotide-binding cleft. Hence, the ribose ring and amide nitrogen of Asn29 cannot interact (Nagarajan *et al.*, 2018). It should be emphasized that switch I, switch II, and various other loops of Eg5, including the loop5, loop7 and the p-loop, are functionally essential in the mitotic protein, and interference with their structural characteristics may affect the enzyme functions. Relative to the inhibitor-free Eg5 structures, the presence of MF, STLC, and ispinesib distorted the flexibility of Eg5, indicating their potential to induce conformational change in the protein. The binding of MF to Eg5 was mostly associated with a reduction in fluctuation of Eg5. However, it appears that the tubulin-binding region gains flexibility of residues after MF interaction (Figure 3-6E), and MF may interfere with Eg5-microtubule interaction as one of its possible Eg5 inhibitory mechanisms. This is in agreement with an earlier report that MF significantly affect microtubule binding to Eg5 and inhibited its microtubule-activated ATPase activities (Ogunwa *et al.*, 2019).

3.3.5. Binding free energy estimation for Eg5-inhibitor complexes

To quantify the effects of small modifications on the complexes, and provide means to partition of free energy, the ligands dissociations energies of ispinesib, STLC and MF in Eg5 model was determined from umbrella sampling (Lemkul and Bevan, 2010). Figure 3-7 shows that the ligand dissociation free energy barrier of ispinesib is significantly higher compared to those of STLC and MF. In fact, in the case of Eg5-ADP-ispinesib, the energy value is around 39 kcal/mol. MF shows a free energy barrier at 28.7 kcal/mol, higher than STLC (25.5 kcal/mol). This result suggests the similar features between the Eg5-ADP-STLC and Eg5-ADP-MF complexes. Another interesting observation is the existence of a plateau region in the energy curve for all inhibitors. Analysis of structures from the simulations for $\xi = 6$ to 8 \AA (for ispinesib) and $\xi = 8$ to 10 \AA (for STLC and MF) shows that ispinesib presents a different temporary stabilized state relative to the STLC and MF. The presence of these stabilized temporary phases for all three inhibitors is due to the different environment, and magnitude of the non-equilibrium contributions. Indeed, at a molecular level, every dissociation event in solution involves slightly different arrangements of atoms and therefore the kinetic data is not explained by a single barrier height but rather by a distribution of barriers. Three different states can be distinguished:

1. Bound state (windows 0–5 for ispinesib, 0-7 for MF, and 0-8 for STLC) where the inhibitors are tightly bound to Eg5 via their numerous charge contacts. This effectively restricts the inhibitors' rotational freedoms such that similar behavior is observed across all trajectories.

2. Transition state (windows 5-10 for ispinesib, 7-10 for MF, and 8-10 for STLC) where inhibitors must undergo some rotation to break out. In this region, the interactions between inhibitors and Eg5 are gradually broken. This corresponds to increasing rotational freedom in the molecules.

3. Electrostatic region (windows 10-14 for ispinesib, 10-14 for MF, and 10-12 for STLC)

where all direct contacts have been severed, and residual electrostatic interactions have been screened by incoming waters. Under weak electrostatic attractions, the inhibitor molecules are more or less rotationally free.

Umbrella sampling results showed that MF has very similar energy values to STLC, a known Eg5 inhibitor. It was also revealed that there are many correspondences between the barrier heights of Eg5-ADP-STLC and Eg5-ADP-MF, suggesting similar manners to obtain dissociation complexes. These data confirm that MF is a promising Eg5 inhibitor.

The Molecular Mechanics-Poisson Boltzmann Surface Area (MM/PBSA) method was also used to calculate the complexes overall free Gibbs energy (i.e. stability). Snapshots of trajectories from 100 ns simulations at every 10 ps of stable intervals were retrieved to serve as inputs for free energy determination. The binding free energies and their corresponding components for Eg5-inhibitor complexes are presented in Table 1. Generally, energy terms that contribute to protein-ligand complex formation are broadly categorized into polar (polar solvation and electrostatic) and non-polar (Van der Waals and non-polar solvation) energies (Kumari and Kumar, 2014). In this study, electrostatic interactions, polar solvation energy and van der Waals were negative whereas non-polar solvation was the only positive energy term for the complexes. This suggests that the major impairment to binding in all Eg5-inhibitor complexes was the non-polar solvation energy whereas electrostatic interactions, polar solvation energy, and van der Waals mainly facilitate ligand binding at the Eg5 allosteric site. In other words, Eg5-ADP-MF, Eg5-ADP-STLC and Eg5-ADP-ispinesib complexes are mainly stabilized by electrostatic, van der Waals, and polar solvation energies.

Notably, electrostatic interaction was a predominant contributor to the total binding energy in all the complexes, whereas Van der Waals interaction energy contributed the least. For STLC and MF complexes, the contributions of all energy terms were comparable. This is consistent with data from umbrella sampling (Figure 3-7). However, the Van der Waals and polar

solvation energies were much lower than those found for ispinesib. The binding energies of Eg5-ADP-Ispinesib, Eg5-ADP-STLC and Eg5-ADP-MF were -96.31, -88.98, and -93.66 kJ/mol, respectively. These results indicate that Eg5 inhibitors bind tightly to the protein in a manner that may be sufficiently strong to induce structural modifications and interfere with the ATPase and motor activities of the enzyme. The energy values also indicated that the binding process was spontaneous at the loop5/ α 2/ α 3 pocket, lending credence to the initial prediction of the allosteric pocket as the actual binding site for MF. Among all the ligands investigated, ispinesib exhibited the highest affinity to the allosteric pocket of Eg5 (Table 1), revealing the favorable interaction between Eg5 and ispinesib, which may be implicated in its inhibitory potency ($IC_{50} = 3$ nM) (Talapatra *et al.*, 2012).

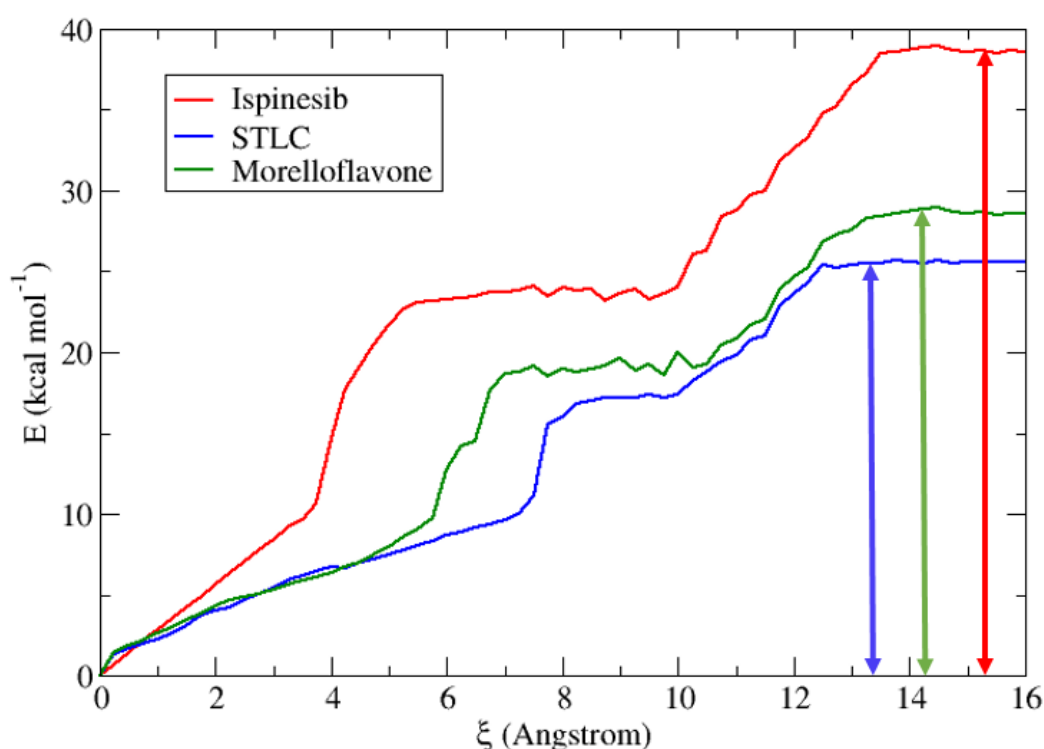


Figure 3-7. Potential of mean force along the reaction coordinate for the dissociation of inhibitors in Eg5 protein. The behavior of ispinesib (red), STLC (blue) and MF (green) are

shown. The vertical solid double-headed arrows indicate the free energy barriers for the inhibitor dissociations.

Table 1. Energy estimation

Energy (kJ/mol)	Eg5-ligand complexes		
	EG5+ADP+Ispinesib	EG5+ADP+STLC	EG5+ADP+MF
Van der Waals	-54.5 ± 8.50	-20.3 ± 9.0	-20.7 ± 8.7
Electrostatic	-103.6 ± 11.0	-158.7 ± 10.7	-156.1 ± 11.1
Polar solvation	-65.1 ± 9.1	-36.1 ± 7.5	-40.1 ± 7.7
Non-polar solvation	126.9 ± 34.2	126.1 ± 34.3	123.2 ± 33.4
Binding energy	-96.31 ± 9.5	-89.0 ± 8.9	-93.7 ± 9.2

3.3.6 MF alters the affinity of nucleotides to the active site of Eg5

Figure 6A shows the predicted binding affinity of ADP on Eg5 in the absence and presence of inhibitors. It was previously shown that the presence of inhibitors changes the stability of Eg5-nucleotide complexes. Here, the binding energy of ADP was lowered by the inhibitors (Figure 3-8A). This may contribute to the suppression of ADP release from the Eg5 active site — an essential mechanism in Eg5 inhibition. The reduced affinity of Eg5 for nucleotides may weaken its affinity to microtubules. To better understand this behavior, the stability of the active site by examined by computing the RMSD and Rg for each biosystem in the absence and presence of the inhibitors. The active site of Eg5 in complex with ATP had lower RMSD values and was

relatively more stable than the ADP counterpart (Figure 3-8B). This is consistent with previous finding that the reduced flexibility in the Eg5-ATP complex was occasioned by the presence of γ -phosphate. Lack of the γ -phosphate in ADP increases the number of potential conformations and thus, lowers the stability of the complex. STLC, ispinesib, or MF had varied effects on the stability of the nucleotide-binding site (Figure 3-8C–E).

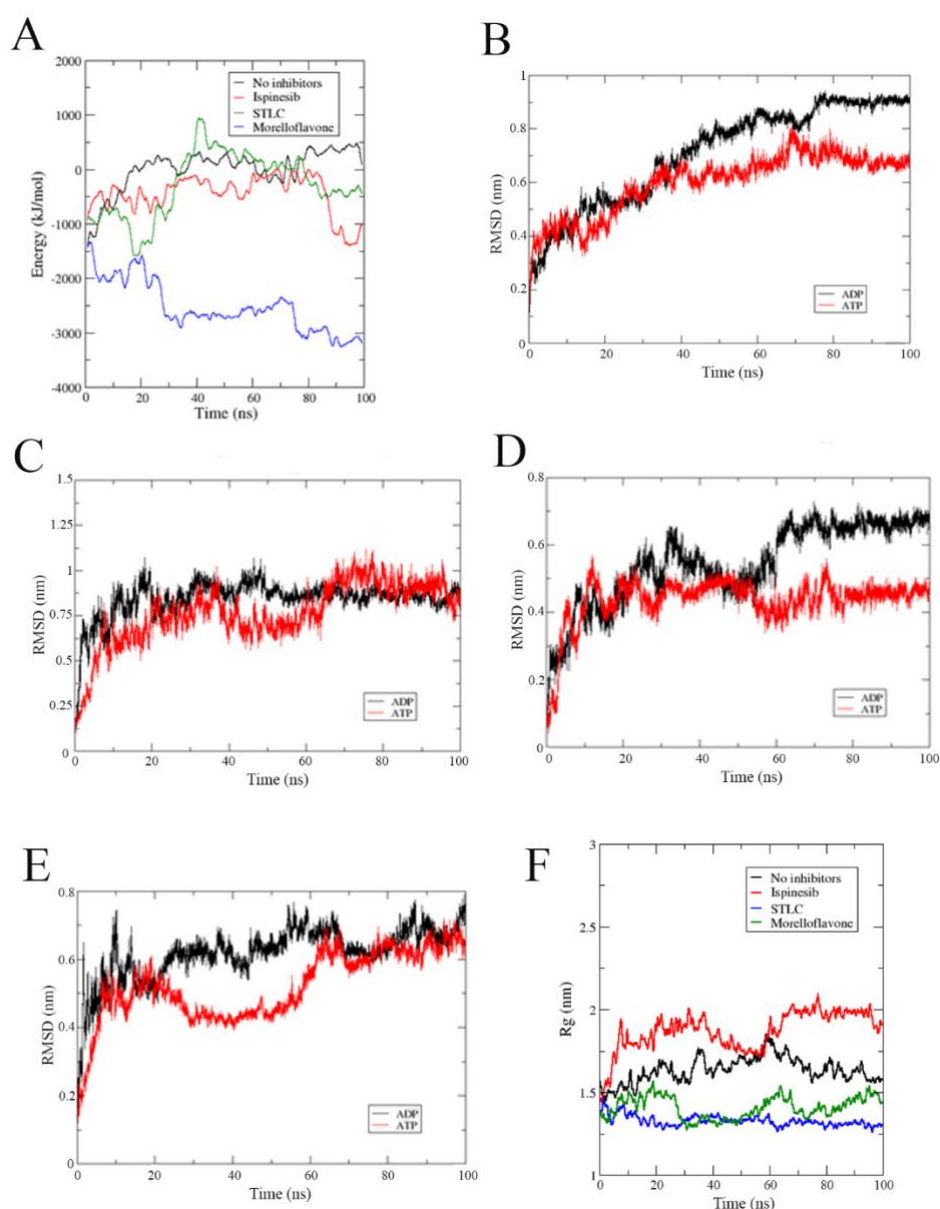


Figure 3-8. (A) Binding affinity of ADP with Eg5 during MD trajectories calculated using MM/PBSA method on the 100 ns trajectories. RMSD profiles of the active site in (B) Eg5-

ADP versus Eg5-ATP, (C) Eg5-ADP-ispinesib versus Eg5-ATP-ispinesib, (D) Eg5-ADP-STLC versus Eg5-ATP-STLC and (E) Eg5-ADP-MF versus Eg5-ATP-MF. (F) Rg of Eg5-ATP complexes.

The Eg5-ATP-inhibitor complexes displayed greater stability for the active site than the Eg5-ADP-inhibitor as deduced from the RMSD plots. It is suggested that the binding of MF, STLC, or ispinesib to Eg5 drives the protein to adjust its allosteric pocket to accommodate the inhibitors. This consequent structural alteration can affect the stability of the nucleotide-binding site which is located roughly 12 Å away from the inhibitor-binding pocket. To obtain more clear information, the Rg of the ATP-binding pocket for the Eg5 complexes was monitored. The Rg values were higher than that of MF-bound Eg5 (Figure 3-8F), indicating that the inhibitor increases the compactness of the active site. A similar result was obtained for STLC, but not for ispinesib, which increased the Rg from 1.55 nm to 1.91 nm. This suggests that ispinesib decreases the degree of compactness in Eg5 at the nucleotide-binding pocket, highlighting again the probable different mode of action of ispinesib compared to MF.

3.4 Conclusion

Eg5 is a validated target for antimitotic agents owing to its importance in cell division. As MF (an anticancer biflavonoid) was previously found to inhibit Eg5 activities, the dynamics of the Eg5-MF interaction at the molecular level was investigated by using atomistic simulation to explain the inhibitory mechanism of the biflavonoid. MF displayed tight binding on the loop5/ α 2/ α 3 pocket of Eg5 in a manner similar to STLC and ispinesib, which implies that the allosteric pocket is its binding site on Eg5. MF binding induced closure of the allosteric pocket through trapping the loop5 in the “closed” conformation, comparable with the previously reported Eg5 crystal structures co-crystallized with potent inhibitors. Structural modifications

of the tubulin-binding region in the presence of MF can compromise the normal binding mode of Eg5 with microtubules as one of the MF mechanisms for inhibiting Eg5 ATPase and motility functions. Upon MF binding, the Eg5 allosteric pocket becomes very compact and stabilized, suggesting a more rigid structure that can contribute to the trapping of Eg5 in the ADP-bound conformation. Taken together, the data show that the inhibition of Eg5 activities by MF indeed involves a stable interaction with the protein at the putative allosteric pocket, and alteration of the conformation of the enzyme. *In vivo* experiments to confirm the inhibitory mechanisms of morelloflavone against Eg5 and crystallization of Eg5-nucleotide-MF shall be undertaken in subsequent research work to gain more insights on the evolution and biochemical implication of the molecular structure of the complexes.

3.5 Supplementary materials

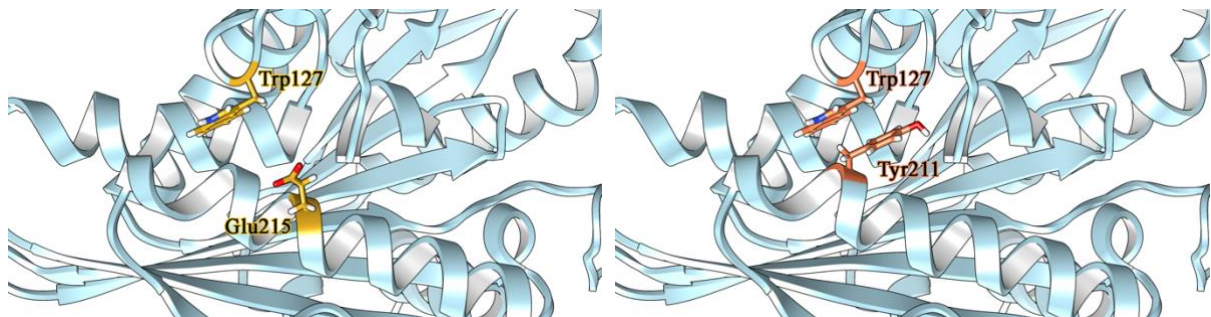
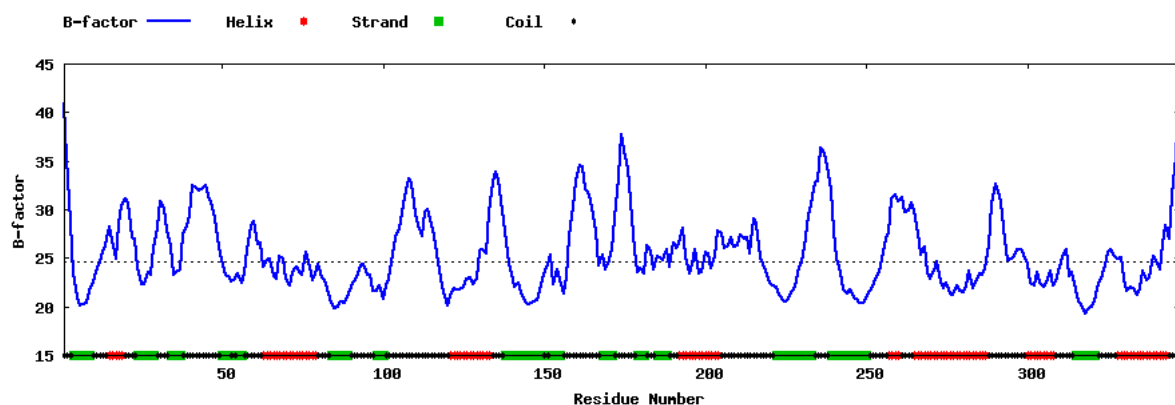


Figure SM3-1. Cartoon representation of Eg5 crystal (motor domain) showing amino acid residues Trp127 and Glu215 (yellow stick), and Trp127 and Tyr211 (orange stick).



correspond to Eg5 in complex with ispinesib and STLC respectively, was compared. It became apparent that atoms with higher values of flexibility compose the amino acids with the highest fluctuation degree. On the contrary, the atoms with the lower flexibility values found on the crystallographic temperature factor compose the amino acids with lowest fluctuation degree. These results confirmed the stability of the MD simulations.

CHAPTER FOUR

General discussion

and

Conclusion

4.1 General discussion

The significance of kinesin Eg5 in cell division and, implication in antimitotic cancer therapy cannot be overemphasized. It is known that inhibition of Eg5 causes formation of monoastrial spindles in dividing cells instead of the normal bipolar spindles required for proper mitosis, leading to mitotic catastrophe and/or apoptosis. This informed my choice of the protein as a target in the current study. Structurally, kinesin Eg5 functions in its homo-tetrameric complex. The motor domain has the nucleotide-binding region and the inhibitor-binding pockets, and was used in this research to study both the structural characteristics and the novel inhibitors binding experiments. In the screening process, the potential inhibitors that bind the active site (ATP-binding pocket) were discarded because their inhibitory effect may not be specific since they can also block activities of other ATP-dependent enzymes. Attention was placed on chemical compounds that can inhibit kinesin Eg5 via binding to the allosteric pocket near the nucleotide-binding site, which is composed of the $\alpha 2$, $\alpha 3$ and loop5. The loop5 in kinesin Eg5 is elongated than that of the other kinesins, conferring specificity to inhibitors that interact with the L5/ $\alpha 2$ / $\alpha 3$ binding site.

As the source of the potential Eg5 inhibitors tested in this study, natural products were preferred because they are readily available, well tolerated with reduced side effects, and can serve as alternative (herbal) medicine. Natural product is also an interesting and reliable pool of various pharmacologically potent ligands with known beneficial health effects. Especially, plant-derived bioactive compounds including the biflavonoids are attractive as source of novel Eg5 inhibitors. The search yielded morelloflavone as novel inhibitor to block both the ATPase and microtubule-gliding functions of kinesin Eg5. The compound belongs to the biflavonoid class of natural compounds, isolated from the *Garcinia spp.* The capacity of the biflavonoid to bind and inhibit Eg5 enzymatic activities appears to depend on the presence of a 3'→8" linkage between the flavonoid constituents of the biflavonoid. To verify this information, a preliminary

and comparative biochemical analysis was done on apigenin and luteolin; the flavonoids constituents of morelloflavone. Results from the *in vitro* experiment confirmed their weak inhibitory effect on Eg5 compared to morelloflavone (Figure 4-1). However, luteolin was more potent than apigenin against the ATPase activity of Eg5.

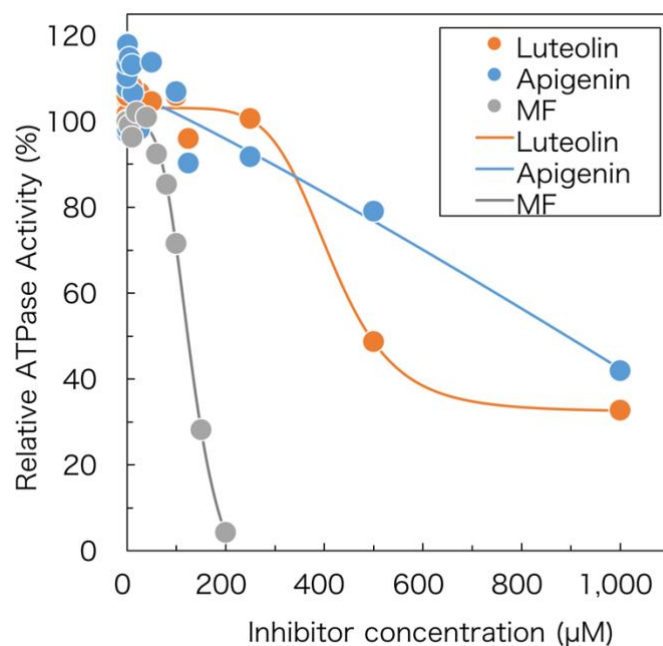
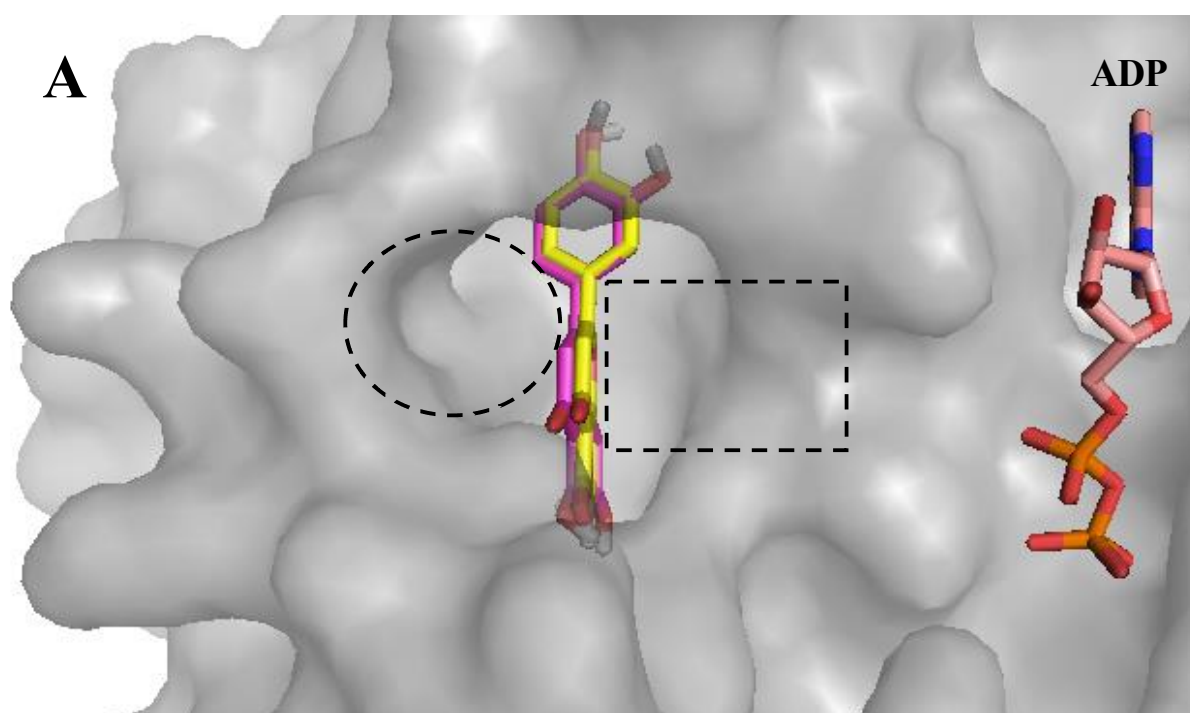


Figure 4-1. Preliminary results to compare Eg5 inhibitory effects of morelloflavone and its constituent flavonoids (apigenin and luteolin).

In silico model of Eg5-luteolin and Eg5-apigenin complexes revealed that the monoflavonoids were completely buried within the L5/ α 2/ α 3 allosteric pocket. Their interaction analysis with the enzyme suggests lower binding affinity which is consistent with their weak inhibition. Both luteolin and apigenin exhibit similar binding pose in the L5/ α 2/ α 3 pocket due to their comparable chemical scaffold (Figure 4-2). Although they lack hydrogen bonds with Eg5 amino acid residues, they apparently displayed hydrophobic interactions which are essential for Eg5 inhibition. The presence of extra hydroxyl group and binding pattern of luteolin might

be responsible for its higher inhibitory effect against ATPase function of Eg5 than the apigenin (Figure 4-1). In Eg5-morelloflavone model, luteolin favourably bind the hydrophobic core of the L5/ α 2/ α 3 pocket while the apigenin unit occupied the solvent-exposed region. This binding mode is lacking in Eg5-luteolin and Eg5-apigenin complexes (Figure 4-2a), and possibly explains the higher potency of morelloflavone. In the interaction pattern of the monoflavonoids, only few Eg5 amino acids residues formed hydrophobic interactions with apigenin and luteolin (Figure 4-2). These observations indicate that morelloflavone inhibits Eg5 activities owing to its chemical scaffold which determines the binding pose and molecular interactions. The numerous hydroxyl moieties in morelloflavone contribute to its bioactivity. Also, the planar position of the aromatic rings improves the binding mode of morelloflavone on Eg5. Although *in silico* screening predicted biflavonoids that are linked at the 3'→8" position with potential to block ATPase and motility functions of Eg5, there is no wet experiment data to support the prediction at this stage. Therefore, biflavonoids such as amentoflavone and hinokiflavone with different linkage types should be tested *in vitro* to ascertain their inhibitory potential on Eg5.



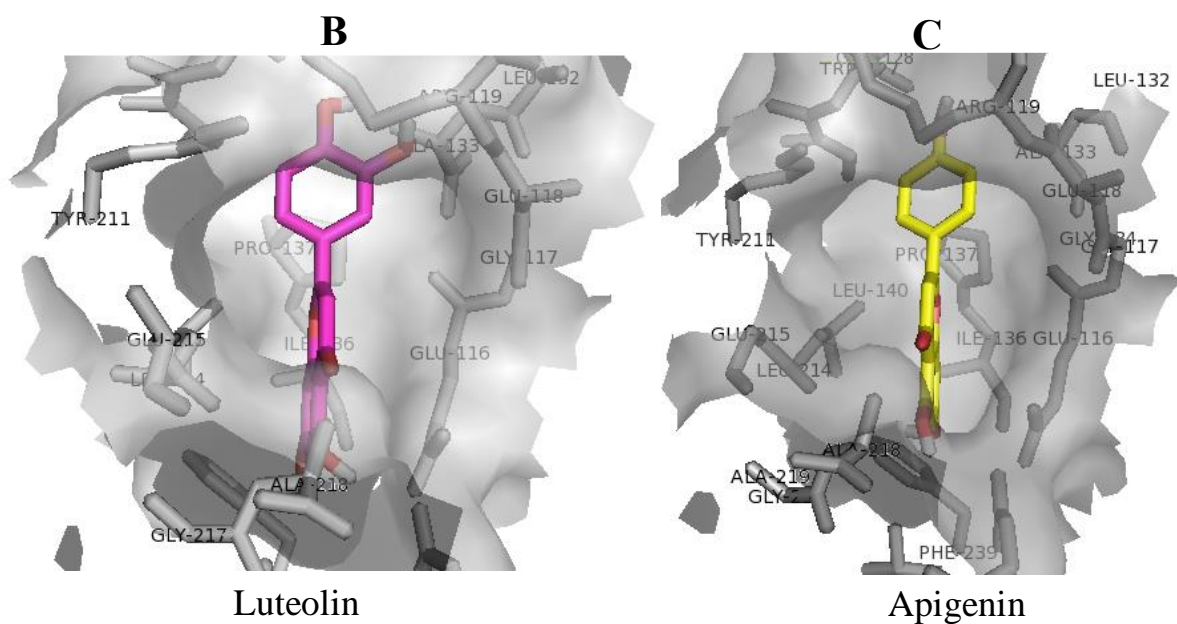


Figure 4-2. (A) *In silico* binding model of apigenin (yellow, stick) and luteolin (magenta, stick), components of morelloflavone, on Eg5 allosteric pocket. Some binding regions, the hydrophobic core (rectangle box) and solvent-exposed area (circle box) are vacant compared to morelloflavone. Molecular interaction of (B) luteolin and (C) apigenin. The binding mode and Eg5 residues that formed hydrogen bond with the flavonoids are different compared to biflavonoid morelloflavone.

In the research work presented in this dissertation, morelloflavone proved effective as inhibitor of Eg5. The chemical structure of the biflavonoid may contribute to the design and development of new Eg5 inhibitors. The moderate potency of the compounds observed in the current work may be related to the absence of some functional groups such as the halogens (F, Cl, and Br), the amine (NH₂), and imine (NH) in the biflavonoids structure. These moieties have been implicated in the potency of Eg5 inhibitors in some previous structure activity related (SAR) studies. It is believed that morelloflavone will be useful in the control of cancer cell proliferation.

4.2 Conclusion

Novel inhibitor of kinesin Eg5 was successfully screened from natural product and evaluated against the biological activities of the mitotic protein. The identified inhibitor, morelloflavone, is a biflavonoid comprising two flavonoids linked particularly in the C3'→C8" position. The interactions and inhibitory effect of morelloflavone on the enzyme were investigated by adopting *in silico* and *in vitro* approaches. The biflavonoid inhibited both the basal and microtubule-activated ATPase activities of Eg5. Furthermore, the biflavonoid suppressed the microtubule-gliding function of the mitotic protein. The *in silico* model showing the Eg5-inhibitor interactions suggests that the novel inhibitor bind at the allosteric pocket of Eg5 and establishing hydrophobic and hydrogen interactions with residues forming the $\alpha 2/\alpha 3/\text{loop}5$ allosteric pocket. These findings support the attribution of folkloric anticancer properties of the *Garcinia dulcis* to its biflavonoid content. Also, kinesin Eg5 is suggested as one of the molecular targets of the anticancer activity of biflavonoids. In addition, morelloflavone represents alternative (herbal) medicine suitable for cancer treatment especially among people living in the rural areas of the world. In this wise, more biflavonoids should be tested against Eg5 to unravel their inhibitory potential, and to ascertain if the inhibitory property is related to the type of linkage between the monoflavonoids. The biflavonoid scaffolds may contribute to the design and development of more potent Eg5 inhibitors. Finally, the screening protocol developed and used in this work will be handy in further discovery of many more novel Eg5 allosteric inhibitors. The X-ray crystallographic determination of Eg5-morelloflavone complex may elucidate more on their precise molecular structures after interaction. Validating the detailed anticancer potency of the novel inhibitor (morelloflavone) may require *in vivo* experiments using animal model and tumor cell lines.

Literature Cited

- Aliev, A.E., Kulke, M., Khaneja, H.S., Chudasama, V., Sheppard, T.D. and Lanigan, R.M. (2014). Motional timescale predictions by molecular dynamics simulations: Case study using proline and hydroxyproline side chain dynamics. *Proteins*, 82: 195–215.
- Anandakrishnan, R., Aguilar, B. and Onufriev, A.V. (2012). H++ 3.0: automating pK prediction and the preparation of biomolecular structures for atomistic molecular modeling and simulation. *Nucleic Acids Res.*, 40(1): 537–541.
- Behnke-Parks, W.M., Vendome, J., Honig, B., Maliga, Z., Moores, C., and Rosenfeld, S. S. (2011). Loop L5 acts as a conformational latch in the mitotic kinesin Eg5. *J. Biol. Chem.*, 286(7), 5242–5253.
- Blangy, A., Lane, H.A., d’Herin, P., Harper, M., Kress, M. and Nigg, E.A. (1995). Phosphorylation by p34cdc2 regulates spindle association of human Eg5, a kinesin-related motor essential for bipolar spindle formation *in vivo*. *Cell*, 83: 1159–1169.
- Brier, S., Carletti, E., DeBonis, S., Hewat, E., Lemaire, D. and Kozielski, F. (2006). The marine natural product adociasulfate-2 as a tool to identify the MT-binding region of kinesins. *Biochemistry*, 45: 15644–15653.
- Brust-Mascher, I., Sommi, P., Cheerambathur, D.K., and Scholey, J.M. (2009). Kinesin-5-dependent poleward flux and spindle length control in *Drosophila* embryo mitosis. *Molecular Biology of the Cell*, 20:1749–1762.
- Chen, G.Y., Kang, Y.J., Gayek, A.S., Youyen, W., Tüzel, E., Ohi, R. and Hancock, W.O. (2017). Eg5 inhibitors have contrasting effects on microtubule stability and metaphase spindle integrity. *ACS Chem. Biol.*, 12(4): 1038–1046.
- Choudhury, B., Kandimalla, R., Bharali, R., Monisha, J., Kunnumakara, A.B., Kalita, K., and Kotoky, J. (2016). Anticancer activity of *Garcinia morella* on T-cell murine lymphoma via apoptotic induction. *Front. Pharmacol.*, 7: 3, doi: 10.3389/fphar.2016.00003.
- Cochran, J.C. and Gilbert, S.P. (2005). ATPase mechanism of Eg5 in the absence of

- microtubules: insight into microtubule activation and allosteric inhibition by monastrol. *Biochemistry*, 44: 16633–16648.
- Cochran, J.C., Sontag, C.A., Maliga, Z., Kapoor, T.M., Correia, J.J. and Gilbert, S.P. (2004). Mechanistic analysis of the mitotic kinesin Eg5. *J. Biol. Chem.*, 279, 38861–38870.
- Compton, D.A. (2000). Spindle assembly in animal cells. *Annu. Rev. Biochem.*, 69: 95–114.
- Cragg, G.M. and Newman, D.J. (2013). Natural products: a continuing source of novel drug leads. *Biochim. Biophys. Acta.*, 1830: 3670–3695.
- Darden, T., York, D. and Pedersen, L. (1993). Particle mesh Ewald: An $N \cdot \log(N)$ method for Ewald sums in large systems. *J. Chem. Phys.*, 98: 10089–10092.
- Debonis, S., Skoufias, D.A., Lebeau, L., Lopez, R., Robin, G., Margolis, R.L., Wade, R.H. and Kozielski, F. (2004). *In vitro* screening for inhibitors of the human mitotic kinesin Eg5 with antimetabolic and antitumor activities. *Cancer Res.*, 3(9): 1079–1090.
- Decha-Dier, U., Hutadilok-Towatana, N., Mahabusarakam, W., Sawangjaroen, K. and Pinkaew, D. (2008). Anti-atherogenic effects of morelloflavone from *Garcinia dulcis* leaves in cholesterol fed rabbits. *J. Nat. Rem.*, 8: 151–159.
- DeLano, W.L. (2002). Pymol: An open-source molecular graphics tool. *CCP4 Newsletter On Protein Crystallography*, 40: 82–92.
- Duan, Y., Wu, C., Chowdhury, S., Lee, M.C., Xiong, G., Zhang, W., Yang, R., Cieplak, P., Luo, R., Lee, T., Caldwell, J., Wang, J. and Kollman, P. (2003). A point-charge force field for molecular mechanics simulations of proteins based on condensed-phase quantum mechanical calculations. *J. Comput. Chem.*, 24: 1999–2012.
- El-Nassan, H.B. (2013). Advances in the discovery of kinesin spindle protein (Eg5) inhibitors as antitumor agents. *Eur. J. Med. Chem.*, 62: 614–31.
- Farrell, C.M., Mackey, A.T., Klumpp, L.M. and Gilbert, S.P. (2002). The role of ATP hydrolysis for kinesin processivity. *J. Biol. Chem.*, 277(19): 17079–17087.

- Fedeli, D., Montani, M., Bordoni, L., Galeazzi, R., Nasuti, C., Correia-Sá, L., Domingues, V.F., Jayant, M., Brahmachari, V., Massaccesi, L., Laudadio, E. and Gabbianelli, R. (2017). *In vivo* and *in silico* studies to identify mechanisms associated with nurr1 modulation following early life exposure to permethrin in rats. *Neuroscience*, 340: 411–423.
- Frisch, M.J., Trucks, G.W., Schlegel, H.B., Scuseria, G.E., Robb, M.A., Cheeseman, J.R., Scalmani, G., Barone, V., Mennucci, B., Petersson, G.A., Nakatsuji, H., Caricato, M., Li, X., Hratchian, H.P., Izmaylov, A.F., Bloino, J., Zheng, G., Sonnenberg, J.L., Hada, M., Ehara, M., Toyota, K., Fukuda, R., Hasegawa, J., Ishida, M., Nakajima, T., Honda, Y., Kitao, O., Nakai, H., Vreven, T., Montgomery, Jr J.A., Peralta, J.E., Ogliaro, F., Bearpark, M., Heyd, J.J., Brothers, E., Kudin, K.N., Staroverov, V.N., Kobayashi, R., Normand, J., Raghavachari, K., Rendell, A., Burant, J.C., Iyengar, S.S., Tomasi, J., Cossi, M., Rega, N., Millam, J.M., Klene, M., Knox, J.E., Cross, J.B., Bakken, V., Adamo, C., Jaramillo, J., Gomperts, R., Stratmann, R.E., Yazyev, O., Austin, A.J., Cammi, R., Pomelli, C., Ochterski, J.W., Martin, R.L., Morokuma, K., Zakrzewski, V.G., Voth, G.A., Salvador, P., Dannenberg, J.J., Dapprich, S., Daniels, A.D., Farkas, O., Foresman, J.B., Ortiz, J.V., Cioslowski, J. and Fox, D.J. (2010). Gaussian 09, revision D.01. Gaussian, Inc., Wallingford CT.
- Gabbianelli, R., Carloni, M., Marmocchi, F., Nasuti, C., Fedeli, D., Laudadio, E., Massaccesi, L. and Galeazzi, R. (2015). Permethrin and its metabolites affects Cu/Zn Superoxide conformation: Fluorescence and *in silico* evidences. *Mol. BioSyst.*, 11: 208–217.
- Galeazzi, R., Bruni, P., Crucianelli, E., Laudadio, E., Marini, M., Massaccesi, L., Mobbili, G. and Pisani, M. (2015). Liposome-based gene delivery systems containing a steroid derivative: computational and small angle X-ray diffraction study. *RSC Adv.*, 5: 54070–54078.

- Galeazzi, R., Mobbili, G., Laudadio, E., Minnelli, C., Amici, A. and Massaccesi, L. (2018). Liposomal formulations for an efficient encapsulation epigallocatechin-3-gallate: an *in silico*/experimental approach, *Molecules*, 23(2): 441.
- Garcia-Saez, I., DeBonis, S., Lopez, R., Trucco, F., Rousseau, B., Thuery, P. and Kozielski, F. (2007). Structure of human Eg5 in complex with a new monastrol-based inhibitor bound in the R configuration. *J. Biol. Chem.*, **282**: 9740–9747.
- Gil, B., Sanz, M.J., Terencio, M.C., Gunasegaran, R., Payá, M. and Alcaraz, M.J. (1997). Morelloflavone, a novel biflavonoid inhibitor of human secretory phospholipase A₂ with anti-inflammatory activity. *Biochem. Pharmacol.*, 53: 733–740.
- Gontijo, V.S., Dos, Santos, M.H. and Viegas, C. Jr. (2017). Biological and chemical aspects of natural biflavonoids from plants: a brief review. *Mini Rev Med Chem.*, 17: 834–862.
- Gontijo, V.S., Januario, J.P., de Souza Judice, W.A., Antunes, A.A., Cabral, I.R., Assis, D.M., Juliano, M.A., Camps, I., Marques, M.J., Junior, C.V. and dos Santos, M.H. (2015). Morelloflavone and its semisynthetic derivatives as potential novel inhibitors of cysteine and serine proteases. *J. Med. Plants Res.*, 9: 426–434.
- Greenwell, M. and Rahman, P.K. (2015). Medicinal plants: their use in anticancer treatment. *Int. J. Pharm. Sci. Res.*, 6, 4103–4112.
- Grossfield, A. (2019). An implementation of WHAM: the Weighted Histogram Analysis Method, version 2.0.9 Available from <https://project-us.mimecast.com/s/uq-tCXD7MEUXy7QnktMii4N?domain=membrane.urmc.rochester.edu> (accessed April, 2019).
- Guido, B.C., Ramos, L.M., Nolasco, D.O., Nobrega, C.C., Andrade, B.Y., Pic-Taylor, A., Neto, B.A. and Corrêa, J.R. (2015). Impact of kinesin Eg5 inhibition by 3,4-dihydropyrimidin-2(1H)-one derivatives on various breast cancer cell features. *BMC Cancer*, 15: 283.

- Hackney, D.D. (1988). Kinesin ATPase: rate-limiting ADP release. *Proc. Natl Acad. Sci., USA* 85: 6314-6318
- Hess, B., Bekker, H., Berendsen, H.J.C. and Fraaije, J.G.E.M. (1997). LINCS: A linear constraint solver for molecular simulations. *J. Comp. Chem.*, 18: 1463–1472.
- Hess, B., Kutzner, C., van der Spoel, D. and Lindahl, E. (2008). GROMACS 4: Algorithms for highly efficient, load-balanced, and scalable molecular simulation. *J. Chem. Theory Comput.*, 4: 435–447.
- Hirokawa, N., Noda, Y., Tanaka, Y. and Niwa, S. (2009). Kinesin superfamily motor proteins and intracellular transport. *Nature Rev. Mol. Cell Biol.*, 10: 682–696.
- human lipoprotein oxidation by morelloflavone and camboginol from *Garcinia dulcis*. *Nat.*
- Humphrey, W., Dalke, A. and Schulten, K. (1996). VMD: visual molecular dynamics, *J. Mol. Graphics.*, 14: 33–38.
- Hutadilok-Towatana, N., Kongkachuay, S. and Mahabusarakam, W. (2007). Inhibition of
- Ishikawa, K., Tohyama, K., Mitsunashi, S. and Maruta, S. (2014). Photocontrol of the mitotic kinesin Eg5 using a novel S-trityl-L-cysteine analogue as a photochromic inhibitor. *J. Biochem.*, 155: 257–263.
- Ito, T., Yokota, R., Watarai, T., Mori, K., Oyama, M., Nagasawa, H., Matsuda, H. and Inuma, M. (2013). Isolation of six isoprenylated biflavonoids from the leaves of *Garcinia subelliptica*. *Chem. Pharm. Bull.*, 61: 551–558.
- Iwu, M.M., Igboko, O.A., Elekwa, O.K., and Tempesta, M.S. (1990). Prevention of thioacetamide-induced hepatotoxicity by biflavanones of *Garcinia kola*. *Phytother. Res.*, 4, 157–159.

- Jakalian, A., David, B.J. and Bayly, C.I. (2002). Fast, efficient generation of high-quality atomic charges. AM1-BCC model: II. Parameterization and validation. *J. Comput. Chem.*, 23: 1623–1641.
- Jeon, Y.J., Jung, S.N., Yun, J., Lee, C.W., Choi, J., Lee, Y.J., Han, D.C. and Kwon, B.M. (2015). Ginkgetin inhibits the growth of DU-145 prostate cancer cells through inhibition of signal transducer and activator of transcription 3 activity. *Cancer Sci.*, 106: 413–420.
- Jiang, C., Chen, Y., Wang, X. and You, Q. (2007). Docking studies on kinesin spindle protein inhibitors: an important cooperative 'minor binding pocket' which increases the binding affinity significantly. *J. Mol. Model.*, 13: 987–992.
- Jorgensen, W.L. and Madura, J.D. (1983). Solvation and conformation of methanol in water. *Am. Chem. Soc.*, 105: 1407–1413
- Kaan, H.Y., Major, J., Tkocz, K., Kozielski, F. and Rosenfeld, S.S. (2013). "Snapshots" of ispinesib-induced conformational changes in the mitotic kinesin Eg5. *J. Biol. Chem.*, 288(25): 18588–18598.
- Kaan, H.Y., Ulaganathan, V., Hackney, D.D., and Kozielski, F. (2009). An allosteric transition trapped in an intermediate state of a new kinesin inhibitor complex. *Biochem. J.*, 425: 55–60.
- Kang, Y.J., Min, H.Y., Hong, J.Y., Kim, Y.S., Kang, S.S. and Lee, S.K. (2009). Ochnaflavone, a natural biflavonoid, induces cell cycle arrest and apoptosis in HCT-15 human colon cancer cells. *Biomol. Ther.*, 17: 282–287.
- Kapitein, L.C., Peterman, E.J., Kwok, B.H., Kim, J.H., Kapoor, T.M., and Schmidt, C.F. (2005). The bipolar mitotic kinesin Eg5 moves on both microtubules that it crosslinks. *Nature*, 435: 114–118.
- Kapoor, T.M., Mayer, T.U., Coughlin, M.L., and Mitchison, T.J. (2000). Probing spindle assembly mechanisms with monastrol, a small molecule inhibitor of the mitotic kinesin,

- Eg5. J. Cell Biol., 150: 975–988.
- Karanjgaokar, C.G., Radhakrishnan, P.V., and Venkataraman, K. (1967). Morelloflavone, a 3 (8-) flavonylflavanone, from the heartwood of *Garcinia morella*. Tetrahedron Lett., 33: 3195–3198.
- Kaseda, K., McAinsh, A.D., and Cross, R.A. (2009). Walking, hopping, diffusing and braking modes of Kinesin-5. Biochemical Society Transactions, 37:1045–1049.
- Kashina, A.S., Baskin, R.J., Cole, D.G., Wedaman, K.P., Saxton, W.M., and Scholey, J.M. (1996). A bipolar kinesin. Nature, 379: 270–272.
- Katiyar, C., Gupta, A., Kanjilal, S. and Katiyar, S. (2012). Drug discovery from plant sources: an integrated approach. Ayu, 33: 10–19.
- Kim, E.D., Buckley, R., Learman, S., Richard, J., Parke, C., Worthylake, D.K., Wojcik, E.J., Walker, R.A. and Kim, S. (2010). Allosteric drug discrimination is coupled to mechanochemical changes in the kinesin-5 motor core. J. Biol. Chem., **285**: 18650–18661.
- Kim, H.P., Park, H., Son, K.H., Chang, H.W. and Kang, S.S. (2008). Biochemical pharmacology of biflavonoids: implications for anti-inflammatory action. Arch. Pharm. Res., 31: 265–273.
- Konoshima, M., Ikeshiro, Y., Nishinaga, A., Matsuura, T., Kubota, T., and Sakamoto, H. (1969). The constitution of flavonoids from *Garcinia spicata* hook f. Tetrahedron Lett., 10: 121–124.
- Kumaresan, J., Kothai, T. and Lakshmi, B.S. (2011). *In silico* approaches towards understanding CALB using molecular dynamics simulation and docking. Mol. Simul., 37: 1053–1061.

- Kumari, R. and Kumar, R. (2014). Open source drug discovery consortium, Lynn, A. g_mmpbsa—A GROMACS tool for high-throughput MM-PBSA calculations. *J. Chem. Inf. Model.*, 54(7): 1951–1962.
- Lad, L., Luo, L., Carson, J.D., Wood, K.W., Hartman, J.J., Copeland, R.A., and Sakowicz, R. (2008). Mechanism of inhibition of human KSP by ispinesib. *Biochemistry*, 47: 3576–3585.
- Laudadio, E., Mobbili, G., Minelli, C., Massaccesi, L. and Galeazzi, R. (2017). Salts influence catechins and flavonoids encapsulation in liposomes: a molecular dynamics investigation, *Mol. Inform.*, 36(11): 1700059.
- Lawrence, C.J., Dawe, K.R., Christie, K.R., Cleveland, D.W., Dawson, S.C., Endow, S.A., Goldstein, L.S.B., Goodson, H.V., Hirokawa, N., Howard, J., Malmberg, R.L., McIntosh, J.R., Miki, H., Mitchison, T.J., Okada, Y., Reddy, A.S., Saxton, W.M., Schliwa, M., Scholey, J.M., Vale, R.D., Walczak, C.E. and Wordeman, L. (2004). A standardized kinesin nomenclature. *J. Cell Biol.*, 167(1): 19–22.
- Lee, H.S. and Zhang, Y. (2012). BSP-SLIM: a blind low-resolution ligand-protein docking approach using predicted protein structures. *Proteins*, 80: 93–110.
- Lee, J.Y., Jung, K.W., Woo, E.R. and Kim, Y. (2008). Docking study of biflavonoids, allosteric inhibitors of protein tyrosine phosphatase 1b. *Bull. Korean Chem. Soc.*, 29: 1479–1484.
- Lee, Y., Lee, J.J., Kim, S., Lee, S.C., Han, J., Heu, W., Park, K., Kim, H.J., Cheong H.K., Kim, D., Kim, H.S. and Lee, K.W. (2014). Dissecting the critical factors for thermodynamic stability of modular proteins using molecular modeling approach. *PLoS One*, 9: e98243.
- Lemkul, J.A. and Bevan, D.R. (2010). Assessing the stability of Alzheimer's amyloid protofibrils using molecular dynamics. *J. Phys. Chem. B*, 114(4): 1652–1660.
- Li, X., Ai, H., Sun, D., Wu, T., He, J., Xu, Z., Ding, L. and Wang, L. (2016). Anti-tumoral

- activity of native compound morelloflavone in glioma. *Oncol. Lett.*, 12(5): 3373–3377.
- Li, X.C., Joshi, A.S., ElSohly, H.N., Khan, S.I., Jacob, M.R., Zhang, Z., Khan, I.A., Ferreira, D., Walker, L.A., Broedel, S.E. Jr., Rauli, R.E. and Cihlar, R.L. (2002). Fatty acid synthase inhibitors from plants: isolation, structure elucidation, and SAR studies. *J. Nat. Prod.*, 65: 1909–1914.
- Li, X.C., Joshi, A.S., Tan, B., El Sohly, H.N., Walker, L.A., Zjawiony, J.K. and Ferreira, D. (2002). Absolute configuration, conformation, and chiral properties of flavanone-(3-8'')-flavone biflavonoids from *Rheedia acuminata*. *Tetrahedron*, 58: 8709–8717.
- Lin, Y.M., Anderson, H., Flavin, M.T., and Pai, Y.S., Mata-Greenwood, E., Pengsuparp, T., Pezzuto, J.M., Schinazi, R.F., Hughes, S.H., and Chen, F.C. (1997). *In vitro* anti-HIV activity of biflavonoids isolated from *Rhus succedanea* and *Garcinia multiflora*. *J. Nat. Prod.*, 60: 884–888.
- Lindorff-Larsen, K., Piana, S., Palmo, K., Maragakis, P., Klepeis, J.L., Dror, R.O. and Shaw, D.E. (2010). Improved side-chain torsion potentials for the Amber ff99SB protein force field. *Proteins*, 78: 1950–1958.
- Luo, L., Carson, J.D., Dhanak, D., Jackson, J.R., Huang, P.S., Lee, Y., Sakowicz, R. and Copeland, R.A. (2004). Mechanism of inhibition of human KSP by monastrol: Insights from kinetic analysis and the effect of ionic strength on KSP inhibition. *Biochem.*, 43(48): 15258–15266.
- Maliga, Z., Kapoor, T.M., and Mitchison, T.J. (2002). Evidence that monastrol is an allosteric inhibitor of the mitotic kinesin Eg5. *Chem. Biol.*, 9: 989–996.
- Mandelkow, E. and Mandelkow, E.M. Kinesin motors and disease. *Trends Cell Biol.*, 2002, 12(12): 585–591.
- Mangiatterra, G., Laudadio, E., Cometti, M., Mobbili, G., Minnelli, C., Massaccesi, L., Biavasco, F., Citterio, B. and Galeazzi, R. (2017). Inhibitors of multidrug efflux pumps

- of *Pseudomonas aeruginosa* from natural sources: An *in silico* high-throughput virtual screening and *in vitro* validation. *Med. Chem. Res.*, 26: 414. doi:10.1007/s00044-016-1761-1.
- Marcus, A.I., Peters, U., Thomas, S.L., Garrett, S., Zelnak, A., Kapoor, T.M., and Giannakakou, P. (2005). Mitotic kinesin inhibitors induce mitotic arrest and cell death in Taxol-resistant and -sensitive cancer cells. *J. Biol. Chem.*, 280: 11569–11577.
- MarvinSketch (version 15.7.27), (2015). calculation module developed by ChemAxon, <http://www.chemaxon.com/products/marvin/marvinsketch/>.
- Masuda, T., Yamashita, D., Takeda, Y., and Yonemori, S. (2005). Screening for tyrosinase inhibitors among extracts of seashore plants and identification of potent inhibitors from *Garcinia subelliptica*. *Biosci. Biotechnol. Biochem.*, 69: 197–201.
- Mayer, T.U., Kapoor, T.M., Haggarty, S.J., King, R.W., Schreiber, S.L. and Mitchison, T.J. (1999). Small molecule inhibitor of mitotic spindle bipolarity identified in a phenotype-based screen. *Science*, 286: 971–974.
- McGrath, M.J., Kuo, I.F., Hayashi, S. and Takada, S. Adenosine triphosphate hydrolysis mechanism in kinesin studied by combined quantum-mechanical/molecular-mechanical metadynamics simulations. *J. Am. Chem. Soc.*, 2013, 135(24): 8908–8919.
- Meagher, K.L., Redman, L.T. and Carlson, H.A. (2003). Development of polyphosphate parameters for use with the AMBER force field. *J. Comput. Chem.*, 24: 1016–1025.
- Miki, H., Okada, Y., and Hirokawa, N. (2005). Analysis of the kinesin superfamily: insights into structure and function. *Trends Cell Biol.*, 15: 467–476.
- Moores, C.A. (2010). Kinesin-5 mitotic motors: Is loop5 the on/off switch? *Cell Cycle*, 9: 1286–1290.
- Myers, S.M. and Collins, I. (2016). Recent findings and future directions for interpolar mitotic kinesin inhibitors in cancer therapy. *Future Med. Chem.*, 8: 463–489.

- Nagarajan, S. and Sakkiah, S. (2018). Exploring a potential allosteric inhibition mechanism in the motor domain of human Eg5. *J. Biomol. Struct. Dyn.*, 13:1–10.
- Nagarajan, S., Skoufias, D.A., Kozielski, F. and Pae, A.N. (2012). Receptor ligand interaction-based virtual screening for novel Eg5/kinesin spindle protein inhibitors. *J. Med. Chem.* 2012, 55, 2561–2573.
- Nakai, R., Iida, S., Takahashi, T., Tsujita, T., Okamoto, S., Takada, C., Akasaka, K., Ichikawa, S., Ishida, H., Kusaka, H., Akinaga, S., Murakata, C., Honda, S., Nitta, M., Saya, H., and Yamashita, Y. (2009). K858, a novel inhibitor of mitotic kinesin Eg5 and antitumor agent, induces cell death in cancer cells. *Cancer Res.*, 69(9):3901-3909.
- Nakazawa, J., Yajima, J., Usui, T., Ueki, M., Takatsuki, A., Imoto, M., Toyoshima, Y.Y. and Osada, H. (2003). A novel action of terpendole E on the motor activity of mitotic kinesin Eg5. *Chem. Biol.*, 10: 131–137.
- Nosè, S. A unified formulation of the constant temperature molecular-dynamics methods. *J. Chem. Phys.* 1984, 81, 511–519.
- Ogo, N., Ishikawa, Y., Sawada, J., Matsuno, K., Hashimoto, A. and Asai, A. (2015). Structure-guided design of novel l-cysteine derivatives as potent KSP inhibitors. *ACS Med. Chem. Lett.*, 6: 1004–1009.
- Ogunwa, T.H., Kenichi, T., Kei, S., Yuka, K., Shinsaku, M. and Takayuki, M. (2019). Morelloflavone as novel inhibitor for mitotic kinesin Eg5. *J. Biochem.* In press.
- Oishi, S., Watanabe, T., Sawada, J., Asai, A., Ohno, H. and Fujii, N. (2010) Kinesin spindle protein (KSP) inhibitors with 2,3-fused indole scaffolds. *J. Med. Chem.*, 53: 5054–5058.
- Omotuyi, O.I. and Ueda, H. (2015). Molecular dynamics study-based mechanism of nefiracetam-induced NMDA receptor potentiation. *Comput. Biol. Chem.*, 55: 14–22.
- Pang, X., Yi, T., Yi, Z., Cho, S.G., Qu, W., Pinkaew, D., Fujise, K. and Liu, M. (2009).

- Morelloflavone, a biflavonoid, inhibits tumor angiogenesis by targeting Rho GTPases and extracellular signal-regulated kinase signaling pathways. *Cancer Res.*, 69: 518–525.
- Parke, C.L., Wojcik, E.J., Kim, S. and Worthylake, D.K. (2010). ATP hydrolysis in Eg5 kinesin involves a catalytic two-water mechanism. *J. Biol. Chem.*, 285(8), 5859–5867.
- Parrinello, M. and Rahman, A. (1981). Polymorphic transitions in single crystals: a new molecular dynamics method. *J. Appl. Phys.*, 52: 7182–7190.
- Pereañez, J.A., Patiño, A.C., Núñez, V. and Osorio, E. (2014). The biflavonoid morelloflavone inhibits the enzymatic and biological activities of a snake venom phospholipase A₂. *Chem. Biol. Interact.*, 220: 94–101.
- Pettersen, E.F., Goddard, T.D., Huang, C.C., Couch, G.S., Greenblatt, D.M., Meng, E.C. and Ferrin, T.E. (2004). UCSF Chimera—a visualization system for exploratory research and analysis. *J. Comput. Chem.*, 25: 1605–1612.
- Pinkaew, D., Cho, S.G., Hui, D.Y., Wiktorowicz, J.E., Hutadilok-Towatana, N., Mahabusarakam, W., Tonganunt, M., Stafford, L.J., Phongdara, A., Liu, M. and Fujise, K. (2009). Morelloflavone blocks injury-induced neointimal formation by inhibiting vascular smooth muscle cell migration. *Biochim. Biophys. Acta*, 1790: 31–39.
- Prod. Res.*, 21: 655–662.
- Rath, O. and Kozielski, F. (2012). Kinesins and cancer. *Nature reviews (cancer)*, 12: 572–539.
- Razzaghi-Asl, N., Sepehri, S., Ebadi, A., Miri, R. and Shahabipour, S. (2015). Molecular docking and quantum mechanical studies on biflavonoid structures as BACE-1 inhibitors. *Struct. Chem.*, 26, 607–621.
- Reddie, K.G., Roberts, D.R. and Dore, T.M. (2006). Inhibition of kinesin motor proteins by adociasulfate-2. *J. Med. Chem.*, 49: 4857–4860.
- Romani, A., Galardi, C., Pinelli, P., Mulinacci, N. and Heimler, D. (2002). HPLC

- quantification of flavonoids and biflavonoids in *Cupressaceae* leaves. *Chromatographia*, 56: 469–474.
- Sadakane, K., Takaichi, M. and Maruta, S. (2018). Photo-control of the mitotic kinesin Eg5 using a novel photochromic inhibitor composed of a spiropyran derivative. *J. Biochem.*, 164: 239–246.
- Saunders, A.M., Powers, J., Strome, S. and Saxton, W.M. (2007). Kinesin-5 acts as a brake in anaphase spindle elongation. *Current Biology: CB*, 17:R453–R454.
- Sawin, K.E., LeGuellec, K., Philippe, M., and Mitchison, T.J. (1992). Mitotic spindle organization by a plus-end-directed microtubule motor. *Nature*, 359:540–543.
- Scarabelli, G. and Grant, B.J. (2014). Kinesin-5 allosteric inhibitors uncouple the dynamics of nucleotide, microtubule, and neck-linker binding sites. *Biophys. J.*, 107(9): 2204–2213.
- Scholey, J.M. (2009). Kinesin-5 in *Drosophila* embryo mitosis: sliding filament or spindle matrix mechanism? *Cell Motility and the Cytoskeleton*, 66:500–508.
- Seeliger, D. and de Groot, B.L. (2010). Ligand docking and binding site analysis with PyMol and Autodock/Vina. *J. Comput. Aided Mol. Des.*, 24: 417–422.
- Sharp, D.J., Rogers, G.C., and Scholey, J.M. (2000). Microtubule motors in mitosis. *Nature*, 407: 41–47.
- Skoufias, D.A., DeBonis, S., Saoudi, Y., Lebeau, L. Crevel, I., Cross, R., Wade, R.H., Hackney, D., and Kozielski, F. (2006). S-trityl-L-cysteine is a reversible, tight binding inhibitor of the human kinesin Eg5 that specifically blocks mitotic progression. *J. Biol. Chem.*, 281: 17559–17569.
- Solowey, E., Lichtenstein, M., Sallon, S., Paavilainen, H., Solowey, E. and Lorberboum-Galski, H. (2014). Evaluating medicinal plants for anticancer activity. *ScientificWorldJournal*, 2014: 721402.

- Stern, B.M. and Murray, A.W. (2001). Lack of tension at kinetochores activates the spindle checkpoint in budding yeast. *Curr. Biol.*, 11: 1462–1467.
- Subramanian, R. and Kapoor, T.M. (2012). Building complexity: insights into self-organized assembly of microtubule-based architectures. *Developmental Cell*, 23:874–885.
- Talapatra, S.K., Schüttelkopf, A.W. and Kozielski, F. (2012). The structure of the ternary Eg5-ADP-ispinesib complex. *Acta Crystallogr. D Biol. Crystallogr.*, 68: 1311–1319.
- Tilio, M., Gambini, V., Wang, J., Garulli, C., Kalogris, C., Andreani, C., Bartolacci, C., Elexpuru Zabaleta, M., Pietrella, L., Hysi, A., Iezzi, M., Belletti, B., Orlando, F., Provinciali, M., Galeazzi, R., Marchini, C. and Amici, A. (2016). Irreversible inhibition of $\Delta 16$ HER2 is necessary to suppress $\Delta 16$ HER2-positive breast carcinomas resistant to Lapatinib., *Cancer Lett.*, 381(1): 76-84.
- Trott, O. and Olson, A.J. (2010). AutoDock Vina: Improving the speed and accuracy of docking with a new scoring function, efficient optimization and multithreading. *J. Comput. Chem.*, 31: 455–461.
- Tuansulong, K.A., Hutadilok-Towatana, N., Mahabusarakam, W., Pinkaew, D., and Fujise, K. (2011). Morelloflavone from *Garcinia dulcis* as a novel biflavonoid inhibitor of HMG-CoA reductase. *Phytother. Res.*, 25: 424–428.
- Turner, P.J. (2005). XMGRACE, Version 5.1.21. Center for Coastal and Land-Margin Research, Oregon Graduate Institute of Science and Technology, Beaverton, OR; 2005.
- Valentine, M.T., Fordyce, P.M., and Block, S.M. (2006). Eg5 steps it up! *Cell Division*, 1:31–38.
- Van Der Spoel, D., Lindahl, E., Hess, B., Groenhof, G., Mark, A.E. and Berendsen, H.J. (2005). GROMACS: fast, flexible, and free. *J. Comput. Chem.*, 26(16): 1701–1718.

- Veeresham, C. (2012). Natural products derived from plants as a source of drugs. *J. Adv. Pharm. Technol. Res.*, 3: 200–201.
- Verdi, L.G., Pizzolatti, M.G., Montanher, A.B., Brighente, I.M., Smânia Júnior, A., Smânia Ed Ede, F.A., Simionatto, E.L. and Monache, F.D. (2004). Antibacterial and brine shrimp lethality tests of biflavonoids and derivatives of *Rheedia gardneriana*. *Fitoterapia*, 75: 360–363.
- Wang, F., Good, J.A., Rath, O., Kaan, H.Y., Sutcliffe, O.B., Mackay, S.P. and Kozielski, F. (2012). Triphenylbutanamines: kinesin spindle protein inhibitors with in vivo antitumor activity. *J. Med. Chem.*, 55: 1511–1525.
- Wang, J., Wolf, R.M., Caldwell, J.W., Kollman, P.A. and Case, D.A. (2004). Development and testing of a general amber force field. *J. Comput. Chem.*, 25(9): 1157–1174.
- Wang, Y., Wu, X., Du, M., Chen, X., Ning, X., Chen, H., Wang, S., Liu, J., Liu, Z., Li, R., Fu, G., Wang, C., McNutt, M.A., Zhou, D. and Yin, Y. (2017). Eg5 inhibitor YL001 induces mitotic arrest and inhibits tumor proliferation. *Oncotarget*, 8(26): 42510–42524.
- Waterhouse, A., Bertoni, M., Bienert, S., Studer, G., Tauriello, G., Gumienny, R., Heer, F.T., de Beer, T.A.P, Rempfer, C., Bordoli, L., Lepore, R. and Schwede, T. (2018). SWISS-MODEL: homology modelling of protein of protein structures and complexes. *Nucleic acids Res.*, 46(W1): W296-W303.
- Weil, D., Garçon, L., Harper, M., Duménil, D., Dautry, F. and Kress, M. (2002). Targeting the kinesin Eg5 to monitor siRNA transfection in mammalian cells. *Biotechniques*, 33:1244–1248.
- Wittmann, T. (2001). Hyman A, Desai A. The spindle: a dynamic assembly of microtubules and motors. *Nat. Cell Biol.*, 3: 28–34.

- Woessner, R., Tunquist, B., Lemieux, C., Chlipala, E., Jackinsky, S., Dewolf, W., Voegtli, W., Cox, A., Rana, S., Lee, P., Walker, D. (2009). ARRY-520, a novel KSP inhibitor with potent activity in hematological and taxane-resistant tumor models. *Anticancer Res.*, 29:4373–4380.
- Wordeman, L. (2010). How kinesin motor proteins drive mitotic spindle function: lessons from molecular assays. *Semin. Cell Dev. Biol.*, 21: 260–268.
- Xiong, M., Wang, L., Yu, H.L., Han, H., Mao, D., Chen, J., Zeng, Y., He, N., Liu, Z.G., Wang, Z.Y., Xu, S.J., Guo, L.Y. and Wang, Y.A. (2016). Ginkgetin exerts growth inhibitory and apoptotic effects on osteosarcoma cells through inhibition of STAT3 and activation of caspase-3/9. *Oncol Rep.*, 35: 1034–1040.
- Yan, Y., Sardana, V., Xu, B., Homnick, C., Halczenko, W., Buser, C.A., Schaber, M., Hartman, G.D., Huber, H.E. and Kuo, L.C. (2004). Inhibition of a mitotic motor protein: where, how, and conformational consequences. *J. Mol. Biol.*, 335: 547–554.
- Yang, H., Figueroa, M., To, M., Baggett, S., Jiang, B., Basile, M.J., Weinstein, I.B. and Kennelly, E.J. (2010). Benzophenones and biflavonoids from *Garcinia livingstonei* fruits. *J. Agric. Food Chem.*, 58: 4749–4755.
- Yao, H., Chen, B., Zhang, Y., Ou, H., Li, Y., Li, S., Shi, P. and Lin, X. (2017). Analysis of the total biflavonoids extract from *Selaginella doederleinii* by HPLC-QTOF-MS and its *in vitro* and *in vivo* anticancer effects. *Molecules*, 22: E325.
- Youngburg, G.E. and Youngburg, M.V. (1930). Phosphorus metabolism. I. A system of blood phosphorus analysis. *J. Lab. Clin. Med.*, 16: 158–166.
- Yu, S., Yan, H., Zhang, L., Shan, M., Chen, P., Ding, A. and Li, S.F.Y. (2017). A review on the phytochemistry, pharmacology, and pharmacokinetics of amentoflavone, a naturally-occurring biflavonoid. *Molecules*, 22: E299.
- Zembower, D.E., Lin, Y.M., Flavin, M.T., Chen, F.C. and Korba, B.E. (1998). Robustaflavone,

a potential non-nucleoside anti-hepatitis B agent. *Antiviral Res.*, 39: 81–88.

Zhang, W. (2011). Exploring the intermediate states of ADP-ATP exchange: A simulation study on Eg5. *J. Phys. Chem. B*, 115(5): 784–795.